

**EFFECT OF THERMAL RADIATION ON MHD MIXED
CONVECTION IN AN ENCLOSER WITH SEMICIRCULAR
HEATER USING KEROSENE BASED CNT NANOFUID**

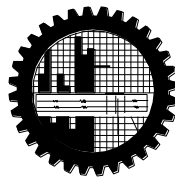
by

Md. Rumman Hossain

Student No. 0419092501

Registration No. 0419092501, Session: April- 2019

MASTER OF SCIENCE
IN
MATHEMATICS




Department of Mathematics



Bangladesh University of Engineering and Technology, Dhaka-1000

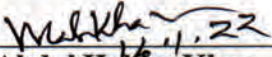
January 16, 2022


The thesis entitled “EFFECT OF THERMAL RADIATION ON MHD MIXED CONVECTION IN AN ENCLOSER WITH SEMICIRCULAR HEATER USING KEROSENE BASED CNT NANOFLUID”, submitted by **Md. Rumman Hossain**, Roll no: 0419092501, Registration No. 0419092501, Session April/2019 has been accepted as satisfactory in partial fulfillment of the requirement for the degree of Master of Science in Mathematics on January 16, 2022.


BOARD OF EXAMINERS

1. 

Dr. Md. Mustafizur Rahman
Professor
Department of Mathematics, BUET, Dhaka-1000

Chairman
(Supervisor)
2. 

Dr. Khandker Farid Uddin Ahmed
~~Head~~ Professor and Head
Department of Mathematics
BUET, Dhaka-1000
Member
(Ex-Officio)
3. 

Dr. Md. Abdul Hakim Khan
Professor
Department of Mathematics, BUET, Dhaka-1000
Member
4. 

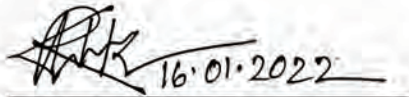
Dr. Nazma Parveen
Professor
Department of Mathematics, BUET, Dhaka-1000
Member
5. 

Dr. Mohammad Arif Hasan Mamun
Professor
Department of Mechanical Engineering, BUET, Dhaka – 1000.
Member
(External)

CANDIDATE'S DECLARATION

I hereby announce that the work which is being presented in this thesis entitled '**EFFECT OF THERMAL RADIATION ON MHD MIXED CONVECTION IN AN ENCLOSER WITH SEMICIRCULAR HEATER USING KEROSENE BASED CNT NANOFUID**', submitted in partial fulfillment of the requirements for the degree of **Master of Science** in Mathematics on January 16, 2022, Bangladesh University of Engineering and Technology, Dhaka-1000 is my own work with proper citation and acknowledgement.

It is hereby declared that this thesis or any part of it has not been submitted elsewhere for any degree or diploma.



16.01.2022

Md. Rumman Hossain


M.Sc. Student

Department of Mathematics

January 16, 2022

CERTIFICATE OF RESEARCH

This is to certify that the work entitled '**EFFECT OF THERMAL RADIATION ON MHD MIXED CONVECTION IN AN ENCLOSER WITH SEMICIRCULAR HEATER USING KEROSENE BASED CNT NANOFLUID**' has been carried out by **Mr. Md. Rumman Hossain** bearing Roll No.: 0419092501, Registration No.: 0419092501, Session: April/2019, of Department of Mathematics, Bangladesh University of Engineering and Technology, Dhaka-1000, Bangladesh in partial fulfillment of the requirements for the degree of **Master of Science** in Mathematics of the aforementioned University, under my supervision.


16.01.2022

Dr. Md. Mustafizur Rahman

Supervisor

Department of Mathematics
Bangladesh University of Engineering
and Technology (BUET)

Dedicated
to
My Parents

ACKNOWLEDGEMENT

All glory to Almighty ALLAH, whose uniqueness, oneness, and completeness are unmatched, and without whose assistance, no task could have been completed.

I am especially grateful to my supervisor, Dr. Mustafizur Rahman, Professor of the Department of Mathematics, Bangladesh University of Engineering, for his advice and encouragement during my studies. I had a fantastic academic experience under his guidance, and his important recommendations and support aided me in planning my further academic pursuits well.

I am thankful from the core of my heart to faculty members of the Department of Mathematics, Bangladesh University of Engineering and Technology, especially, to Prof. Dr. Khandker Farid Uddin Ahmed, Head, Department of Mathematics, Prof. Dr. Md. Abdul Hakim Khan, Prof. Dr. Md. Manirul Alam Sarker, Prof. Dr. Md. Abdul Alim, Prof. Dr. Md. Zafar Iqbal Khan, Prof. Dr. Nazma Parveen, Dr. Mohammed Forhad Uddin, Prof. Dr. Salma Parvin, Prof. Dr. Ms. Rehana Nasrin and all other teachers of this department for their guidance and supports.

I am also grateful to my elder brother, Md. Abul Kalam Azad, Assistant Professor. Department of Natural Sciences, IUT(OIC), Gazipur, Bangladesh for initiating this research. This thesis would not have been feasible without his cooperation, exceptional recommendations, persistent encouragement, strong curiosity, constructive critique, and amicable discussions.

Finally, but certainly not least, I want to express my gratitude for the love and support of my family members who prayed for my success and well-being. I am indebted to them for their unfailing kindness, patience, and encouragement.

ABSTRACT

Oil-based nanofluids are used to strengthen the stability of nanofluids as well as their thermophysical properties when they are exposed to high temperature. For this study, heat transfer enhancement on time dependent combined convective flow were examined numerically. A lid-driven square cavity with a semicircular heater on the bottom wall is selected as fluid domain with kerosene-based CNT nanofluid, that is considered for an unsteady, laminar, newtonian, incompressible, and mixed convection flow in the existence of radiative heat flux and magnetic field. The upper wall slides to the x-direction with an isothermal temperature value of T_c and constant velocity u_0 , whilst the semi-circular heater stays at isothermal temperature T_h with a radius of $0.25L$ and $T_h > T_c$. The other walls of the fluid domain are considered insulated, so there is no heat transfer took place in those regions. The governing two-dimensional equations and associated boundary conditions were presented mathematically for the considered physical problem. The governing equations and boundary conditions are transformed into non-dimensional form and solved using a finite-element approach based on Galerkin weighted residuals. The thermal conductivity and dynamic viscosity models incorporated nanoparticle Brownian motion. The simulations were carried out with a range of values for the radiation parameter Rd ($= 0 - 2$), the Hartmann number Ha ($= 0 - 50$), the solid volume fraction ϕ ($= 0\% - 10\%$), the Reynolds number Re ($= 50 - 200$), and the Richardson number Ri ($= 0.1-10$). Numerous features such as streamlines, isotherms, heat transfer rate of the semicircular heater Nu_h and thermophysical properties such as Drag force of the moving lid, fluid temperature gradient θ_f , fluid pressure gradient $Grad P$, average fluid temperature θ_{av} , fluid bulk temperature θ_b velocity magnitude of the fluid were described for dimensionless time τ ($= 0 - 1$) and the aforesaid parameters. The results show that the indicated parameters have a strong influence on the flow phenomena and temperature field inside the cavity, but have a negligible effect for higher value of dimensionless time. It is worth noted that after a while, the considered parameter exhibits consistent behavior.

TABLE OF CONTENTS

<u>Items</u>	<u>Page</u>
BOARD OF EXAMINERS	ii
CANDIDATE’S DECLARATION.....	iii
CERTIFICATE OF RESEARCH.....	iv
ACKNOWLEDGEMENT	vi
ABSTRACT.....	vii
NOMENCLATURE.....	xi
LIST OF TABLES	xiii
LIST OF FIGURES	xiv
CHAPTER 1	1
INTRODUCTION.....	1
1.1 MODES OF HEAT TRANSFER.....	2
1.1.1 Conduction.....	2
1.1.2 Convection	2
1.1.3 Radiation	3
1.2 MIXED CONVECTION HEAT TRANSFER IN CAVITIES [1]	3
1.3 MAGNETOHYDRODYNAMICS	4
1.3.1 Fluid Mechanics Aspect.....	5
1.3.2 Applications of Magnetohydrodynamics	6
1.4 THERMAL RADIATION [5].....	7
1.4.1 Thermal Radiation in Nature.....	8
1.4.2 Thermal Radiation in Engineering.....	8
1.4.3 Thermal Radiation and Thermodynamics.....	9
1.5 NANOFUIDS	11
1.5.1 Theoretical Model of Nanofluid’s Thermal Conductivity	11
1.5.2 Theoretical Model of Nanofluids’ Viscosity	13
1.5.3 Density and Specific Heat of Nanofluids.....	14
1.6 DIMENSIONLESS PARAMETERS.....	14
1.6.1 Radiation Parameter.....	14
1.6.2 Hartmann Number.....	15
1.6.3 Solid Volume Fraction	15
1.6.4 Reynolds Number	16
1.6.5 Prandtl Number	17
1.6.6 Richardson Number	17

1.7 LITERATURE REVIEW.....	18
1.8 APPLICATIONS	24
1.9 MOTIVATION	24
1.10 OBJECTIVES OF THE PRESENT STUDY.....	25
1.11 OUTLINE OF THE THESIS	26
CHAPTER 2	27
PROBLEM FORMULATION.....	27
2.1 MODEL DEFINITION.....	28
2.2 GOVERNING EQUATIONS	29
2.3 INITIAL AND BOUNDARY CONDITIONS(DIMENSIONAL FORM)	30
2.4 NANOFUIDS PROPERTIES.....	30
2.5 DIMENSIONAL ANALYSIS	31
2.5.1 Approximation of $\frac{\partial q_R}{\partial y}$	32
2.5.2 Non Dimensional Governing Equations with Boundary Conditions	33
2.6 CALCULATION OF PHYSICAL AND HYDRODYNAMIC PROPERTIES .	34
2.7 NUMERICAL ANALYSIS	35
2.7.1 Finite Element Formulation and Computational Procedure	35
2.7.2 Grid Size Sensitivity Test	39
2.7.3 Code Validation	40
CHAPTER 3	42
RESULTS AND DISCUSSION	42
3.1 EFFECT OF RADIATION PARAMETER.....	42
3.1.1 Effect on Flow Movement	42
3.1.2 Effect on the Temperature in the Flow Field	44
3.1.3 Effect on the Velocity Magnitude.....	44
3.1.4 Effect on Drag Force.....	46
3.1.5 Effect on the Pressure Gradient	47
3.1.6 Effect on the Fluid Temperature Gradient	47
3.1.7 Effect on the Mean Heat Transfer Rate	49
3.1.8 Effect on Average Fluid Temperature	50
3.1.9 Effect on the Bulk Temperature of the Fluid	50
3.2 EFFECT OF HARTMANN NUMBER.....	51
3.2.1 Effect on Flow Movement	51
3.2.2 Effect on the Temperature in the Flow Field	53
3.2.3 Effect on the Velocity Magnitude.....	55
3.2.4 Effect on Drag Force.....	56
3.2.5 Effect on the Pressure Gradient	57

3.2.6 Effect on the Mean Heat Transfer Rate	58
3.2.7 Effect on the Fluid Temperature Gradient	59
3.2.8 Effect on Average Fluid Temperature	60
3.2.9 Effect on the Bulk Temperature of the Fluid	61
3.3 EFFECT OF SOLID VOLUME FRACTION	62
3.3.1 Effect on Flow Movement	62
3.3.2 Effect on the Temperature in the Flow Field	64
3.3.3 Effect on the Velocity Magnitude	66
3.3.4 Effect on Drag Force	67
3.3.5 Effect on the Pressure Gradient	68
3.3.6 Effect on Mean Heat Transfer Rate.....	69
3.3.7 Effect on Fluid Temperature Gradient	70
3.3.8 Effect on the Average Fluid Temperature.....	71
3.3.9 Effect on Bulk Temperature of the Fluid	72
3.4 EFFECTS OF REYNOLDS NUMBER.....	73
3.4.1 Effect on Flow Movement	73
3.4.2 Effect on the Temperature in the Flow Field	74
3.4.3 Effect on the Velocity Magnitude	76
3.4.4 Effect on Drag Force.....	77
3.4.5 Effect on the Pressure Gradient	78
3.4.6 Effect on the Mean Heat Transfer Rate	79
3.4.7 Effect on the Fluid Temperature Gradient	80
3.4.8 Effect on Average Fluid Temperature	81
3.4.9 Effect on the Bulk Temperature of the Fluid	82
3.5 EFFECT OF RICHARDSON NUMBER.....	83
3.5.1 Effect on Flow Movement	83
3.5.2 Effect on the Temperature in the Flow Field	85
3.5.3 Effect on the Velocity Magnitude.....	87
3.5.4 Effect on Drag Force.....	88
3.5.5 Effect on the Pressure Gradient	89
3.5.6 Effect on the Mean Heat Transfer Rate	90
3.5.7 Effect on the Fluid Temperature Gradient	91
3.5.8 Effect on Average Fluid Temperature	92
3.5.9 Effect on the Bulk Temperature of the Fluid	93
CHAPTER 4	94
CONCLUSIONS.....	94
4.1 SUMMARY OF THE MAJOR OUTCOMES.....	94
4.2 FURTHER WORKS	96
REFERENCES.....	97

NOMENCLATURE

B_0	magnetic field induction (N/Am ²)
c_p	specific heat at constant pressure (J/kg.K)
E_b	Blackbody Radiation
g	gravitational acceleration (ms ⁻²)
h	convective heat transfer coefficient (W/m ² .K)
H	height of the cavity (m)
Ha	Hartmann number
k	thermal conductivity of fluid (Wm ⁻¹ K ⁻¹)
L	length of the cavity (m)
n	dimensional distance either along x or y direction (m)
N	Any direction
N_α	quadratic shape function
Nu	Average Nusselt number
p	pressure with dimation (Nm ⁻²)
P	Pressure without dimension
Pl	Plank Number
Pr	Prandtl number
Ra	Rayleigh number
Rd	Radiation prameter
Ri	Richardson Number
Re	Reynolds number
t	Dimensional time (s)
T	Dimensional temperature (k)
S_x	surface tractions along X-axis
S_y	surface tractions along Y-axis
T	dimensional fluid temperature (K)
ΔT	dimensional temperature difference (K)
u	velocity in x-direction (m/s)
U	dimensionless horizontal velocity
v	velocity in y-direction (m/s)
V	dimensionless vertical velocity
\bar{A}	cavity area (m ²)
u, v	Velocity component with dimension (ms ⁻¹)
U, V	Velocity component without dimension
x, y	Dimensional cartesian coordinates
X, Y	Dimensionless cartesian coordinates

Greek symbols

α	thermal diffusivity (m^2s^{-1})
β	coefficient of thermal expansion (K^{-1})
θ	dimensionless fluid temperature
$\Delta\theta$	dimensionless temperature difference
ψ	stream function
ϕ	solid volume fraction
ε	Emissivity
μ	Dynamic viscosity of the fluid ($\text{kgm}^{-1}\text{s}^{-1}$)
ν	kinematic viscosity of the fluid (m^2s^{-1})
κ	Average absorption coefficient (m^{-1})
η	Dimensionless optical thickness
ρ	density of the fluid (kgm^{-3})
σ	Electrical conductivity ($\Omega^{-1}.\text{m}^{-1}$)
σ_s	Stefan-Boltzmann constant

Subscripts

av	average
CNT	Carbon nanotube
f	fluid
h	heated wall
i	inlet state
nf	nanofluid
s	solid nanoparticle

LIST OF TABLES

2.1	Thermo physical properties of fluid and nanoparticle [Kavitha et al.[62]]	29
2.2	Grid test for, $Ri = 1$, $Ha = 10$, $Re = 100$, $Pr = 23.004$, $Rd = 1$, $\tau = 0.1$ and $\phi = 0.05$	40

LIST OF FIGURES

2.1	Schematic diagram for the problem with boundary conditions and co-ordinate system.	28
2.2	Mesh generation of the enclosure.	39
2.3	Grid test for the representative values of $Ri = 1$, $Ha = 10$, $Re = 100$, $Pr = 23.004$, $Rd = 1$, $\tau = 0.1$ and $\phi = 0.05$	40
2.4.a	Comparison of the average Nusselt number on Ri between the present results and Malleswarm et al. [68] for $Ha = 25$, $Re = 100$, $Pr = 0.054$, $L_H = 1/3m$ and $\varepsilon_2 = 1/2m$.	41
2.4.b	Comparison of the average Nusselt number on Ha between the present results and Sheikholeslami et al. [69] for $Ra = 10^5$, $Pr = 6.2(Al_2O_3 \text{ water})$, $Rd = 1$ and $\varepsilon = 0$.	41
3.1.1	Effect of radiation parameter, Rd on streamlines for changed values of dimensionless time τ at $Re = 100$, $Ri = 1$, $Ha = 10$, $\phi = 0.05$.	43
3.1.2	Effect of radiation parameter, Rd on isotherms for changed values of dimensionless time τ at fixed values of $Re = 100$, $Ri = 1$, $Ha = 10$, $\phi = 0.05$.	45
3.1.3	Effect of radiation parameter, Rd and dimensionless time τ on velocity fields at the fixed values of $Re = 100$, $Ri = 1$, $Ha = 10$, $\phi = 0.05$.	46
3.1.4	Effect of radiation parameter, Rd and dimensionless time τ on drag force of the moving lid at the fixed values of $Re = 100$, $Ri = 1$, $Ha = 10$, $\phi = 0.05$.	47
3.1.5	Effect of radiation parameter, Rd and dimensionless time τ on pressure gradient of the fluid at the fixed values of $Re = 100$, $Ri = 1$, $Ha = 10$, $\phi = 0.05$.	48
3.1.6	Effect of radiation parameter, Rd and dimensionless time τ on fluid temperature gradient at the fixed values of $Re = 100$, $Ri = 1$, $Ha = 10$, $\phi = 0.05$.	48
3.1.7	Effect of radiation parameter, Rd and dimensionless time τ on mean heat transfer rate from the heated surface at the fixed values of $Re = 100$, $Ri = 1$, $Ha = 10$, $\phi = 0.05$.	49

3.1.8	Effect of radiation parameter, R_d and dimensionless time τ on the average temperature of the fluid at the fixed values of $Re = 100$, $Ri = 1$, $Ha = 10$, $\phi = 0.05$.	50
3.1.9	Effect of radiation parameter, R_d and dimensionless time τ on bulk temperature of the fluid at the fixed values of $Re = 100$, $Ri = 1$, $Ha = 10$, $\phi = 0.05$.	51
3.2.1	Effect of Hartmann number, Ha on streamlines for changed values of dimensionless time τ at $Re = 100$, $Ri = 1$, $R_d = 1$, $\phi = 0.05$.	52
3.2.2	Effect of Hartmann number, Ha on isotherms for changed values of dimensionless time τ at $Re = 100$, $Ri = 1$, $R_d = 1$, $\phi = 0.05$.	54
3.2.3	Effect of Hartmann number, Ha and dimensionless time τ on velocity fields at the fixed values of $Re = 100$, $Ri = 1$, $R_d = 1$, $\phi = 0.05$.	55
3.2.4	Effect of Hartmann number, Ha and dimensionless time τ on Drag force of the moving lid at the fixed values of $Re = 100$, $Ri = 1$, $R_d = 1$, $\phi = 0.05$.	57
3.2.5	Effect of Hartmann number, Ha and dimensionless time τ on pressure gradient of the field at the fixed values of $Re = 100$, $Ri = 1$, $R_d = 1$, $\phi = 0.05$.	58
3.2.6	Effect of Hartmann number, Ha and dimensionless time τ on mean heat transfer rate from the heated surface at the fixed values of $Re = 100$, $Ri = 1$, $R_d = 1$, $\phi = 0.05$.	59
3.2.7	Effect of Hartmann number, Ha and dimensionless time τ on fluid temperature gradient at the fixed values of $Re = 100$, $Ri = 1$, $R_d = 1$, $\phi = 0.05$.	60
3.2.8	Effect of Hartmann number, Ha and dimensionless time τ on average temperature of the fluid at the fixed values of $Re = 100$, $Ri = 1$, $R_d = 1$, $\phi = 0.05$.	61
3.2.9	Effect of Hartmann number, Ha and dimensionless time τ on bulk temperature of the fluid at the fixed values of $Re = 100$, $Ri = 1$, $R_d = 1$, $\phi = 0.05$.	62
3.3.1	Effect of solid volume fraction, ϕ on streamlines for changed values of dimensionless time τ at $Re = 100$, $Ri = 1$, $R_d = 1$, $Ha = 10$.	63
3.3.2	Effect of solid volume fraction, ϕ on isotherms for changed values of dimensionless time τ at $Re = 100$, $Ri = 1$, $R_d = 1$, $Ha = 10$.	65

3.3.3	Effect of solid volume fraction, ϕ and dimensionless time τ on velocity fields at the fixed values of $Re = 100$, $Ri = 1$, $Ha = 10$, $Rd = 1$.	66
3.3.4	Effect of solid volume fraction, ϕ and dimensionless time τ on Drag force of the moving lid at the fixed values of $Re = 100$, $Ri = 1$, $Ha = 10$, $Rd = 1$.	67
3.3.5	Effect of solid volume fraction, ϕ and dimensionless time τ on pressure gradient of the fluid at the fixed values of $Re = 100$, $Ri = 1$, $Ha = 10$, $Rd = 1$.	68
3.3.6	Effect of solid volume fraction, ϕ and dimensionless time τ on mean heat transfer rate from the heated surface at the fixed values of $Re = 100$, $Ri = 1$, $Ha = 10$, $Rd = 1$.	69
3.3.7	Effect of solid volume fraction, ϕ and dimensionless time τ on fluid temperature gradient at the fixed values of $Re = 100$, $Ri = 1$, $Ha = 10$, $Rd = 1$.	70
3.3.8	Effect of solid volume fraction, ϕ and dimensionless time τ on the average temperature of the fluid at the fixed values of $Re = 100$, $Ri = 1$, $Ha = 10$, $Rd = 1$.	71
3.3.9	Effect of solid volume fraction, ϕ and dimensionless time τ on bulk temperature of the fluid at the fixed values of $Re = 100$, $Ri = 1$, $Ha = 10$, $Rd = 1$.	72
3.4.1	Effect of Renolds number, Re on streamlines for changed values of dimensionless time τ at $\phi = 0.05$, $Ri = 1$, $Rd = 1$, $Ha = 10$.	74
3.4.2	Effect of Renolds number, Re on isotherms for changed values of dimensionless time τ at $\phi = 0.05$, $Ri = 1$, $Rd = 1$, $Ha = 10$.	75
3.4.3	Effect of Renolds number, Re and dimensionless time τ on velocity fields at the fixed values of $\phi = 0.05$, $Ri = 1$, $Rd = 1$, $Ha = 10$.	76
3.4.4	Effect of Renolds number, Re and dimensionless time τ on Drag force of the moving lid at the fixed values of $\phi = 0.05$, $Ri = 1$, $Rd = 1$, $Ha = 10$.	77
3.4.5	Effect of Renolds number, Re and dimensionless time τ on pressure gradient at the fixed values of $\phi = 0.05$, $Ri = 1$, $Rd = 1$, $Ha = 10$.	78
3.4.6	Effect of Renolds number, Re and dimensionless time τ on mean heat transfer rate from the heated surface at the fixed values of $\phi = 0.05$, $Ri = 1$, $Rd = 1$, $Ha = 10$.	79
3.4.7	Effect of Renolds number, Re and dimensionless time τ on fluid temperature gradient at the fixed values of $\phi = 0.05$, $Ri = 1$, $Rd = 1$, $Ha = 10$.	80

3.4.8	Effect of Renolds number, Re and dimensionless time τ on average temperature of the fluid at the fixed values of $\phi = 0.05$, $Ri = 1$, $Rd = 1$, $Ha = 10$.	81
3.4.9	Effect of Renolds number, Re and dimensionless time τ on bulk temperature of the fluid at the fixed values of $\phi = 0.05$, $Ri = 1$, $Rd = 1$, $Ha = 10$.	82
3.5.1	Effect of Richardson number, Ri on streamlines for changed values of dimensionless time τ at $\phi = 0.05$, $Re = 100$, $Rd = 1$, $Ha = 10$.	84
3.5.2	Effect of Richardson number, Ri on isotherms for changed values of dimensionless time τ at $\phi = 0.05$, $Re = 100$, $Rd = 1$, $Ha = 10$.	86
3.5.3	Effect of Richardson number, Ri and dimensionless time τ on velocity field at the fixed values of $\phi = 0.05$, $Re = 100$, $Rd = 1$, $Ha = 10$.	87
3.5.4	Effect of Richardson number, Ri and dimensionless time τ on on Drag force of the moving lid at the fixed values of $\phi = 0.05$, $Re = 100$, $Rd = 1$, $Ha = 10$.	88
3.5.5	Effect of Richardson number, Ri and dimensionless time τ on pressure gradient of the fluid at the fixed values of $\phi = 0.05$, $Re = 100$, $Rd = 1$, $Ha = 10$.	89
3.5.6	Effect of Richardson number, Ri and dimensionless time τ on mean heat transfer rate from the heated surface at the fixed values of $\phi = 0.05$, $Re = 100$, $Rd = 1$, $Ha = 10$.	90
3.5.7	Effect of Richardson number, Ri and dimensionless time τ on on fluid temperature gradient at the fixed values of $\phi = 0.05$, $Re = 100$, $Rd = 1$, $Ha = 10$.	91
3.5.8	Effect of Richardson number, Ri and dimensionless time τ on average temperature of the fluid at the fixed values of $\phi = 0.05$, $Re = 100$, $Rd = 1$, $Ha = 10$.	92
3.5.9	Effect of Richardson number, Ri and dimensionless time τ on bulk temperature of the fluid at the fixed values of $\phi = 0.05$, $Re = 100$, $Rd = 1$, $Ha = 10$.	93

CHAPTER 1

INTRODUCTION

The study of thermal radiation of gases has a fundamental importance in understanding many phenomena in engineering systems such as combustion and motion and energy transport processes involving radiating gases. This chapter provides a general introduction to applied thermodynamics of nanofluids, which includes mixed convection heat transfer phenomena that occurs under different areas of applications in the field of engineering, such as silicon mirror cooling, electronic cooling, vehicle cooling, transformer cooling, nuclear reactors, lakes and reservoirs, and solar applications, etc. Mixed convection heat transfer in a channel with a cavity in the presence of magnetic field is a new branch of thermo-fluid mechanics. Here convection means the flow of heat through in liquid or gasses along with the flow of the mass itself. Hence convection is classically assumed as a large-scale level of heat transfer. Basically, radiation is the transmission of energy (and thus heat) directly through electromagnetic waves. To describe the heat transport phenomenon, strong background of the hydrodynamics, the convective heat transfer mechanism and the electromagnetic field are pre-requisite as they have a symbiotic relationship. On the other hand heat transfer properties of thermo fluid play an important role in the development of energy-efficient heat transfer equipment. Numerous analysts are inquisitive about the think of MHD liquid flow because of its significant applications within the forms of designing, vitality generations, planetary and sun powered plasma liquid flow frameworks, attractive field control of fabric handing framework, half breed attractive impetus framework for space travel, businesses, biomedical science. The rest of this preliminary chapter is as follows. Since this thesis is the effect of thermal radiation on MHD Mixed convection in an enclosure with semicircular heater using kerosene based CNT nanofluid so it is organized in a flowing manner.

Following is the remainder of this chapter's content: Using kerosene-based CNT nanofluids, we will investigate the effect of thermal radiation on MHD mixed convection in an enclosure with a semicircular heater. First, we cover the various

forms of heat transfer in section 1.1. Section 1.2 discusses mixed convection heat transfer in a cavity. Magnetohydrodynamics (MHD) characteristics are described in section 1.3 for the objectives of this study. In section 1.4, the topic of thermal radiation as it relates to this research was briefly discussed. A short discussion on Nanofluids is presented in 1.5. In 1.6, Dimensionless parameters and their definitions are discussed. Literature related to this study has been presented briefly in section 1.7. Then application, the motivation behind selection of the present problem and objective of the current study are described in sections 1.8 to 1.10 respectively. Finally, in section 1.11, a brief outline of the remainder of the thesis has been presented.

1.1 MODES OF HEAT TRANSFER

Heat transfer is the movement of thermal energy from one area to another because of temperature differences. Conduction, Convection, and Radiation are three separate forms of heat transport. Once both mediums reach the same temperature, heat transmission is halted.

1.1.1 Conduction

Conduction is the process by which energy is transferred from a substance's more energetic particles to nearby less energetic ones as a consequence of particle interactions. Conduction occurs in solids, liquids, and gases. Conduction occurs in gases and liquids as a result of collisions and diffusion of molecules during their random motion; in solids, it occurs as a result of the combination of the vibrations of molecules in a lattice and energy transfer through free electrons. The rate of heat conduction across a medium is determined by its shape, thickness, and composition, as well as the temperature differential across the medium [1].

1.1.2 Convection

Convection is the heat transmission process that occurs when a fluid is subjected to bulk fluid motion as a consequence of a temperature differential. There are two forms of convection heat transfer: natural convection and forced convection. When convection happens spontaneously, it is referred to as natural (or free) convection. In

this example, buoyancy effects generated by the temperature differential in the fluid and gravitational force create fluid motion. If, on the other hand, the fluid motion is induced artificially by an external source such as a blower or fan, the heat transfer mode is referred to as forced convection [1].

1.1.3 Radiation

Radiation is the energy that is released by matter in the form of electromagnetic waves (or photons) as a consequence of changes in the atom's or molecule's electrical state. In contrast to conduction and convection, radiation does not need the existence of an intervening medium. Indeed, heat transmission by radiation is quicker and exhibits no loss of efficiency in a vacuum. This is how the sun's energy is transmitted to the earth. Radiation is a volumetric phenomena, and all solids, liquids, and gases, to variable degrees, emit, absorb, or transmit radiation. However, radiation is often thought of as a surface phenomena for materials such as metals, wood, and rocks that are opaque to heat radiation [1].

1.2 MIXED CONVECTION HEAT TRANSFER IN CAVITIES [1]

Mixed convection in cavities is a current issue, since cavities filled with fluid are critical components of a diverse range of engineering and geophysical systems. Induced flow and heat transfer in a hollow are fundamentally different from those in an exterior mixed convection boundary layer. In contrast to the external mixed convection boundary layer caused by the heat transfer interaction between a single wall and a very large fluid reservoir, mixed convection in a cavity is the result of a complex interaction between finite size fluid systems in thermal communication with all the surrounding walls. The intricacy of this internal interaction is what accounts for the range of flows that may occur inside a cavity.

The mixed convection phenomena in cavities varies according to the geometry and direction of the cavity. Cavity phenomena may be classified informally into two categories based on their possible technical uses.

1. Vented cavity and
2. Lid-driven cavity

In a vented cavity, the interaction between the external forced stream given by the inlet and the buoyancy-driven fluxes created by the heat source allows for dynamic flows. As a result, understanding the fluid flow and heat transmission properties of mixed convection in a vented cavity is critical. However, the fluid flow and heat transfer in a lid-driven cavity, where the flow is induced by a shear force caused by the motion of a lid combined with the buoyancy force caused by the non-homogeneous temperature of the cavity wall, presents another problem that has been extensively studied by researchers in order to understand the interaction between buoyancy and shearing forces in such flow situation. In a mixed convection regime, the interplay between buoyancy-driven and shear-driven flows within a confined cavity is highly complicated. As a result, it is critical to comprehend the fluid flow and heat transmission properties of mixed convection in a lid-driven cavity.

1.3 MAGNETOHYDRODYNAMICS

Magnetohydrodynamics (MHD) is a branch of research that studies the flow of electrically conducting fluids in the presence of electric and magnetic fields. The velocity of the conducting fluid through the magnetic field produces electric currents that alter the magnetic field, and the magnetic field's influence on these currents produces mechanical forces that affect the fluid. MHD, on the other hand, is often viewed as a very modern field of study. The sciences of astrophysics and geophysics have made the most significant contribution to our knowledge of such events. It has long been considered that the majority of matter in the cosmos exists in the plasma or highly ionized state, and much of the fundamental understanding in the field of electromagnetic fluid dynamics stems from these investigations. MHD also explains several natural phenomena. The sea's movements produce a magnetic field that disrupts the earth's magnetic field. Ocean motions are driven by the electromagnetic force created by the interaction of currents and the earth's magnetic field. The MHD was first used in astrophysical and geophysical issues, and it is still highly useful in these fields. MHD concepts are used in the design of heat exchangers, pumps, and flow meters, as well as in space craft engine, control, and re-entry, as well as in designing innovative power producing systems and confinement techniques for controlled fusion. Electromagnets with fluid conductors, different energy conversion

or storage devices, and magnetically controlled lubrication by conducting fluids, among other things, are all possible MHD uses. Shercliffe provides a detailed analysis of magnetohydrodynamics (MHD) [1].

In classical MHD, are supplemented by Gauss' law:

$$\nabla \cdot \vec{B} = 0. \quad (1.1)$$

Ampere's law for non-relativistic MHD, which neglects the displacement currents for slow MHD phenomena, has the form

$$\vec{J} = \nabla \times \vec{B} / \mu_0. \quad (1.2)$$

In standard MHD, $\nabla \cdot \vec{B} = 0$. However, for MHD numerical simulations, where numerical generation of $\nabla \cdot \vec{B} \neq 0$ [2] it is useful to know the form of the equations for $\nabla \cdot \vec{B} \neq 0$.

1.3.1 Fluid Mechanics Aspect

Local parameters of the fluid, such as pressure and velocity, should be properly specified as averages across components that are enormous in relation to the microscopic structure of matter but tiny in contrast to the scale of macroscopic events. The fluid in MHD is electrically conductive. It is not magnetic; the only way it impacts a magnetic field is by electric currents running through it. Because it includes free charges (ions or electrons) that may flow endlessly, the fluid conducts. According to non-relativistic electromagnetic theory, a charged particle like an electron is subjected to three different types of forces [3]. The total force on a particle per unit of its charge is $f_e = \vec{E} + \vec{v} \times \vec{B}$. This is referred to as the Lorentz force. Electromagnetic body forces operate on the fluid, and the fluid's motion in the presence of an electromagnetic field may cause an electromotive force, so altering the fields. This implies the assumption of local quasi-equilibrium, which enables the state of the fluid at any place to be represented by a few variables that are connected in the same way as if the fluid were in equilibrium. Thus, the fluid may be considered incompressible, homogeneous, and isotropic in both the mathematical and electrical senses. The mathematical models utilized in this study are identical to those

used in classical fluid mechanics. The electromagnetic field's only action is to induce a coupling in the equation of motion through the electromagnetic body force [3].

1.3.2 Applications of Magnetohydrodynamics

There are a number of important cosmic situations in which magnetohydrodynamics is useful [4].

- i. Sunspots: Magnetic fields divide the solar spectrum's spectral lines, as has been known since 1908.(Zeeman effect). It has been inferred that the sunspots are the seat of strong fields ($\sim 10^3$ gauss).
- ii. Stellar magnetic fields: It is known, again from the Zeeman splitting of spectral lines, that a number of stars possess quite strong magnetic fields (10^3 to 10^4 gauss). These may change significantly in as little as a few days, and may even reverse entirely within this time.
- iii. The geomagnetic field: The Earth has a dense fluid core that is believed to be electrically conductive. The main magnetic field of the Earth (<0.7 gauss) is thought to originate from currents flowing in this core.
- iv. Supernova remnants: In the Crab Nebula, the light is strongly polarized, which is characteristic of synchrotron radiation, which is the radiation produced by electrons that have been accelerated in an electromagnetic field. Magnetic fields of 10^{-4} gauss have been inferred.
- v. Galactic field: There seems to be strong evidence that a general Galactic magnetic field ($\sim 10^{-5}$ gauss) exists. It has also been proposed that this field is responsible for keeping the spiral arms from collapsing due to gravity.
- vi. The flow meter: When a conducting fluid runs through an insulating pipe across which a continuous magnetic field is produced, a potential gradient (proportional to the flow speed) is formed and may be monitored by probes placed in the walls of the pipe. The flow rate may thus be measured without, for example, polluting the fluid in the pipe. (The technique is used to measure the flow of blood.)

- vii. Direct conversion of energy: Electricity is often generated in the following manner from the chemical energy contained in fossil fuels such as coal or oil. The fuel is burnt, and the resulting heat is utilized to produce high pressure steam. This then powers a turbine connected to a dynamo. $(T_1 - T_2)/T_1$ where T_1 and T_2 are the upper and lower absolute temperatures of the cycle; in practice, it is usually significantly less. The efficiency can be improved in theory by increasing T_1 but in practice the loss of strength in materials (e.g. the walls of the combustion chamber) at high temperatures is a limitation. Assume that the gases are burnt at high temperatures in a flame that is kept away from the walls. By adding a perpendicular magnetic field, the kinetic energy of the hot ionized gas in the flame may be transformed directly into electrical energy: a potential gradient is generated in a direction perpendicular to field and motion, and currents can be taken off by electrodes inserted in the gas. A pulsed system, in which the alternating current produced in a container of gas by cyclic pulsations (over a stable impressed field) generates a fluctuating magnetic field outside it, is an alternate idea. This would serve as the main coil of a transformer, with the secondary being an external circuit located near the container.
- viii. The electromagnetic pump: This device is, in a sense, the converse of (vii). The Lorentz force, which is formed when mutually perpendicular magnetic fields and electric currents are introduced perpendicular to the pipe, forces a conducting fluid in a pipe to flow. A device like this has been used to circulate liquid sodium conveying heat from a fission reactor's core to an exterior heat exchanger.

1.4 THERMAL RADIATION [5]

Energy emanates from all types of matter under all situations and at all times. Thermal radiation is caused by random fluctuations in the quantized internal energy levels of emitting materials. Temperature is a measure of an object's internal energy level, and the nature of the variations may be attributed to its temperature. When energy is emitted, it spreads like an electromagnetic wave (EM). The quantities of radiation emitted and absorbed depend on the material's physical and chemical

qualities, as well as its internal energy level, as measured by temperature. Radiation may be released by a variety of ways. Thermal radiation emissions are caused by spontaneous fluctuations in quantized energy, and the temperature of matter reflects the average size of such levels. This is referred to as incandescence. Radiation is also emitted as a result of non-thermal events. Some chemical processes, for example, may promote emission. This process is known as chemiluminescence, which is responsible for the blue hue of a natural gas flame, as well as bioluminescence.

1.4.1 Thermal Radiation in Nature

Thermal radiation is essential to the natural events that influence our everyday lives, beginning with the sun. The sun turns hydrogen fuel into helium and heat radiation. Radiation is the sole way to convey thermal energy across a vacuum, and hence the technique by which energy is carried from the sun to the planets of the solar system. Solar energy evaporates water from the seas, irrigates land masses, and creates ocean currents. Climatic zones and seasonal changes are created by differences in the sun angle of incidence at distinct latitudes and as the planet tilts on its axis. Photosynthesis converts solar irradiation into chemical energy, which serves as the basis for almost all plant and animal life on Earth. The temperature of the planet, which supports chemical processes that sustain organic life, is governed by a balance between absorbed and released solar energy. The sky appears blue on a clear day because solar irradiation is dispersed by nitrogen and oxygen molecules in the air, as well as extremely small dust and pollen particles. The majority of creatures on Earth sense by reflected solar radiation, which has a peak emission intensity aligned with the center of the visible spectrum (approximately 550 nm, green light). It is worth noting that the shortwavelength (blue) of the visible spectrum is poorly absorbed in compared to the longwavelength (red), which is frequent in blue-hued underwater scenes [5].

1.4.2 Thermal Radiation in Engineering

Thermal radiation is also useful in many technical applications, particularly when temperatures are high. The amount of energy transferred between two objects by conduction and convection is proportional to the temperature difference between

them. The transferred energy may be a function of the difference between T_1^n and T_2^n for natural (free) convection or if changing impacts of property are included, where n power can be somewhat greater than 1 and can exceed 2. The difference in the fourth power of two distant bodies' absolute temperatures ($n = 4$) determines thermal radiation transmission. When temperature-dependent material properties are used in the calculations, the radiative flux may be proportional to a larger power n of absolute temperatures, emphasizing the significance of radiation transmission at high temperatures. Radiation plays a role in the transfer of energy in furnaces, combustion chambers, fires, rocket plumes, spacecraft atmospheric entry, high-temperature heat exchangers, and chemical explosions. Thermal radiation is critical in the creation of electricity. Around 80% of the world's energy is produced by the burning of fossil fuels, and heat transfer through radiation inside boilers and combustion chambers is crucial for thermal efficiency and pollutant emissions. Thermal radiation is critical in designing more energy-efficient building energy systems and architectural design choices. Even at very low temperatures, radiation is a crucial component of thermal management systems for spacecraft and cryogenic insulation systems, among other uses. Because these systems are mostly vacuum, the only means to transport energy is by radiation. Because of the sun, the planet, and deep space, spaceship radiative heating and cooling varies greatly. Skylab, a space station that orbited the Earth from 1973 to 1979 but only functioned for 24 weeks after launch in May 1973, is a well-known illustration of the need of spacecraft heat regulation. During launch, Skylab lost a critical radiation shield meant to protect the space station from solar radiation, and a replacement made of Mylar arrived 11 days later. Furthermore, the examples above represent just a tiny portion of the many engineering systems that use thermal radiation heat transfer [5].

1.4.3 Thermal Radiation and Thermodynamics

The First Law of Thermodynamics (energy conservation) and the Second Law of Thermodynamics are the foundations of thermal radiation laws. The application of the First Law is typically simple. The First Law stipulates that the absorbed, reflected, and, in the case of semitransparent surfaces, transmitted radiation must all be perfectly balanced by the radiation incident on the surface. The application of the

First Law is typically quite simple. The First Law stipulates that the absorbed, reflected, and, in the case of semitransparent surfaces, transmitted radiation must all be perfectly balanced by the radiation incident on the surface. By increasing the control volume to include mass, it is feasible to link radiative transfer to other forms of heat transmission. The pace at which a surface's temperature increases or heat is carried through it may be connected to the net rate at which radiation is absorbed by it. In the case of a participating medium, the difference between absorbed and emitted radiation at every position in a coupled radiation-advection-diffusion equation is transformed into a volumetric radiative energy source term. The notions of the Second Law are just as important, if not more so. The process by which systems establish thermal equilibrium with their environment is known as energy transmission. When a system is thermally balanced with its environment, it is in a condition of uniform thermal potential, and there can be no net, spontaneous energy transfer across the system's borders until some effort is performed. This is Clausius's proclamation of Thermodynamics' Second Law, which has been the subject of several arguments and debates. The link between macroscopic and microscopic energy conditions necessitates the existence of a particular probability density function (PDF) P_i for their respective energy conditions. The Boltzmann distribution is usually used to refer to

$$p_i \propto \left(-\frac{E_i}{k_b T} \right)$$

where E_i denotes the energy of state i and $k_b = 1.381 \times 10^{-23}$ J/K Boltzmann's constant. Atoms and molecules at local thermodynamic equilibrium (LTE) have sufficient random interactions to generate the Boltzmann distribution. Microscopic reversibility is another concept from the Second Law of Thermodynamics that has an effect on radiative transmission. Simply defined, microscopic reversibility requires that a process be reduced to its most fundamental and predictable form. For example, conservation of linear momentum may be used to estimate the adiabatic scattering (reflection) of a gas molecule across a completely smooth surface [5].

1.5 NANOFUIDS

The addition of small particles into base fluid to boost heat conductivity has been used since the Maxwell treatise was established. With recent advancements in nanotechnology, it is now possible to produce nanometer-sized particles (nanoparticles) with reasonable ease. Because of their tiny size, nanoparticles quickly fluidize within the base fluid, and as a result, channel obstruction and erosion in channel walls are no longer a concern. When it comes to suspension stability, it was shown that using correct dispersants may avoid particle sedimentation. For nanofluid preparation, a variety of particle materials are employed. In nanofluid research, Al_2O_3 , CuO , TiO_2 , SiC , TiC , Ag , Au , Cu , and Fe nanoparticles are widely utilized. Carbon nanotubes are also used because of their extraordinarily high longitudinal (axial) heat conductivity. The common working fluids of heat transfer applications, such as water, ethylene glycol, and motor oil, are generally employed in the creation of nanofluids. Some additives are added to the mixture in modest quantities to increase the stability of nanoparticles inside the base fluid. The sizes of nanoparticles utilized in nanofluid production are typically less than 100 nm. Nanofluid research has made use of particles as tiny as 10 nm. When particles are not spherical but rod or tube-shaped, their diameter is still less than 100 nm, but their length may be measured in micrometers. It should also be mentioned that, owing to the clustering phenomenon, particles with sizes on the order of micrometers may form clusters [1].

1.5.1 Theoretical Model of Nanofluid's Thermal Conductivity

There are two (2) types of models used to estimate the thermal conductivity of nanofluids. They are static and dynamic models, respectively. Maxwell and Hamilton Crosser models are typical static models, as seen in Equations (1.3) and (1.4), respectively [1].

$$\frac{k_{eff}}{k_f} = \frac{k_p + 2k_f + 2\phi(k_p - k_f)}{k_p + 2k_f - \phi(k_p - k_f)} \quad (1.3)$$

$$\frac{k_{eff}}{k_f} = \frac{k_p + (n-1)k_f - (n-1)\phi - (k_p - k_f)}{k_p + (n-1)k_f + \phi(k_p - k_f)} \quad (1.4)$$

The Maxwell model is based on the notion of heat transmission by conduction through a stagnant suspension of spherical particles [6]. Both models are based on particle volume fractions and the thermal conductivity of the particle base fluid. However, the Maxwell model is only applicable to spherical particles. Because of the insertion of the shape component, n , the Hamilton Crosser model is suitable for both spherical and cylindrical particles. Several studies have improved on these traditional models by include the influence of the interfacial layer [7]. Each particle is assumed to be surrounded by an ordered layer. The presence of an ordered layer increases the volume percentage of nanoparticles. Yu and Choi [8] enhanced the Hamilton Crosser model to account for nonspherical nanoparticles. The interface is described as a confocal ellipsoid with a solid particle in this model. Model of thermal conductivity that includes particles Jang and Choi [9] initiate Brownian motion. Brownian motion, according to the authors, is a significant element in the heat transmission of nanoparticles floating in a base fluid. This is in contrast to the conventional method, which believes discrete particles remain stationary and immobile. The suggested model is based on a number of phenomena, including collision between base fluid molecules, thermal diffusion of collision between nanoparticles owing to Brownian motion, and thermal contact of dynamic nanoparticles with base fluid molecules.

Prasher et al. produced another well-known model based on Brownian motion [10]. The suggested model takes into account the influence of nanoparticle-liquid interfacial heat resistance. The authors claimed that the increased thermal conductivity of nanofluids is due to localized convection caused by the Brownian motion of nanoparticles. The suggested model combines conduction and convection models from Maxwell-Garnett (MG). Despite the fact that various models have been created, there is currently no model available to precisely forecast the thermal conductivity of nanofluids (Khanafer and Vafai [6]). As a result, Corcione [11] and Khanafer and Vafai [6] created empirical models based on experimental data from the literatures. For example, Khanafer and Vafai's model is valid and applicable to water-based Al_2O_3 and CuO -based nanofluids.

1.5.2 Theoretical Model of Nanofluids' Viscosity

Several variables impact the viscosity of nanofluids. Particle volume fraction, operating temperature, and nanofluid theology behavior are the most important aspects. A few analytical methods for predicting the viscosity behavior of nanofluids are available. It's important to note that the majority of the models are based on Einstein's groundbreaking work. His concept is based on a linearly viscous fluid with dilute spherical particles ($\delta < 2\%$). The proposed formulation is shown in Equation (1.5) [1]

$$\frac{\mu_{nf}}{\mu_f} = (1 + 2.5\phi) \quad (1.5)$$

The limitations of this formula are as follows: it examines only non-interacting particles and fluids with minimal inertia force. Since then, other researchers have developed different models to address Einstein's model's constraints. Brinkman[12] expanded Einstein's model for greater particle volume concentrations, as seen in Equation (1.6)

$$\mu_{nf} = \frac{1}{(1 - \phi)^{2.5}} \mu_f \quad (1.6)$$

Another researcher, Batchelor[13] focused on the hydrodynamic and Brownian impact of spherical particles as seen in Equation (1.7)

$$\frac{\mu_{nf}}{\mu_f} = (1 + 2.5\phi + 6.2\phi^2) \quad (1.7)$$

Lundgren[14] developed a Taylor series formulation as shown in Equation (1.8)

$$\frac{\mu_{eff}}{\mu_f} = \frac{1}{(1 - 2.5\phi)} = (1 + 2.5\phi + 6.25\phi^2 + \dots) \quad (1.8)$$

Nguyen et al. [15] presented viscosity correlation for water based copper oxide (CuO) and alumina (Al₂O₃) nanofluid as shown in Equations (1.9 - 1.11)

$$\frac{\mu_{nf}}{\mu_f} = (1.475 - 0.319\phi + 0.051\phi^2 - 0.009\phi^3) \text{ for CuO} \quad (1.9)$$

$$\frac{\mu_{nf}}{\mu_f} = (1 + 0.025\phi + 0.015\phi^2) \text{ for } 36\text{nm Al}_2\text{O}_3 \quad (1.10)$$

$$\frac{\mu_{nf}}{\mu_f} = (0.904e^{0.1483\phi}) \text{ for } 47\text{nm Al}_2\text{O}_3 \quad (1.11)$$

1.5.3 Density and Specific Heat of Nanofluids

To the best of the author's knowledge, most researchers used single formulation to determine the density of nanofluids [1]. The density formulation is shown in Equation (1.12).

$$\rho_{nf} = (1 - \phi)\rho_f + \phi\rho_p \quad (1.12)$$

Similar formulation has also been used by other researchers (Namburu et al. [16] and Kulkarni et al. [17]). From the formulation, it seems that the density of nanofluids tends to increase with the increase of particle volume fraction.

The common formulation for specific heat used by researchers is shown in Equation (1.13). Specific heat tends to reduce with particle volume fraction.

$$C_{p,nf} = \frac{(1 - \phi)\rho_f C_{p,f} + \phi\rho_p C_{p,p}}{\rho_{nf}} \quad (1.13)$$

1.6 DIMENSIONLESS PARAMETERS

The dimensionless parameters can be considered as measures of the relative importance of certain aspects of the flow. Some dimensionless parameters related to the present study are discussed below:

1.6.1 Radiation Parameter

Thermal radiation is electromagnetic radiation that is produced as a result of the thermal motion of matter particles. Thermal radiation is produced when heat created by the movement of charges (electrons and protons in common forms of matter) is transformed to electromagnetic radiation. The emission of electromagnetic waves from any substance with a temperature higher than absolute zero is known as thermal

radiation. The conversion of thermal energy into electromagnetic energy is reflected in thermal radiation [18].

$$\begin{aligned}
 \text{Radiation Parameter, } Rd &= \text{Plank Constants} \times \text{Optical Thickness} \\
 &= \text{Plank Constants} \times \text{Absorption} \times \text{Cavity Length} \\
 &= \frac{16 \times \text{Boltzmann Constant} \times \text{Temperature of the upper wall}}{\text{Thermal Conductivity of fluid}} \times \kappa L \\
 &= \frac{16\sigma T_c^3}{k} \times \kappa L
 \end{aligned}$$

1.6.2 Hartmann Number

Hartmann number is the ratio of electromagnetic force to the viscous force first introduced by Hartmann [1]. It is denoted and defined by $Ha = B_0 L \sqrt{\frac{\sigma}{\mu}}$

Where, B_0 is the magnetic field, L is the characteristic length scale, σ is the electric conductivity and μ is the viscosity. In addition, it is a dimensionless quantity characterizing flow of conducting fluid in a transvers magnetic field, being the product of the magnetic flux density, a representative length and the square root of the ratio of electric conductivity to viscosity.

1.6.3 Solid Volume Fraction

The Solid volume fraction ϕ_i is defined as the volume of a constituent V_i divided by the volume of all constituents of the mixture V prior to mixing $\phi_i = \frac{V_i}{\sum_j V_j}$

Being dimensionless, its unit is 1; it is expressed as a number. The volume fraction coincides with the volume concentration in ideal solutions where the volumes of the constituents are additive (the volume of the solution is equal to the sum of the volumes of its ingredients). The sum of all volume fractions of a mixture is equal to

$$1: \sum_i^N V_i = V; \sum_i^N \phi_i = 1$$

The volume fraction (percentage by volume, vol%) is one way of expressing the composition of a mixture with a dimensionless quantity; mass fraction (percentage by weight, wt%) and mole fraction (percentage by moles, mol%) are others. Volume percent is a common expression of a solution's concentration. It is the volume fraction expressed with a denominator of 100, and thus is defined as:

$$\text{Volume Percent} = \frac{\text{Volume of Solute}}{\text{Volume of Solution}} \times 100\%$$

Volume percent is usually used when the solution is made by mixing two fluids, such as liquids or gases. However, percentages are only additive for ideal gases. The percentage by volume (vol%) is one way of expressing the composition of a mixture with a dimensionless quantity; mass fraction (percentage by weight, wt%) and mole fraction (percentage by moles, mol%) are others [1].

1.6.4 Reynolds Number

The transition from laminar to turbulent flow depends on the surface geometry, surface roughness, flow velocity, surface temperature and type of fluid, among other things. In 1883, Osborn Reynolds discovered that the flow regime depends mainly on the ratio of the inertia forces to friction forces in the fluid. This ratio is called the Reynolds number, which is a dimensionless quantity, and is defined as

$$\begin{aligned}
Re &= \frac{\text{inertia Force}}{\text{Friction Force}} = \frac{\text{Mass} \times \text{Accelaretion}}{\text{Shering Stress} \times \text{Cross sectional Area}} \\
&= \frac{\text{Volume} \times \text{Density} \times (\text{Velocity} / \text{Time})}{\mu \times (\text{Velocity} / \text{Length}) \times \text{Cross Sectional Area}} \\
&= \frac{(\text{Length})^3 \times \text{Density} \times (\text{Length} / \text{Time})}{\mu \times (\text{Length})^2} \\
&= \frac{\text{Length} \times \text{Density} \times \text{Velocity}}{\mu} = \frac{L \times \rho \times V}{\mu} = \frac{LV}{\mu / \rho} = \frac{LV}{\nu}
\end{aligned}$$

Here V , L , ρ and μ . are characteristic values of reference velocity, characteristic length, density and coefficient of viscosity of the fluid flow, respectively and $\nu = \frac{\mu}{\rho}$ is the kinematic viscosity [1].

1.6.5 Prandtl Number

The relative thickness of the velocity and the thermal boundary layers are best described by the dimensionless parameter Prandtl number, defined as

$$Pr = \frac{\nu}{\alpha} = \frac{\text{Viscous diffusion rate}}{\text{Thermal diffusion rate}} = \frac{c_p \mu}{k}$$

Where ν is the kinematic viscosity, $\nu = \frac{\mu}{\rho}$, α is the thermal diffusivity and

$$\alpha = \frac{k}{(\rho c_p)}, \quad \mu \text{ is the dynamic viscosity, } k \text{ is the thermal conductivity, } c_p \text{ is the}$$

specific heat and ρ is the density. It is named after Ludwing Prandtl, who introduced the concept of boundary layer in 1904 and made significant contributions to boundary layer theory. The Prandtl number of fluids ranges from less than 0.01 for liquid metals to more than 100,000 for heavy oils [1].

1.6.6 Richardson Number

Richardson Number is a dimensionless number that indicates the ratio of the buoyancy term to the flow shear term. It is named after by English mathematician “Lewis Fry Richardson”. In thermal convection issues, the Richardson number

indicates the relative significance of natural and forced convection. In this context, the Richardson number is denoted and defined as

$$Ri = \frac{g\beta(T_h - T_c)L}{V^2} \quad (1.15)$$

where g stands for gravity acceleration, β for thermal expansion coefficient, T_h for hot wall temperature, T_c for reference temperature, L for characteristic length, and V for typical velocity.

Additionally, the Richardson number can be represented as a combination of the Grashof and Reynolds numbers, as follows:

$$Ri = \frac{Gr}{Re^2} \quad (1.16)$$

Natural convection is typically negligible when $Ri < 0.1$, forced convection is negligible when $Ri > 10$, and neither is negligible when $0.1 < Ri < 10$. Except in the case of very low forced flow velocities, forced convection is generally considerable in comparison to natural convection. However, buoyancy often plays a substantial role in defining the laminar–turbulent transition of a mixed convective flow. The Richardson number is helpful in the construction of water-filled thermal energy storage tanks [19].

1.7 LITERATURE REVIEW

Fluid flow and heat transfer in different types of cavities such as rectangular, square, and trapezoidal focused by buoyancy and shears have been calculated widely in the literature. Simultaneous convection of buoyancy and forced convection is called as combined or mixed convection, which is of great interest in engineering applications such as nuclear reactors, lakes and reservoirs, cooling process of electronic devices, solar applications, combustion chambers, food processing and float glass production in industry. Various researchers investigated the effects of mixed convective flows in cavities, channels by using analytical, experimental and numerical methods [20]–[23]. An experimental investigation was conducted by Ghorbani et al. [24] experimentally investigated the mixed convection heat transfer in a coil-in-shell heat

exchanger for various Reynolds numbers, various tube-to-coil diameter ratios and different dimensionless coil pitch. They showed that the equivalent diameter of shell is the best characteristic length. Bengisen and Hakan [25] examined the two-dimensional problem in a Lid-driven unit square cavity for mixed convection heat transfer with adiabatic horizontal walls and heated vertical walls. They found that convective heat transfer is smaller in case of middle centered partial magnetic field than the other cases. Xia Chen et al. [26] studied on mixed convection heat transfer of Hitec salt in one-, two-, and three-sided heating conditions in pipes. They observed that double side heating has the strongest buoyancy effect and three-sided heating is lowest and the nonuniformity of the heat transfer process in one-sided heating is the highest. Rahman et al [27] numerically investigated the MHD mixed convection in a channel with a fully or partially heated cavity by using finite element method. By using finite-element technique they found two different cases and Rayleigh numbers.

Magnetohydrodynamics is a branch of fluid dynamics which studies the movement of an electrically-conducting fluid in a magnetic field. The study of magnetohydrodynamics (MHD) concludes the electrically conducting fluids, magnetic field, liquid metals. Basically it is a physical-mathematical outline that concerns the dynamics of magnetic fields which is electrically conducting fluids by plasmas and liquid metals. Swedish physicist Hannes Alfvén (1908-1995) discovered the magnetohydrodynamics effects and its applications in different parts of plasma physics in 1942. The initial concept behind MHD is that magnetic fields can induce currents in a moving conductive fluid. Sheremet et al. [28] introduced the mathematical modelling of MHD free convection in an inclined wavy enclosure filled with a Cu–water nanofluid in the presence of an isothermal corner heater. With the help of finite difference method of second-order accuracy they solved MHD natural convection of Cu-water nanofluid within an inclined wavy cavity with a corner heater. Mansour et al. [29] studied A numerical investigation of magnetohydrodynamic mixed convection in a square lid-driven cavity filled with gyrotactic micro-organism. Rabbia et al. [30] investigated the present study is concerned with the comparison of heat transfer performance between semi-circular and triangular notches in lid-driven cavities. The purpose of this investigation is to study heater

geometry effect on pure mixed convection heat transfer. Ferrofluid has been considered as the working fluid. The flow and thermal field have been studied and discussed by streamline and isothermal contours respectively. Öztop et al.[31] studied the thermal and dynamical behavior of fluid in an enclosure with two semicircular heaters on the bottom wall for MHD natural convection. They showed that distance between two heaters affected the thermal and flow field and Hartmann number was a controlling parameter for heat transfer. Hasanuzzaman et al.[32] numerically investigated the MHD effect for natural convection in a trapezoidal cavity with different wall boundary condition. They found that heat transfer rate is increased for decreasing value of Hartmann number. Selimefendigil and Oztop [33] observed the MHD mixed convection in a flexible walled and nanofluids filled lid-driven cavity with volumetric heat generation by using CuO-nanofluid and elastic side wall. They noticed that the local and averaged heat transfer enhance as the value of solid volume fraction of the nanoparticle increases and this is more effective for higher values of Richardson number where heat transfer process is effective. Barnoon et al. [34] studied the mixed convection and entropy generation in a square cavity containing nanofluid flow and heat transfer in a cavity with rotating cylinders. They found that heat transfer increases when Hartmann number, Richardson number, and volume fraction are reduced. Rashad et al. [35] investigated magneto-hydrodynamic mixed convection in a lid-driven square cavity filled with Cu–water nanofluid by considering the partial slip effect along the horizontal lid-driven walls. They demonstrated that the shortest length of the heat source/sink located midway between the vertical walls provides the best convective heat transfer, and that the best direction of the horizontal walls is when they are both lid-driven to the left.

The investigation of radiative flux in mixed convection with nanofluids and MHD are both intriguing areas of research. The Lorentz force slows convection currents when a liquid is radiative and subjected to a magnetic field, hence an external magnetic field can be used to govern manufacturing operations. Thermal radiation has long been recognized as being relevant in space technology and high-temperature operations. In the polymer manufacturing business, protection of trustworthy resources in the building industry, thermal radiation is also vital for managing the heat transfer process [36]. In recent years, many researchers have investigated the

fluid flow behavior in a lid driven cavity and elucidated the augmentation of heat transfer. Bhuiyan et al. [37] numerically studied the thermal characteristics in a microstructure-filled porous cavity with mixed convection and they found, there is a strong relation of the aspect ratio and the width of the inlet as a fraction of the width (I/W). Entropy generation increases with the increase of the value I/W . Rahman et al. [27] performed a study in a channel with a square cavity with magnetohydrodynamic (MHD) mixed convection. They observed that for the higher values of the magnetic field the length of the heater became insignificant. But there is a relation with the inclination angle in a lid-driven triangular enclosure which was investigated by Çolak et al. [38] also worked on a lid-driven cavity with mixed convection. They used the heater orientation to control the heat transfer effectiveness, vorticity. They showed that the inclination can increase the heat transfer rate by around 324%. They also concluded that the Darcy number can increase the average Nusselt number up to 10 times. Sheikholeslami et al. [39] numerically studied the magnetic effect with introducing nanofluid in a cavity with a tilted elliptic cylinder and they observed that heat transfer rate increases with the inclination angle.

Magnetohydrodynamics has a significant role in terms of the heat transfer rate in a lid driven cavity with a channel flow [40]. Shekaramiz et al. [41] considered a wavy triangular cavity for a heat transfer enhancement study using MHD. They found that entropy increases with the magnetic field initially, and at a certain period it becomes constant. Davood Toghraie [42] investigated the influence of MHD mixed convection flow of Cu-water nanofluid in a trapezoidal cavity across a wide range of Richardson number, nanoparticle volume fraction, and Hartman number. He discovered that the average Nusselt number on the bottom wall is affected by dimensionless parameters as well as tilt angles. A magnetic field also reduces the velocity profile. Furthermore, he employed nanoparticles to increase the Nusselt number. Azad et al. [43] carried out a study on mixed convection in a channel with a cavity-heated wall and concluded that the flow velocity and heat transfer rate reduced with the rise of Hartman number. They also declared that it is a control parameter for heat transfer and fluid flow. Hussain et al. [44] investigated the impact of the inclined magnetic field in the lid-driven curvilinear cavity. They concluded that the inclination angle for the magnetic field is a control parameter for heat and

mass transfer. They also stated that there is an optimal inclination angle value. Krishna et al. [45] numerically investigated unsteady MHD convective rotating flow which passes a vertical moving porous surface. They found that with the increase of the rotation parameter the velocity increases. They also considered radiation in the study and concluded that it affects the heat transfer rate. In another study, Sheikholeslami et al. [46] put focus on the Magnetohydrodynamic ferrofluid radiation. They also found that the heat transfer rate enhances the buoyancy forces and the radiation.

Nanofluid is now widely used to enhance the heat transfer rate in almost all heat transfer-related applications [47]. In the cavity lid-driven profile, the nanofluid plays a significant role in the increase of the heat transfer rate. Krishna et al. [48] used a non-Newtonian Casson hybrid nanofluid over an exponentially accelerated vertical moving porous surface. They found that the heat absorption decreases with the decrease of the nanofluid volume fractions. Kumar et al. [47] worked on metal based nanofluid with various concentrations and they found that the CeO_2 – MWCNT/water nanofluid ensured the best performance.

The last century has seen an explosion of research and inventions utilizing remarkable applications of nanofluids in fields such as power generation, process engineering, building technology, air conditioning and refrigeration systems, solar energy, heat pipes, electrical cooling, and processing plants and many others. The number of research studies on nanofluids is increasing in response to the increased interest in and demand for nanofluids as heat transfer fluids. This is evident from the quantity of articles produced. Nanofluids are a widely used material in thermal engineering applications[49]. Due to its high thermal conductivity, which ensures better heat transfer rate, it has become trendy in research. Jain et al. [50] experimentally worked on Al_2O_3 water-based nanofluid using Rainbow Schlieren Deflectometry. They noticed that thermal boundary layer thickness decreases with the nanofluid concentration. Mei et al. [51] tried to investigate the magnetic field effect in a smooth and corrugated tube using Fe_3O_4 -water nanofluid of four different concentrations. They concluded that by increasing the nanofluid concentrations and magnetic field intensity, the heat transfer rises.

Hybrid nanofluids are also used for thermal enhancement in the heat transfer application. Siddiqui et al. [52] investigated graphene hybrid nanofluid's evaporation and boiling performance with different mixing configurations and droplet sizes. They built different models which can predict the evaporation rate with droplet size and mixing ratio in the range of 25° to 100° temperature. Modi et al. [53] performed a study on Al₂O₃ water-based nanofluid considering nucleate pool boiling. They concluded that evaporation increases the heat transfer rate and natural convection leads to heat transfer rise using nanofluid. Gholinia et al. [54] numerically studied the heat transfer effect of CNTs/(C₂H₆O₂-H₂O) hybrid nanofluid considering a magnetic field in a porous stretching cylinder. Authors concluded that Reynolds number, Magnetic parameter, and Squeeze number decrease the heat transfer rate.

Many researchers introduced magnetohydrodynamics and radiation in increasing the heat transfer rate. Hosseinzadeh et al. [55] investigated the effect of different parameters considering MHD and radiation using (CH₂OH)₂ nanofluid. And found that the nanofluid solid volume fraction and magnetic field increase the friction coefficient and lower the heat transfer rate. Srinivasulu et al. [56] numerically worked on Williamson nanofluid considering the inclined magnetic field using the RKF-45 technique. They concluded that the magnetic parameter increases the temperature profile and reduces with the rise of the Prandtl number. Toghraie [42] numerically investigated the effect of MHD in a trapezoidal cavity using Cu-water nanofluid. The author observed that the velocity profile changes with the decrease of magnetic field intensity. Dehghani et al. [57] worked on MHD flow in a grooved channel using Al₂O₃ nanofluid to see the effect of MHD. They observed that the heat transfer enhances when the fluid velocity and the Hartman number rise. El-Shorbagy et al. numerically worked on heat transfer augmentation in a trapezoidal channel in the presence of porous medium and mixed convection. They concluded that with the decrease of Richardson number, heat transfer increases. Selimefendigil et al. [58] worked on a nanofluid-filled cavity considering mixed convection and MHD. They observed that the magnetic inclination angle 60° and 90° report the highest Lorentz force. Heat transfer enhances around 29% when the 4% nanofluid concentration is used.

Mixed convection plays a vital role in heat transfer augmentation. Selimefendigil [59] worked on the mixed convection using nanofluid in a cavity flow. They observed that the Richardson number has a vital role in heat transfer. Ismael et al. [60] worked on a nanofluid-filled cavity with mixed convection, constant heat flux, and MHD. They noticed that natural convection decreases by the increase of the length of the heat source.

Additionally, dispersion of carbon nanotubes in engine oil like kerosene oil is significant due to the high viscosity of the base oil and the nanotubes filament shape. Although nanofluid stability is important, just a few investigations have been conducted on dispersion of carbon nanotubes within base oils [61].

1.8 APPLICATIONS

Thermal radiation and heat transfer with MHD mixed convection have a great interest because they are used in a wide variety of engineering and industrial manufacturing processes, including aerodynamics, wire drawing, hot rolling, extrusion of plastic and rubber sheets, glass blowing, condensation of metallic plates, fiber spinning and others. Additionally, thermal radiation is used in a variety of ways in solar energy systems. Due to its wide applications in engineering, such as geophysical thermal and insulation engineering, design of pebble-bed nuclear reactors, crude oil drilling, ceramic processing, geothermal energy conversion, use of fibrous material in building thermal insulation, catalytic reactors, and compact heat exchangers, convective flow and heat transfer with MHD has a large number of investigators. Hydromagnetic flow in microgeometry is used in microelectrochemical cell transport, microheat exchangers, and microchip cooling. Microelectromechanical systems (MEMS) and nanoelectromechanical systems (NEMS) have recently gained enormous attention due to their wide application in heating or cooling microreactor devices.

1.9 MOTIVATION

According to the analysis of the literature, relatively a few numerical studies on MHD mixed convection heat transfer in a lid-driven square cavity with radiative heat

flow have been conducted. The study of mixed convection in a cavity-filled channel is critical for a variety of engineering applications. The investigation of mixed convection effects in cavities with nanofluids in the presence of magnetic and radiation effects is critical for a variety of technical applications. According to the brief review, while there is a wealth of published work on increasing heat transfer rates using nanofluids, there are just a few research on the influence of solid volume fraction on mixed convection and thermal radiation in a lid-driven cavity in the presence of a magnetic field. As a result, this research intends to extend the work of Rahman et al. [31] by examining the influence of solid volume fraction on mixed convection with kerosene oil-based CNT nanofluid in the presence of radiative heat flux and magnetic effect. As far as the authors are aware, no further studies have been done on the influence of particle volume fraction in a cavity filled with kerosene oil-based CNT nanofluid under conditions of radiative heat flux and magnetic field.

1.10 OBJECTIVES OF THE PRESENT STUDY

According to a study of previous work, the MHD mixed convection in a lid-driven square cavity employing nanofluids and radiation has not been investigated yet. The investigation will be conducted numerically using a precise numerical approach, and the resulting data will be represented graphically using streamlines, isotherms, and associated graphs and charts.

The specific objectives of the present research work are as follows:

- To modify the mathematical model for the proposed study.
- To investigate the effects of governing parameters namely Radiation parameter, Hartmann number, Richardson number and solid volume fraction on the flow and thermal fields within the enclosure.
- To observe the velocity and temperature profile as well as overall heat transfer rate from the heat source for the aforementioned parameters.
- To compare the present result with other related published results.

The current numerical analysis is likely to aid in the hunt for more efficient and superior renewable energy technology. This model may be used to address the

difficulty of improving heat transmission in solar thermal collectors and human medical devices.

1.11 OUTLINE OF THE THESIS

There are four chapters in this dissertation. A brief introduction with goal and purpose is offered in Chapter 1. A literature review of previous work on nanofluids, MHD mixed convection, thermal radiation, and heat transfer is also included in this chapter. Different features of past research have been comprehensively described in this state-of-the-art review. Then, for the presentation of fluid flow and heat transfer effects in cavities or channels, a post-mortem of a recent historical event is presented. The numerical computing approach for the issue of viscous incompressible flow is presented in Chapter 2. In this work, the finite element approach is used and discussed in details. Using a kerosene oil-based CNT nanofluid, we examined the impact of MHD on mixed convection flow in a lid-driven square cavity with radiative heat flux.

A comprehensive parametric investigation on the influence hydrodynamic characteristics of kerosene oil-based CNT nanofluid of a lid driven cavity in the presence of magnetic effect is presented in Chapter 3. The effects of significant factors such as the Radiation parameter, Hartmann number, solid volume fraction, Reynolds number, and Richardson number, as well as their related hydrodynamic properties, are investigated. The findings are given as streamline and isotherm contours, as well as relevant plots for the thermophysical properties of the fluid.

Finally, in Chapter 4, the dissertation is completed with conclusions and comparisons. Eventually, suggestions for additional research into the current problem are provided.

CHAPTER 2

PROBLEM FORMULATION

Ordinary or partial differential equations have been studied numerically and analytically as mathematical models of physical events. Fluid mechanics and heat transfer's governing partial differential equations are solved for a finite number of flows. To obtain a numerical solution, we must employ a discretization approach that converts the differential equations to a system of algebraic equations that can be solved on a computer. Approximations are applied to small domains in space and/or time, resulting in numerical solutions that provide results at discrete locations in space and time. As with experimental data, the accuracy of numerical solutions are dependent on the quality of the discretization used.

Computational fluid dynamics (CFD) includes the construction of a set of numbers that approximates a real life system. The outcome of computation process increases system performance knowledge. Engineers need CFD algorithms that produce physically realistic results with high accuracy on finite grids. Activities in the broad field of computational fluid dynamics range from the automation of well-established engineering design methods to the use of detailed Navier-Stokes equation solutions as substitutes for experimental research into the nature of complex flows. CFD has been used to solve a variety of fluid dynamics problems. It is more commonly used in engineering fields where the geometry is complicated or there is an important feature that cannot be dealt with using standard methods.

Theoretical or experimental flow and heat transfer analysis can be performed in thermodynamics. Due to their restricted flexibility and applications, experimental investigation of such problems has not gained much favor in the field of thermodynamics. It requires different investigations necessitating a separate experimental requirement/arrangement for each changes in the geometry/limit circumstances, which in turn makes it particularly unfavorable from the time-bound and economical perspective.

The remainder of this chapter is as follows. First of all model definition are given in section 2.1. In sections 2.2 and 2.3, the proper mathematical model (both governing equations and boundary conditions) is discussed. Afterwards, in Section 2.4 and 2.5 nanofluids properties and dimensional analysis are discussed respectively. Then Calculation of Physical and hydrodynamic properties are calculated in section 2.6. Finally, details numerical analysis is explored in section 2.7.

2.1 MODEL DEFINITION

In a lid-driven square cavity filled with kerosene-based CNT nanofluid is considered for an unsteady, Newtonian, incompressible and laminar mixed convection flow in the presence of a magnetic field and radiative heat flux. Kerosene and Carbon nanotubes (CNT nanoparticles) are expected to be of homogeneous shape, size and in thermal equilibrium with no slip between the two media. It is necessary to utilize dimensional coordinates with the x -axis measuring along the bottom wall and the y -

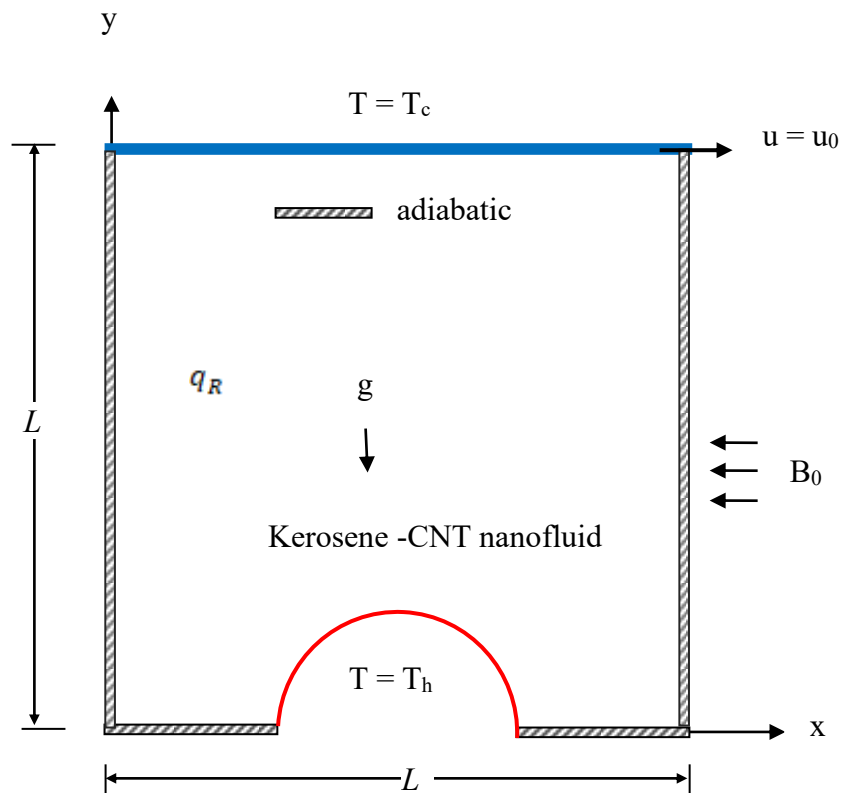


Figure 2.1: Schematic diagram for the problem with boundary conditions and coordinate system

axis being normal to it measuring along the left wall in order to make the model. Figure 2.1 depicts the model's configuration and boundary conditions. L is the length of the square cavity. The top wall moves to the right with constant velocity u_0 and isothermal temperature T_c , while the semi-circular heater is maintained at isothermal temperature T_h with a radius of $0.25L$ and $T_h > T_c$. The remaining walls of the enclosure are thermally insulated. Table 2.1 lists the nanofluid's thermophysical properties as reported on [62]. Additionally, the fluid's Joule heating impact and the effect of viscous dissipation are minimal. The cavity's four walls are believed to be stiff and impermeable. The acceleration due to gravity is in the negative y direction. The fluid is thought to be under the Boussinesq approximation.

Table 2.1: Thermophysical properties of fluid and nanoparticle [62].

Properties	Fluid (Kerosene)	Solid (CNT)
P [kg/m ³]	783.0	1600
C_p [J/kg.K]	2090	796.0
K [W/m.K]	0.145	3000
$\beta \times 10^{-5}$ [K ⁻¹]	99	44

2.2 GOVERNING EQUATIONS

Based on the above assumptions the followings are the governing equations in dimensional cartesian coordinates form:

Continuity Equation

$$\frac{\partial u}{\partial x} + \frac{\partial v}{\partial y} = 0 \quad (2.1)$$

Momentum Equations

$$\frac{\partial u}{\partial t} + u \frac{\partial u}{\partial x} + v \frac{\partial u}{\partial y} = -\frac{1}{\rho_{nf}} \frac{\partial p}{\partial x} + \frac{\mu_{nf}}{\rho_{nf}} \left(\frac{\partial^2 u}{\partial x^2} + \frac{\partial^2 u}{\partial y^2} \right) \quad (2.2)$$

$$\frac{\partial v}{\partial t} + u \frac{\partial v}{\partial x} + v \frac{\partial v}{\partial y} = -\frac{1}{\rho_{nf}} \frac{\partial p}{\partial y} + \frac{\mu_{nf}}{\rho_{nf}} \left(\frac{\partial^2 v}{\partial x^2} + \frac{\partial^2 v}{\partial y^2} \right) + \frac{\sigma_{nf} B_0^2}{\rho_{nf}} v + \frac{(\rho\beta)_{nf}}{\rho_{nf}} g(T - T_c) \quad (2.3)$$

Energy Equations

$$\frac{\partial T}{\partial t} + u \frac{\partial T}{\partial x} + v \frac{\partial T}{\partial y} = \alpha_{nf} \left(\frac{\partial^2 T}{\partial x^2} + \frac{\partial^2 T}{\partial y^2} \right) - \frac{1}{(\rho c_p)_{nf}} \frac{\partial q_R}{\partial y} \quad (2.4)$$

The variables and their associated values are indicated in the nomenclature.

2.3 INITIAL AND BOUNDARY CONDITIONS(DIMENSIONAL FORM)

The boundary conditions for the present problem are specified as follows

$$\left. \begin{aligned}
 &\text{For } t = 0 : u = v = 0, T = 0, p = 0 \\
 &\text{For } t > 0 : u = v = 0, T = T_h \text{ when } y = 0; 0.25L \leq x \leq 0.75L \\
 &\quad u = u_0, v = 0, T = T_c \text{ when } y = L; 0 \leq x \leq L \\
 &\quad u = v = 0, \frac{\partial T}{\partial N} = 0 \text{ when } x = 0, L; 0 \leq y \leq L \\
 &\quad u = v = 0, \frac{\partial T}{\partial N} = 0 \text{ when } y = 0; 0 \leq x \leq 0.25L, 0.75L \leq x \leq L
 \end{aligned} \right\} \quad (2.5)$$

where N denotes the surface normal along x or y.

2.4 NANOFUIDS PROPERTIES

The following formulas are used to calculate the effective density ρ_{nf} , specific heat $(c_p)_{nf}$, thermal expansion coefficient β_{nf} , viscosity μ_{nf} , and thermal diffusivity α_{nf} of nanofluids those occur in equations (2.1)–(2.4) [63]:

$$\rho_{nf} = (1 - \phi)\rho_f + \phi\rho_s \quad (2.6)$$

$$(\rho c_p)_{nf} = (1 - \phi)(\rho c_p)_f + \phi(\rho c_p)_s \quad (2.7)$$

$$(\rho\beta)_{nf} = (1 - \phi)(\rho\beta)_f + \phi(\rho\beta)_s \quad (2.8)$$

$$\mu_{static} = \frac{\mu_f}{(1 - \phi)^{2.5}} \quad (2.9)$$

$$\alpha_{nf} = \frac{k_{nf}}{(\rho c_p)_{nf}} \quad (2.10)$$

The effective thermal conductivity of nanofluids k_{nf} for solid–liquid mixtures of low solid concentrations is presented in the Maxwell model as bellow:

$$k_{static} = \frac{k_s + 2k_f - 2\phi(k_f - k_s)}{k_s + 2k_f\phi(k_f - k_s)} k_f \quad (2.11)$$

The aforementioned Maxwell model (equation 2.11) does not consider the particles Brownian motion. However, it has been demonstrated experimentally that the Brownian motion of nanoparticles has a significant impact on the heat transport performance of nanofluids [64]. Kalbani et al. [64] presented a model for calculating

nanofluid thermal conductivity that includes both a static and a Brownian motion. Both particle size and particle volume fraction influence temperature dependency, as do the types of particle and base fluid combinations. In this investigation authors considered that model and is given bellow:

$$k_{nf} = k_{static} + k_{Brownian} \quad (2.12)$$

in which k_{static} represents thermal conductivity defined in the Maxwell model presented in equation (2.11). However, Brownian k , the thermal conductivity component amplified by dispersed nanoparticles' erratic motion, might be advocated as bellow:

$$k_{Brownian} = \frac{\phi \rho_p c_{p,p}}{2} \sqrt{\frac{2K_B T_{ref}}{3\pi d \mu_{static}}} \quad (2.13)$$

A significant contribution of this work is the combined influence of the Maxwell model and Brownian motion are considered for thermal conductivity and dynamic viscosity of the nanofluid and is given bellow:

$$k_{nf} = \frac{k_s + 2k_f - 2\phi(k_f - k_s)}{k_s + 2k_f\phi(k_f - k_s)} k_f + \frac{\phi \rho_p c_{p,p}}{2} \sqrt{\frac{2K_B T_{ref}}{3\pi d \mu_{nf}}} \quad (2.14)$$

Further investigation of laminar Al₂O₃-water based nanofluid in an L-shape enclosure was carried out by Sheikholeslami et al. [65], who estimated the effective viscosity of the nanofluid. In this study, the authors used the effective viscosity of the nanofluid rather than the Brinkman model (Equation 2.9), as shown below:

$$\mu_{eff} = \mu_{static} + \mu_{Brownian} = \frac{\mu_f}{(1-\phi)^{2.5}} + \frac{k_{Brownian}}{k_f} \times \frac{\mu_f}{Pr_f} \quad (2.15)$$

2.5 DIMENSIONAL ANALYSIS

The following dimensionless variables are introduced to make the governing equations and corresponding boundary conditions (2.1)– (2.5) in nondimensional form in order to simplify them:

$$\left. \begin{aligned} X = \frac{x}{L}, Y = \frac{y}{L}, U = \frac{u}{u_0}, V = \frac{v}{u_0}, P = \frac{p}{\rho_{nf} u_0^2}, \theta = \frac{T - T_c}{T_h - T_c} \end{aligned} \right\} \quad (2.16)$$

2.5.1 Approximation of $\frac{\partial q_R}{\partial y}$

According to Shohel and Roydon [66] a simplified mathematical approach for approximating the $\frac{\partial q_R}{\partial y}$ term is as follows:

$$\frac{\partial q_R}{\partial y} = 4\kappa E_b - \kappa \int_{\Omega} Id\Omega \quad (2.17)$$

the monochromatic absorption coefficient, solid angle, and blackbody emissive power are represented by κ , Ω , and E_b , respectively. A boundary's effect is represented by the second component on the right side in Equation (2.17) and can be expressed by

$$\int_{\Omega} Id\Omega \approx 2\pi(I_{t \rightarrow t} + I_{l \rightarrow t}) \quad (2.18)$$

where $I_{0,t}$, $I_{0,l}$, ε_t , ε_l , ρ_t and ρ_l , denote the intensity of radiation, emissivity, and reflectivity for the top and bottom walls, respectively. It is assumed that $I_{t \rightarrow t}$ and $I_{l \rightarrow t}$ remain constant across the fluid thickness between the cold and hot walls (Fig. 1). As a result, $I_{t \rightarrow t}$ and $I_{l \rightarrow t}$ became synonymous. Each of the streams can be approximated as a combination of emission εI_0 and reflection ρI by using the formulas:

$$\left. \begin{aligned} I_{t \rightarrow t} &= \varepsilon_t I_{0t} + \rho_t I_{l \rightarrow t} \\ I_{l \rightarrow t} &= \varepsilon_l I_{0l} + \rho_l I_{t \rightarrow t} \end{aligned} \right\} \quad (2.19)$$

Solving the equation [18] for $I_{t \rightarrow t}$ and $I_{l \rightarrow t}$ yield

$$\left. \begin{aligned} I_{t \rightarrow t} &= \frac{\varepsilon_t I_{0t} + \rho_t \varepsilon_l I_{0l}}{1 - \rho_t \rho_l} \\ I_{l \rightarrow t} &= \frac{\varepsilon_l I_{0l} + \rho_l \varepsilon_t I_{0t}}{1 - \rho_t \rho_l} \end{aligned} \right\} \quad (2.20)$$

Plugin the above value of $\left(\frac{1}{\varepsilon_l} - \frac{1}{2}\right)E_{bl} + \left(\frac{1}{\varepsilon_t} - \frac{1}{2}\right)E_{bt}$ in Equation.(18) and

considering the relations $\rho + \varepsilon = 1$ (transmissivity ≈ 0) and $\pi I = E_b$ which gives the following:

$$\int_{\Omega} Id\Omega \approx 4 \frac{\left(\frac{1}{\varepsilon_t} - \frac{1}{2}\right) E_{bt} + \left(\frac{1}{\varepsilon_t} - \frac{1}{2}\right) E_{bl}}{\left(\frac{1}{\varepsilon_t} - \frac{1}{2}\right) + \left(\frac{1}{\varepsilon_t} - \frac{1}{2}\right)} \quad (2.21)$$

Considering that emissivity of the top and lower walls is identical ($\varepsilon_t = \varepsilon_l$) and from Eqs. (2.17) and (2.21) we get

$$\frac{\partial q_R}{\partial y} = 4\kappa \left[E_b - \frac{1}{2}(E_{bt} + E_{bl}) \right] \quad (2.22)$$

The mean emissive power E_{b0} can be substituted for $\frac{E_{bt} + E_{bl}}{2}$ in the following expression. E_b and E_{b0} can also be written as $\sigma_e T^4$ and $\sigma_e T_c^4$ respectively, where σ_e is the Stefan–Boltzmann constant. By the Taylor series expansion of T at $T = T_0$ yields

$$\left. \begin{aligned} f(T) = T^4 &= \sum_{n=0}^{\infty} \frac{(T - T_c)^n}{n!} \left[\frac{d^n}{dT^n} f(T) \right]_{T=T_c} \\ &= T_c^4 + 4(T - T_c)T_c^3 + \frac{12(T - T_c)^2}{2} T_c^2 + \frac{24(T - T_c)^3}{6} T_c + \frac{24(T - T_c)^4}{24} \end{aligned} \right\} \quad (2.23)$$

Neglecting after the second term of Equation (2.23) and applying the hypothesis of E_b and E_{b0} Eqs. [22] and [23] yields

$$\frac{\partial q_R}{\partial y} \approx 16\kappa\sigma_e T_c^3 (T - T_c) \quad (2.24)$$

2.5.2 Non Dimensional Governing Equations with Boundary Conditions

Using the relations from Equations. (2.16) and (2.24) in Eqs. (2.1) – (2.4) and (2.5), the dimensionless governing equations are as follows:

$$\frac{\partial U}{\partial X} + \frac{\partial V}{\partial Y} = 0 \quad (2.25)$$

$$\frac{\partial U}{\partial \tau} + U \frac{\partial U}{\partial X} + V \frac{\partial U}{\partial Y} = -\frac{\partial p}{\partial x} + \frac{\mu_{nf}}{\rho_{nf}} \frac{1}{\text{Re}} \left(\frac{\partial^2 U}{\partial X^2} + \frac{\partial^2 U}{\partial Y^2} \right) \quad (2.26)$$

$$\left. \begin{aligned} \frac{\partial V}{\partial \tau} + U \frac{\partial V}{\partial X} + V \frac{\partial V}{\partial Y} &= -\frac{\partial p}{\partial Y} + \frac{\mu_{nf}}{\rho_{nf}} \frac{\rho_f}{\mu_f} \frac{1}{\text{Re}} \left(\frac{\partial^2 V}{\partial X^2} + \frac{\partial^2 V}{\partial Y^2} \right) + \\ \frac{(\rho\beta)_{nf}}{\rho_{nf}\beta_f} Ri\theta - \frac{\mu_{nf}}{\rho_{nf}} \frac{\rho_f}{\mu_f} \frac{Ha^2 V}{\text{Re}} \end{aligned} \right\} \quad (2.27)$$

$$\frac{\partial \theta}{\partial \tau} + U \frac{\partial \theta}{\partial X} + V \frac{\partial \theta}{\partial Y} = \frac{1}{\text{Re Pr}} \left(\frac{\partial^2 \theta}{\partial X^2} + \frac{\partial^2 \theta}{\partial Y^2} \right) - \frac{Rd \cdot L \theta}{\text{Re Pr}} \quad (2.28)$$

The nondimensional parameters are used in Equations (2.26) – (2.28) as follows:

$$\text{Reynolds number } \text{Re} = \frac{u_0 L}{\nu_{nf}}, \text{ Prandtl number } \text{Pr} = \frac{\nu_{nf}}{\alpha_{nf}}, \text{ Optical thickness } \eta = \kappa L,$$

$$\text{Radiation parameter } Rd = pl \times \eta = \frac{16 \sigma_e T_c^3 \kappa L}{k}, \text{ Hartmann number } Ha = \frac{LB_0 \sqrt{\sigma_{nf}}}{\sqrt{\mu_{nf}}},$$

$$\text{Richardson number } Ri = \frac{Ra}{\text{Re}^2 \text{Pr}}.$$

And its pertinent boundary conditions presented below:

$$\text{For } \tau = 0 : U = V = 0; \theta = 0; P = 0$$

$$\text{For } \tau > 0 : U = V = 0; \theta = 1 \text{ when } Y = 0; \frac{1}{4} \leq X \leq \frac{3}{4}$$

$$U = 1; V = 0; T = 0 \text{ when } Y = 1; 0 \leq X \leq 1$$

$$U = V = 0; \frac{\partial \theta}{\partial N} = 0 \text{ when } X = 0, 1; 0 \leq Y \leq 1$$

$$U = V = 0; \frac{\partial \theta}{\partial N} = 0 \text{ when } Y = 0; 0 \leq X \leq \frac{1}{4}, \frac{3}{4} \leq X \leq 1$$

(2.29)

2.6 CALCULATION OF PHYSICAL AND HYDRODYNAMIC PROPERTIES

Averaged Nusselt number are calculated over the entire semicircular heater and defined as follows:

$$Nu_{av} = - \left(\frac{k_{nf}}{kf} \right) \frac{4L}{\pi} \int_{1/4}^{3/4} \frac{\partial \theta}{\partial Y} dX \quad (2.30)$$

Drag force of the moving lid calculated as follows

$$F_D = \int_0^1 \left. \frac{\partial U}{\partial Y} \right|_{Y=1} dX \quad (2.31)$$

Bulk temperature of the fluid domain is as follows

$$\theta_b = \iint_A \frac{\theta}{\rho_{nf}} dA \quad (2.32)$$

Pressure gradient magnitude is given below:

$$\text{Grad } P = \iint_A \sqrt{P_x^2 + P_y^2} dA \quad (2.33)$$

Average temperature of the fluid domain is defined below

$$\theta_{av} = \iint_A \frac{\theta}{A} dA \quad (2.34)$$

Temperature gradient magnitude of the fluid is as follows:

$$\text{Grad } \theta = \iint_A \sqrt{\theta_x^2 + \theta_y^2} dA \quad (2.35)$$

Magnitude of Velocity field calculated as below:

$$\text{Velocity field} = \sqrt{U^2 + V^2} \quad (2.36)$$

2.7 NUMERICAL ANALYSIS

The governing nondimensional equations (2.25) – (2.28) associated with initial and boundary conditions (2.29) are numerically solved using the Galerkin weighted residual finite element technique.

2.7.1 Finite Element Formulation and Computational Procedure

To derive the finite element equations, the method of weighted residuals as described by Zienkiewicz and Taylor [67] is applied to the Equations (2.25) – (2.29) as

$$\int_A N_\alpha \left(\frac{\partial U}{\partial X} + \frac{\partial V}{\partial Y} \right) dA = 0 \quad (2.37)$$

$$\int_A N_\alpha \left(\frac{\partial U}{\partial \tau} + U \frac{\partial U}{\partial X} + \frac{\partial V}{\partial Y} \right) dA = - \int_A H_\lambda \left(\frac{\partial P}{\partial X} \right) dA + \frac{\mu_{nf}}{\rho_{nf} \nu_f} \frac{1}{\text{Re}} \int_A N_\alpha \left(\frac{\partial^2 U}{\partial X^2} + \frac{\partial^2 U}{\partial Y^2} \right) dA \quad (2.38)$$

$$\left. \begin{aligned} \int_A N_\alpha \left(\frac{\partial V}{\partial \tau} + U \frac{\partial V}{\partial X} + V \frac{\partial V}{\partial Y} \right) dA &= - \int_A H_\lambda \left(\frac{\partial P}{\partial Y} \right) dA \\ &+ \frac{\mu_{nf}}{\rho_{nf} \nu_f} \frac{1}{\text{Re}} \int_A N_\alpha \left(\frac{\partial^2 V}{\partial X^2} + \frac{\partial^2 V}{\partial Y^2} \right) dA \\ &+ \frac{(\rho\beta)_{nf}}{\rho_{nf} \beta_f} \text{Ri} \int_A N_\alpha \theta dA - \frac{\rho_f \sigma_{nf}}{\rho_{nf} \sigma_f} \frac{Ha^2}{\text{Re}} \int_A N_\alpha V dA \end{aligned} \right\} \quad (2.39)$$

$$\left. \int_A N_\alpha \left(\frac{\partial \theta}{\partial \tau} + U \frac{\partial \theta}{\partial X} + V \frac{\partial \theta}{\partial Y} \right) dA = \frac{\alpha_{nf}}{\alpha_f} \frac{1}{Re Pr} \int_A N_\alpha \left(\frac{\partial^2 \theta}{\partial X^2} + \frac{\partial^2 \theta}{\partial Y^2} \right) dA \right\} \quad (2.40)$$

$$+ \frac{\alpha_{nf}}{\alpha_f} \frac{R_d L}{Re Pr} \int_A N_\alpha \theta dA$$

Then apply Gauss's theorem into Equations (2.38) – (2.40) to generate the boundary integral terms associated with the surface tractions and heat flux. After that the Eqns. (2.38) – (2.40) become

$$\left. \int_A N_\alpha \left(\frac{\partial U}{\partial \tau} + U \frac{\partial U}{\partial X} + V \frac{\partial U}{\partial Y} \right) dA + \int_A H_\lambda \left(\frac{\partial P}{\partial X} \right) dA + \right\} \quad (2.41)$$

$$\frac{\mu_{nf}}{\rho_{nf} \nu_f} \frac{1}{Re} \int_A \left(\frac{\partial N_\alpha}{\partial X} \frac{\partial U}{\partial X} + \frac{\partial N_\alpha}{\partial Y} \frac{\partial U}{\partial Y} \right) dA = \int_{S_0} N_\alpha S_x dS_0$$

$$\left. \int_A N_\alpha \left(\frac{\partial V}{\partial \tau} + U \frac{\partial V}{\partial X} + V \frac{\partial V}{\partial Y} \right) dA + \int_A H_\lambda \left(\frac{\partial P}{\partial Y} \right) dA + \right\} \quad (2.42)$$

$$\frac{\mu_{nf}}{\rho_{nf} \nu_f} \frac{1}{Re} \int_A \left(\frac{\partial N_\alpha}{\partial X} \frac{\partial V}{\partial X} + \frac{\partial N_\alpha}{\partial Y} \frac{\partial V}{\partial Y} \right) dA - \frac{(\rho \beta)_{nf}}{\rho_{nf} \beta_f} Ri \int_A N_\alpha \theta dA +$$

$$\frac{\rho_f \sigma_{nf}}{\rho_{nf} \sigma_f} \frac{Ha^2}{Re} \int_A N_\alpha V dA = \int_{S_0} N_\alpha S_y dS_0$$

$$\left. \int_A N_\alpha \left(\frac{\partial \theta}{\partial \tau} + U \frac{\partial \theta}{\partial X} + V \frac{\partial \theta}{\partial Y} \right) dA + \frac{\alpha_{nf}}{\alpha_f} \frac{1}{Re Pr} \int_A \left(\frac{\partial N_\alpha}{\partial X} \frac{\partial \theta}{\partial X} + \frac{\partial N_\alpha}{\partial Y} \frac{\partial \theta}{\partial Y} \right) dA + \right\} \quad (2.43)$$

$$\frac{\alpha_{nf}}{\alpha_f} \frac{R_d L}{Re Pr} \int_A N_\alpha \theta dA = \int_{S_w} N_\alpha q_{1w} dS_w$$

Surface tractions (S_x, S_y) along outflow boundary S_0 are specified in Equations. (2.41-2.42), and velocity components and fluid temperature or heat flux (q_w) that flow into or out of domain via wall boundary S_w are specified in Equations.(2.43).

This analysis is concerned with U , V , θ and P . To get the mentioned unknowns six node triangular element is considered for FE equations. Pressure is taken only at the vertex node whereas velocity components and temperature are considered at every node of the element. Consequently, pressure is associated with lower order polynomial which satisfies the continuity equation. Higher order derivative of the differential Equations.(2.25 – 2.28), the velocity component and temperature distributions, as well as linear interpolation for the pressure distribution are given bellow: $U(X, Y, \tau) = N_\beta U_\beta$ (2.44)

$$V(X, Y, \tau) = N_\beta V_\beta \quad (2.45)$$

$$\theta(X, Y, \tau) = N_\beta \theta_\beta \quad (2.46)$$

$$P(X, Y, \tau) = H_\lambda P_\lambda \quad (2.47)$$

where $\beta = 1, 2, \dots, 6$; $\lambda = 1, 2, 3$.

Substituting the element velocity component distributions, the temperature distribution, and the pressure distribution from Eqns. (2.44)-(2.47) into Eqns (2.37) and Eqns. (2.41) – (2.43) we get the following finite element Eqns.:

$$K_{\alpha\beta^x} U_\beta + K_{\alpha\beta^y} V_\beta = 0 \quad (2.48)$$

$$K_{\alpha\beta\gamma^x} U_\beta U_\gamma + K_{\alpha\beta\gamma^y} V_\beta V_\gamma + M_{\lambda\mu^x} P_\mu + \left(\frac{\mu_{nf}}{\rho_{nf} \nu_f} \frac{1}{Re} \right) (S_{\alpha\beta^{xx}} + S_{\alpha\beta^{yy}}) U_\beta = Q_{\alpha^u} \quad (2.49)$$

$$\left. \begin{aligned} & K_{\alpha\beta\gamma^x} U_\beta V_\gamma + K_{\alpha\beta\gamma^y} V_\beta V_\gamma + M_{\alpha\mu^y} P_\mu + \left(\frac{\mu_{nf}}{\rho_{nf} \nu_f} \frac{1}{Re} \right) (S_{\alpha\beta^{xx}} + S_{\alpha\beta^{yy}}) V_\beta \\ & - \frac{(\rho\beta)_{nf}}{\rho_{nf} \beta_f} Ri K_{\alpha\beta} \theta_\beta + \frac{\rho_f \sigma_{nf}}{\rho_{nf} \sigma_f} \frac{Ha^2}{Re} K_{\alpha\beta} V_\beta = Q_{\alpha^v} \end{aligned} \right\} \quad (2.50)$$

$$\left. \begin{aligned} & K_{\alpha\beta\gamma^x} U_\beta \theta_\gamma + K_{\alpha\beta\gamma^y} V_\beta \theta_\gamma + \frac{\alpha_{nf}}{\alpha_f} \frac{1}{Re Pr} (S_{\alpha\beta^{xx}} + S_{\alpha\beta^{yy}}) \theta_\beta \\ & + \frac{\alpha_{nf}}{\alpha_f} \frac{R_d L}{Re Pr} \int N_\alpha \theta dA = Q_{\alpha^\theta} \end{aligned} \right\} \quad (2.51)$$

where the coefficients in element matrices are in the form of the integrals over the element area and along the element edges S_0 and S_w as

$$\left. \begin{aligned} & K_{\alpha\beta^x} = \int_A N_\alpha N_{\beta,x} dA; K_{\alpha\beta^y} = \int_A N_\alpha N_{\beta,y} dA; K_{\alpha\beta\gamma^x} = \int_A N_\alpha N_\beta N_{\gamma,x} dA; \\ & K_{\alpha\beta\gamma^y} = \int_A N_\alpha N_\beta N_{\gamma,y} dA; K_{\alpha\beta} = \int_A N_\alpha N_\beta dA; S_{\alpha\beta^{xx}} = \int_A N_{\alpha,x} N_{\beta,x} dA; \\ & S_{\alpha\beta^{yy}} = \int_A N_{\alpha,y} N_{\beta,y} dA; M_{\lambda\mu^x} = \int_A H_\lambda H_{\mu,x} dA; M_{\alpha\mu^y} = \int_A H_\alpha H_{\mu,y} dA; \\ & Q_{\alpha^u} = \int_{S_0} N_\alpha S_x dS_0; Q_{\alpha^v} = \int_{S_0} N_\alpha S_y dS_0; Q_{\alpha^\theta} = \int_{S_w} N_\alpha q_w dS_w; \end{aligned} \right\} \quad (2.52)$$

These element matrices have been analyzed in closed-form and are ready to be numerically simulated. For the sake of brevity, the derivation for these element

matrices has omitted and detailed calculations are available in the thesis written by A. K. Azad [1]. Nonlinearity exists in the resulting finite element Eqns (2.48 – (2.51). Boundary conditions are imposed on the nonlinear algebraic equations thus obtained. This results in a series of algebraic equations with the incremental unknowns.

$$\begin{bmatrix} K_{uu} & K_{uv} & K_{u\theta} & K_{up} \\ K_{vu} & K_{vv} & K_{v\theta} & K_{vp} \\ K_{\theta u} & K_{\theta v} & K_{\theta\theta} & 0 \\ K_{pu} & K_{pv} & 0 & 0 \end{bmatrix} \begin{bmatrix} \Delta u \\ \Delta v \\ \Delta \theta \\ \Delta p \end{bmatrix} = \begin{bmatrix} F_{\alpha^u} \\ F_{\alpha^v} \\ F_{\alpha^\theta} \\ F_{\alpha^p} \end{bmatrix} \quad (2.53)$$

here

$$\left. \begin{aligned} K_{uu} &= K_{\alpha\beta\gamma^x} U_\beta + K_{\alpha\beta\gamma^x} U_\gamma + K_{\alpha\beta\gamma^y} V_\beta + \left(\frac{\mu_{nf}}{\rho_{nf} \nu_f} \frac{1}{Re} \right) (S_{\alpha\beta^{xx}} + S_{\alpha\beta^{yy}}); \\ K_{uv} &= K_{\alpha\beta\gamma^y} U_\gamma; K_{u\theta} = 0; K_{up} = M_{\alpha\mu^x}; K_{vu} = K_{\alpha\beta\gamma^x} V_\gamma; K_{vp} = M_{\alpha\mu^y}; \\ K_{vv} &= K_{\alpha\beta\gamma^x} U_\beta + K_{\alpha\beta\gamma^y} V_\gamma + K_{\alpha\beta\gamma^y} V_\gamma + \left(\frac{\mu_{nf}}{\rho_{nf} \nu_f} \frac{1}{Re} \right) (S_{\alpha\beta^{xx}} + S_{\alpha\beta^{yy}}); \\ K_{v\theta} &= -\frac{(\rho\beta)_{nf}}{\rho_{nf} \beta_f} \frac{Ra}{Re^2 Pr} K_{\alpha\beta}; K_{\theta u} = K_{\alpha\beta\gamma^x} \theta_\gamma; K_{\theta v} = K_{\alpha\beta\gamma^y} \theta_\gamma; \\ K_{\theta\theta} &= K_{\alpha\beta\gamma^x} U_\beta + K_{\alpha\beta\gamma^y} V_\beta + \frac{\alpha_{nf}}{\alpha_f} \frac{1}{Re Pr} (S_{\alpha\beta^{xx}} + S_{\alpha\beta^{yy}}); \\ K_{pu} &= M_{\alpha\mu^x}; K_{pv} = M_{\alpha\mu^y}; \text{ and } K_{\theta p} = K_{p\theta} = K_{pp} = 0 \end{aligned} \right\} \quad (2.54)$$

The Newton-Raphson iteration approach is used to solve a set of global nonlinear algebraic equations in MATLAB. The convergence requirement is considered for every variable which is less than δ so as to $|\Psi^{m+1} - \Psi^m| < \delta = 10^{-5}$, here m is the number of iteration and $\Psi = \Psi(U, V, \theta)$

There are various advantages of using FEM when compared to other numerical approaches. FEM is used to determine the equations for each element before it is built, which is one of them. As a result, adding new parts through refining of existing ones is not a huge issue. The method's use of a set of finite elements to create

computational domains with irregular geometries makes it a useful tool for solving boundary value issues in a variety of engineering applications.

2.7.2 Grid Size Sensitivity Test

To ensure the accuracy of the numerical results of this study, a grid independence analysis was carried out for the representative values of $Ri = 1$, $Ha = 10$, $Re = 100$, $Pr = 23.004$, $Rd = 1$, $\tau = 0.1$ and $\phi = 0.05$. In this study, a non-uniform six node triangular element grid scheme was used. The extreme value of Nu_{av} and average fluid temperature θ_{av} was employed as a sensitivity measure of the solution's correctness, and both numerical value accuracy and computing time were chosen as the monitoring variable represented in Table 2.2 and Figure 2.3 The magnitude of the average Nusselt number and average fluid temperature for the 12742 elements is found to be fairly similar to the values obtained for the other higher elements. Consequently, 12742 triangular elements were taken for this study. Figure 2.2 illustrates the mesh structure of considered physical domain's using triangular finite elements.

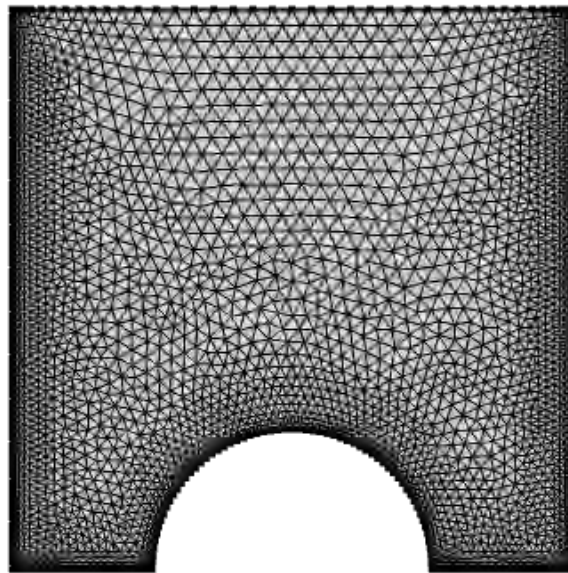
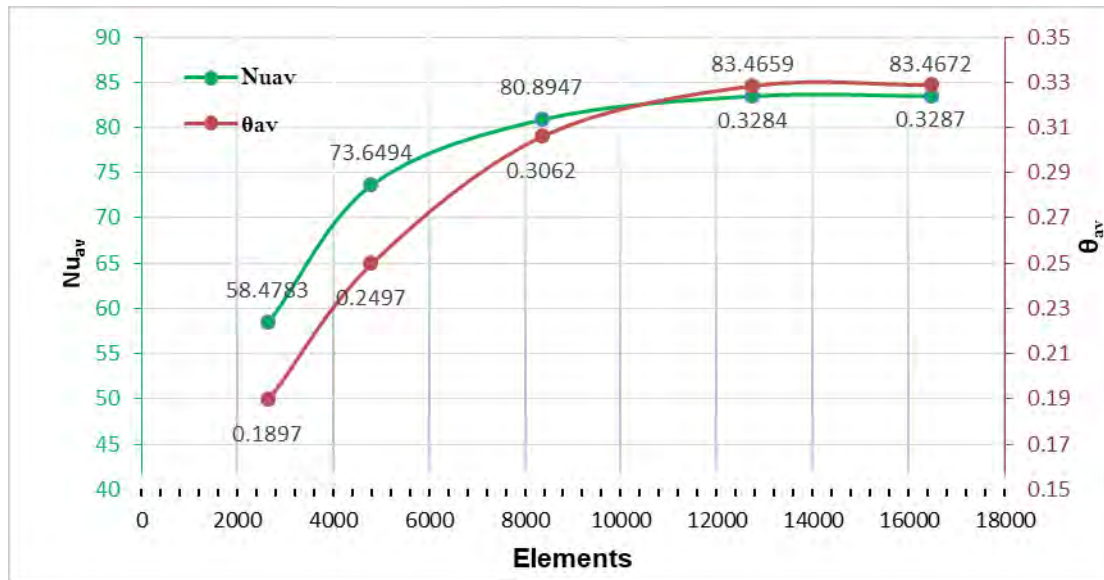


Figure 2.2: Mesh generation of the enclosure

Table 2.2: Grid test for $Ri = 1$, $Ha = 10$, $Re = 100$, $Pr = 23.004$, $Rd = 1$, $\tau = 0.1$ and $\phi = 0.05$

Elements	2638	4784	8356	12742	16467
Nu_{av}	58.4783	76.6494	80.8947	83.4659	83.4672
θ_{av}	0.1897	0.2497	0.3062	0.3284	0.3287
Time(m)	2.4	2.8	3.1	3.4	6.9

**Figure 2.3:** Grid test for the representative values of $Ri = 1$, $Ha = 10$, $Re = 100$, $Pr = 23.004$, $Rd = 1$, $\tau = 0.1$ and $\phi = 0.05$

2.7.3 Code Validation

The accuracy of this study is checked with the available literature using the current code for average heat transfer rate from the heated surface. First, as stated in Malleswaran et al. [68], MHD mixed convection in a lid driven square cavity with a heater in the left wall and fielded with electrically conducting fluid with low Prandtl number (0.054) for $Re = 100$, $Ha = 25$ heater length $L_H = 1/3$ m and center of the heater from bottom $\varepsilon_2 = 1/2$ m and illustrated in Figure 2.4 (a). It is then validated again with the numerical results of Sheikholeslami et al. [69] for MHD free convection of thermal radiation on Al_2O_3 -water nanofluid flow in a square cavity with a heat source having length $L/3$ and centrally positioned on the bottom surface for $Ra = 10^5$, viscous dissipation parameter $\varepsilon = 0$ and radiation parameter $Rd = 1$ as shown in Figure 2.4 (b). These illustrations show that the current results and past investigations are in excellent accord .

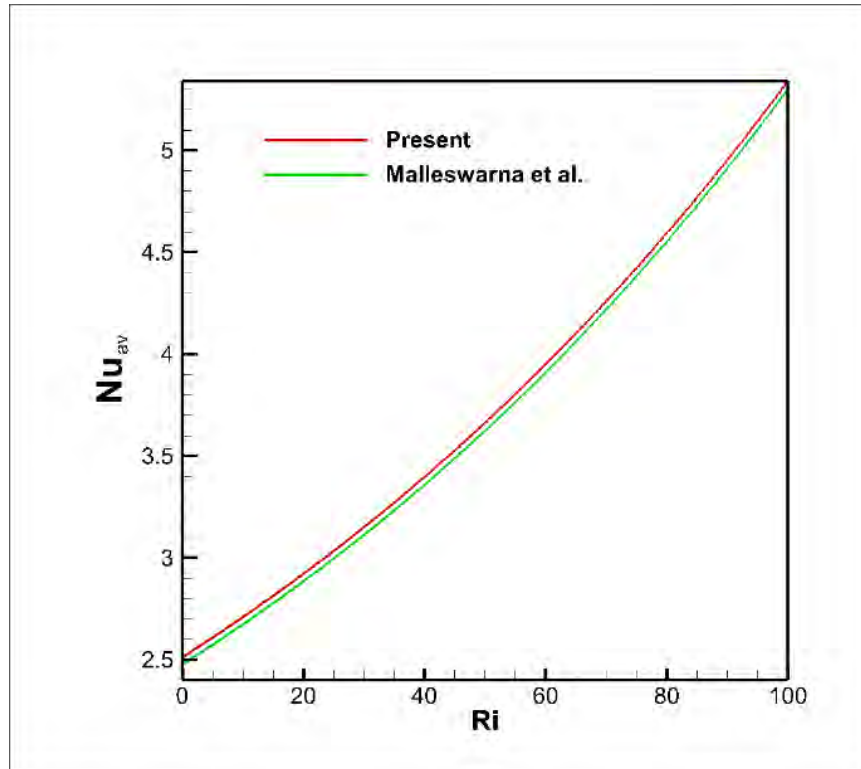


Figure 2.4(a): Comparison of the average Nusselt number on Ri between the present results and Malleswarana et al. [68] for $Ha = 25$, $Re = 100$, $Pr = 0.054$, $L_H = 1/3m$ and $\varepsilon_2 = 1/2m$.

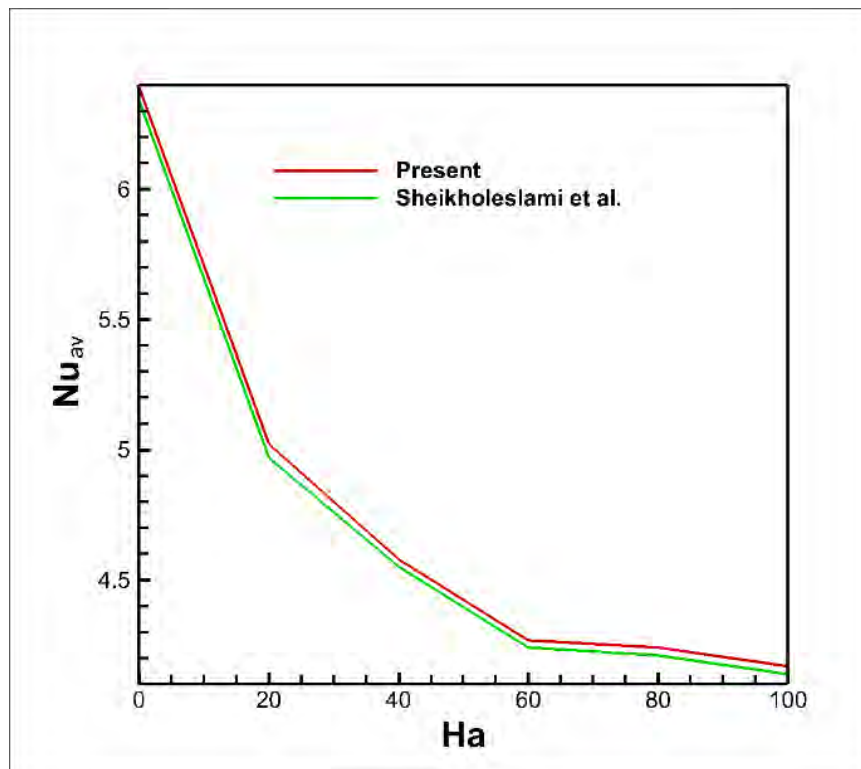


Figure 2.4(b): Comparison of the average Nusselt number on Ha between the present results and Sheikholeslami et al. [69] for $Ra = 10^5$, $Pr = 6.2(\text{Al}_2\text{O}_3\text{-water})$, $Rd = 1$ and $\varepsilon = 0$.

CHAPTER 3

RESULTS AND DISCUSSION

The present study analyzed the effect hydrodynamic properties of kerosene oil-based *CNT* nanofluid of a lid driven cavity in presence of magnetic effect. The numerical results are provided in order to determine the impact of the factors that have been taken into consideration. The system's dimensionless parameters, such as the Radiation Parameter (Rd), the Hartmann number (Ha), the solid volume fraction (ϕ), the Reynolds number (Re), and the Richardson number (Ri), as well as their associated hydrodynamic characteristics, are explored. The results are presented in the form of streamline and isotherm contours, as well as the appropriate plots for the hydrodynamic characteristics for the parameters in consideration. Additionally, the heat transfer rate of the heated surface is shown in terms of the average Nusselt number (Nu_h), as well as the dimensionless average fluid temperature (θ_{av}).

3.1 EFFECT OF RADIATION PARAMETER

In this section, the different hydrodynamic behaviour and heat transfer phenomena due to radiation have been discussed and illustrated for different values of dimensionless time ($\tau = 0.1, 0.5, \text{ and } 1$) at $Re = 100, Ha = 10, Ri = 1, Pr = 23.004$ and $\phi = 0.05$.

3.1.1 Effect on Flow Movement

The velocity profile shows vorticity along the fluid domain as the flow passes over the semi-circular heater. Figure 3.1.1 depicts velocity streamlines with different radiation magnitude and dimensionless time. Radiation has a substantial effect which is observed. When the radiation increases the vorticity of the fluid is also increased gradually over the flow-field. Radiation magnitudes vary from 0 to 2 to get the significant changes. Considering the situation from the transient state point of view, the vorticity has also been increased with the dimensionless time.

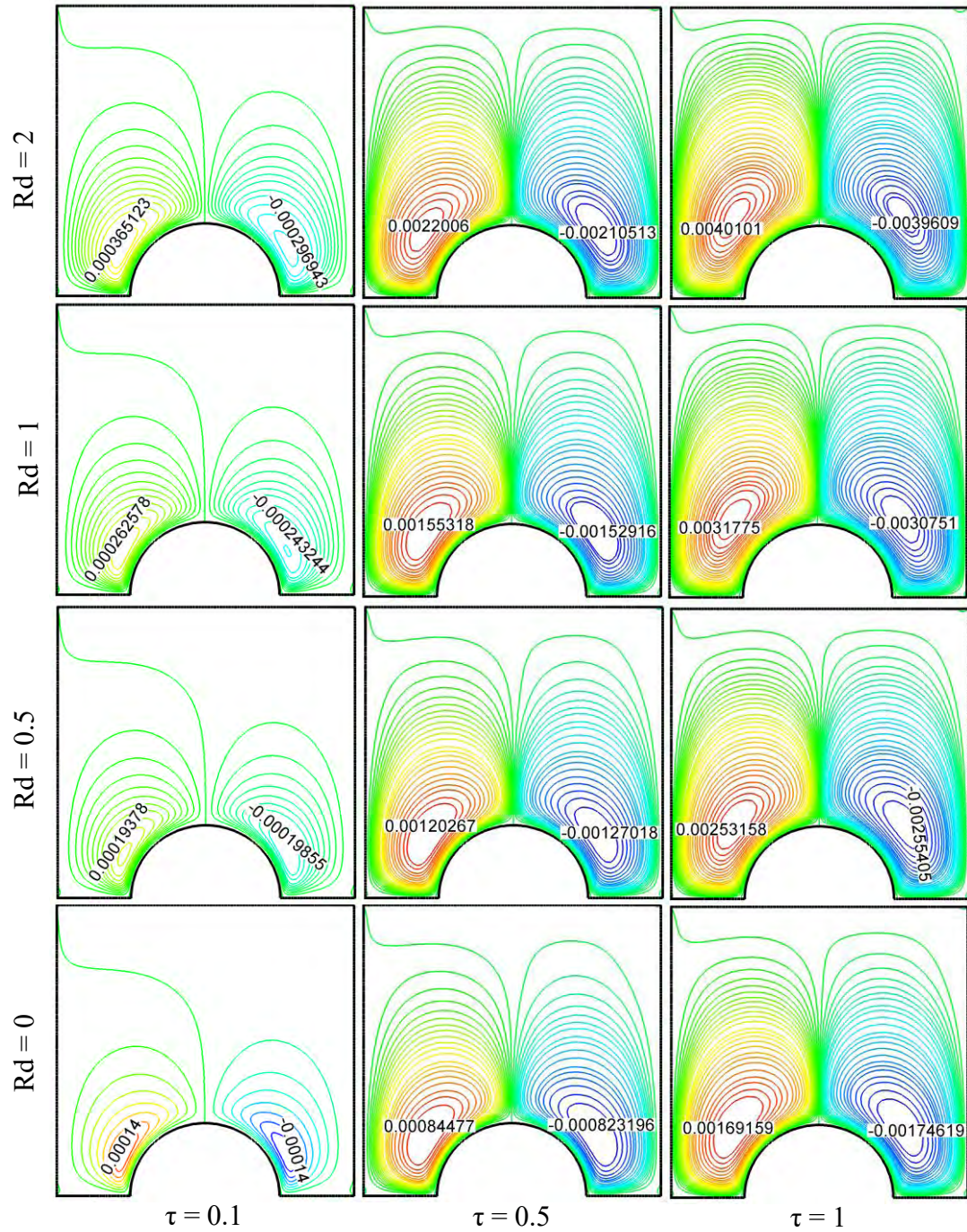


Figure 3.1.1: Effect of radiation parameter, Rd on streamlines for changed values of dimensionless time τ at $Re = 100$, $Ri = 1$, $Ha = 10$, $\phi = 0.05$, $Pr = 23.004$.

It is also notable that vorticity has been generated on both sides of the semicircular heated profile. For both sides, the vorticity increased gradually with the increase of radiation and time. So, it is concluded that fluid streamlines have a denotation of fluid flow behaviour which have a declaration that the higher radiation and the increasing time steps ensures the higher vorticity of the fluid flow.

3.1.2 Effect on the Temperature in the Flow Field

Figure 3.1.2 represents the isotherm plot with varying the radiation parameter and the dimensionless time. It is obvious from the plot that the radiation has an impact on convective heat transfer over the fluid domain. Like vorticity of the fluid flow, the temperature of the fluid over the semi-circular profile is changing by the increase of radiation. The fluid temperature is increased almost 3 times at the near-wall after increasing the radiation from 0 to 2. Additionally, it is assumed that as the time length increases, the temperature increases as a constant heat flux passes through the heated surface until it reaches the same point. The temperature increases commensurately at each step of time throughout the study.

3.1.3 Effect on the Velocity Magnitude

Varying the radiation parameter has an impact on fluid velocity. Figure 3.1.3 (a) shows a plot of velocity field against dimensionless time changing the radiation from 0 to 2. The velocity magnitude is increasing by the increase of the radiation parameter and remains constant with the corresponding parameter for infinite increments of time. The reason is thermal radiation is a form of heat generation and when thermal radiation intensity increases the link binding the fluid particle components loosens and the fluid velocity increases. For a better representation, a surface plot has been shown in Figure 3.1.3 (b) which describes that the changing of radiation ensures an impact on the velocity magnitude of the fluid. It also increases with time as the transient state.

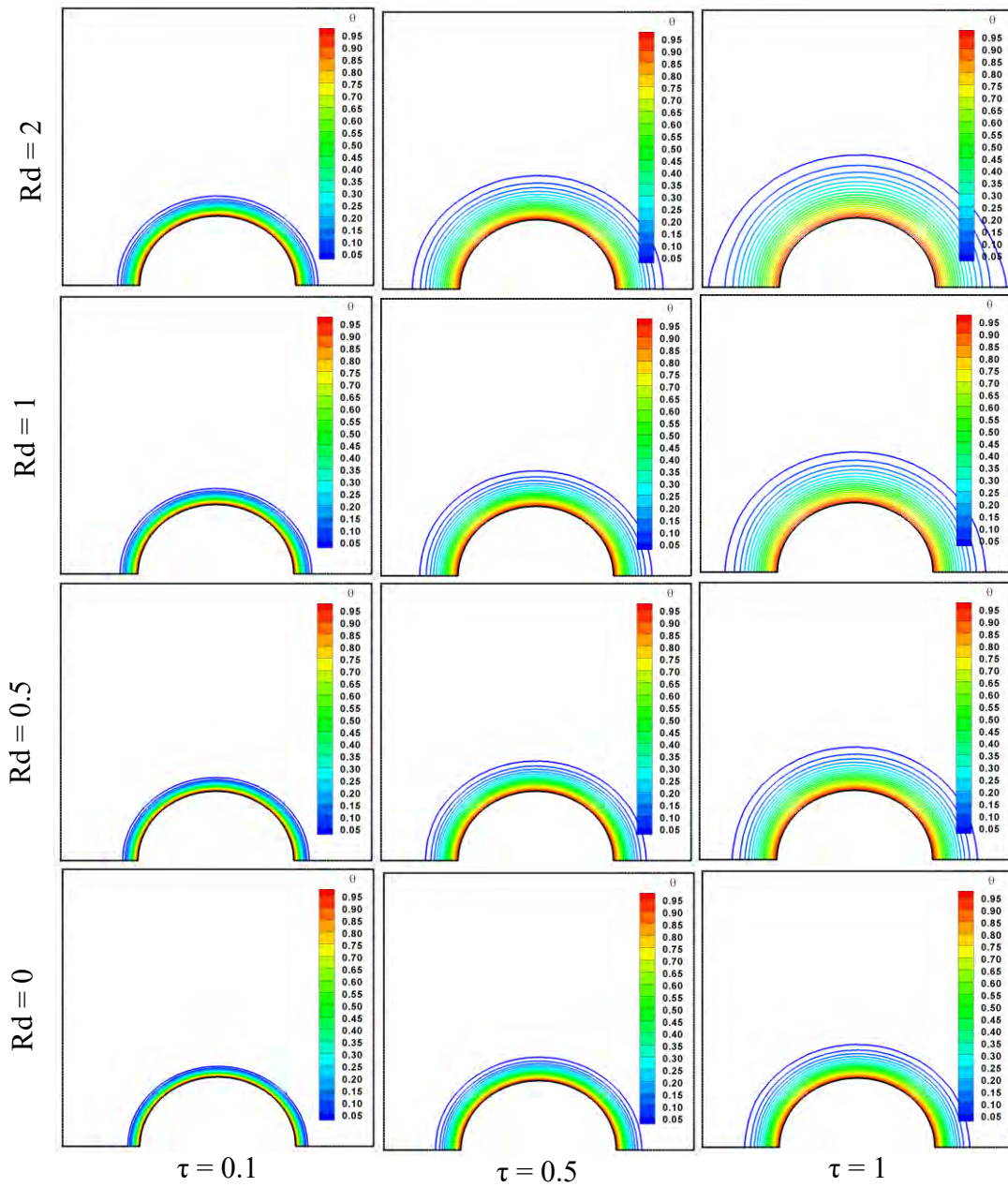


Figure 3.1.2: Effect of radiation parameter, Rd on isotherms for changed values of dimensionless time τ at fixed values of $Re = 100$, $Ri = 1$, $Ha = 10$, $\phi = 0.05$, $Pr = 23.004$.

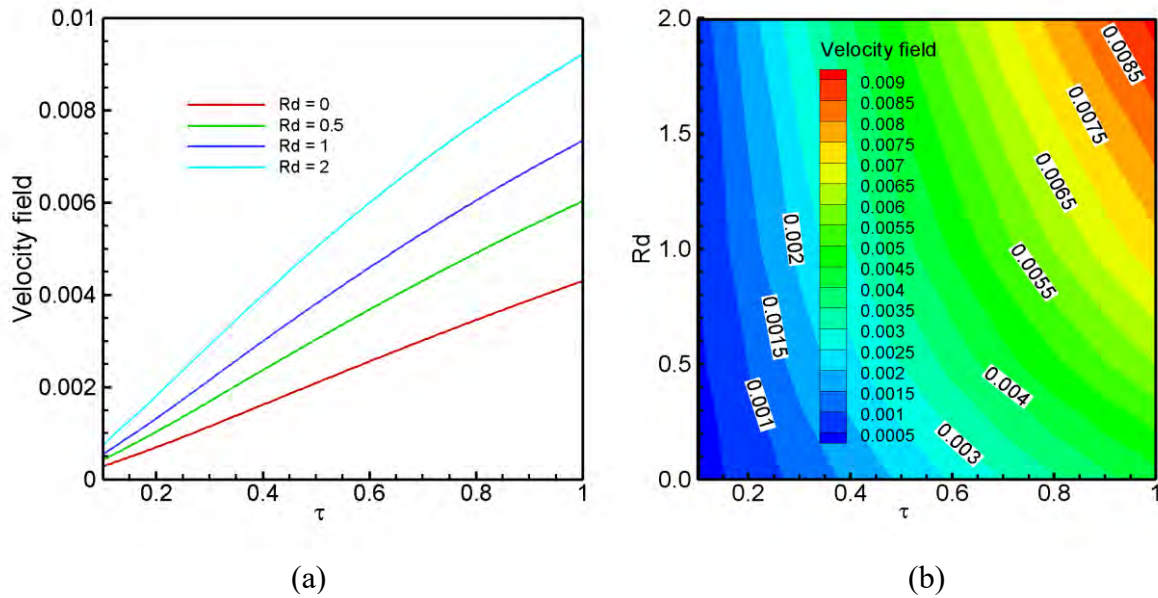


Figure 3.1.3: Effect of radiation parameter, Rd and dimensionless time τ on velocity fields at the fixed values of $Re = 100$, $Ri = 1$, $Ha = 10$, $\phi = 0.05$, $Pr = 23.004$.

3.1.4 Effect on Drag Force

A type of friction or fluid resistance is drag. It is a force that acts in the opposite direction of the relative motion of any moving object in relation to a fluid. As velocity increases throughout the time and with changing of radiation parameter, there must be an effect on drag force. Drag force is the proportion of the square of the velocity magnitude of the fluid, so there will be an increase of drag force with the increase of velocity. Figure 3.1.4 (a) shows a line graph of drag force against dimensionless time varying the radiation from 0 to 2. It is observed that the drag force increases by the increase of radiation parameter, as same as the velocity magnitude and the drag force remains constant with the corresponding parameter for infinite increments of time. In figure 3.1.4 (b), a surface plot of the study has been shown which describes that the increasing radiation ensures an impact on drag force by the increase of radiation magnitude. Similarly, it is notable from the figure that the higher the radiation and dimensionless time, the higher the drag force.

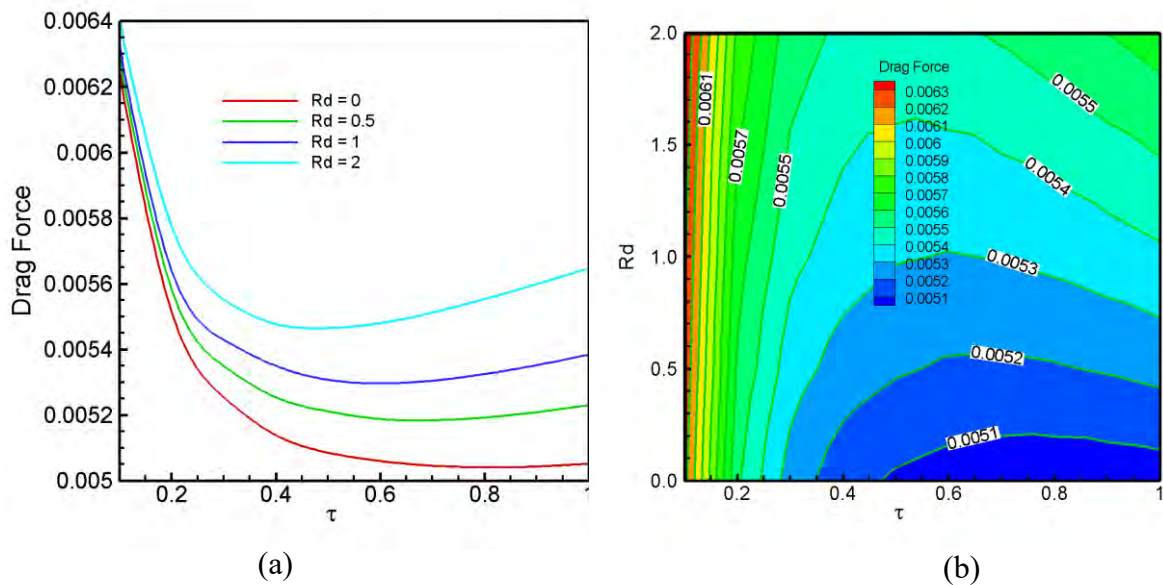


Figure 3.1.4: Effect of radiation parameter, Rd and dimensionless time τ on Drag force of the moving lid at the fixed values of $Re = 100$, $Ri = 1$, $Ha = 10$, $\phi = 0.05$, $Pr = 23.004$.

3.1.5 Effect on the Pressure Gradient

As previously discussed, the drag force increases with the increase of radiation, there should be a variation of pressure in the fluid domain. The pressure gradient has also been shown with varying radiation and dimensionless time. In Figure 3.1.5 (a) shows that the pressure gradient increases by differing the value of radiation, and with the dimensionless time from the transient point of view. It is because the pressure increases with the increment of the drag force. There is a significant high pressure at the inlet side of the semicircular heated region, and there is a pressure drop on the passed flow region. Also in Figure 3.1.5 (b) shows the surface plot where it denotes the pressure gradient increases with the increase of radiation parameter. Also, it increases with dimensionless time.

3.1.6 Effect on the Fluid Temperature Gradient

So far, it has been discussed about the hydrodynamic effects due to radiation. Earlier, isotherms plots showed the fluid temperature variation over the domain through the

streamline. Here, a discussion on the convective heat transfer effect on varying the radiation will take place for both the fluid and heated surface regions.

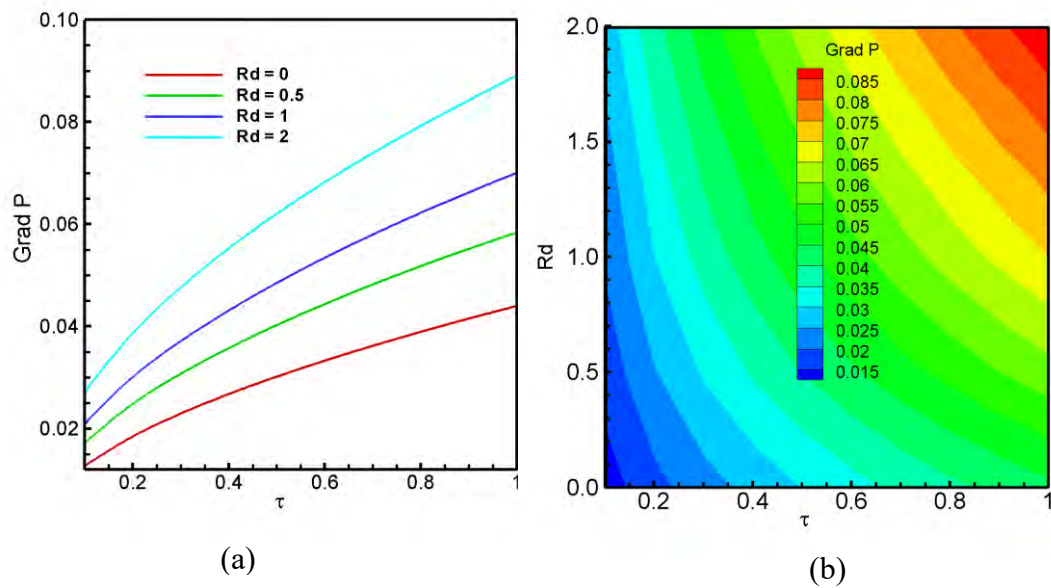


Figure 3.1.5: Effect of radiation parameter, Rd and dimensionless time τ on pressure gradient of the fluid at the fixed values of $Re = 100$, $Ri = 1$, $Ha = 10$, $\phi = 0.05$, $Pr = 23.004$.

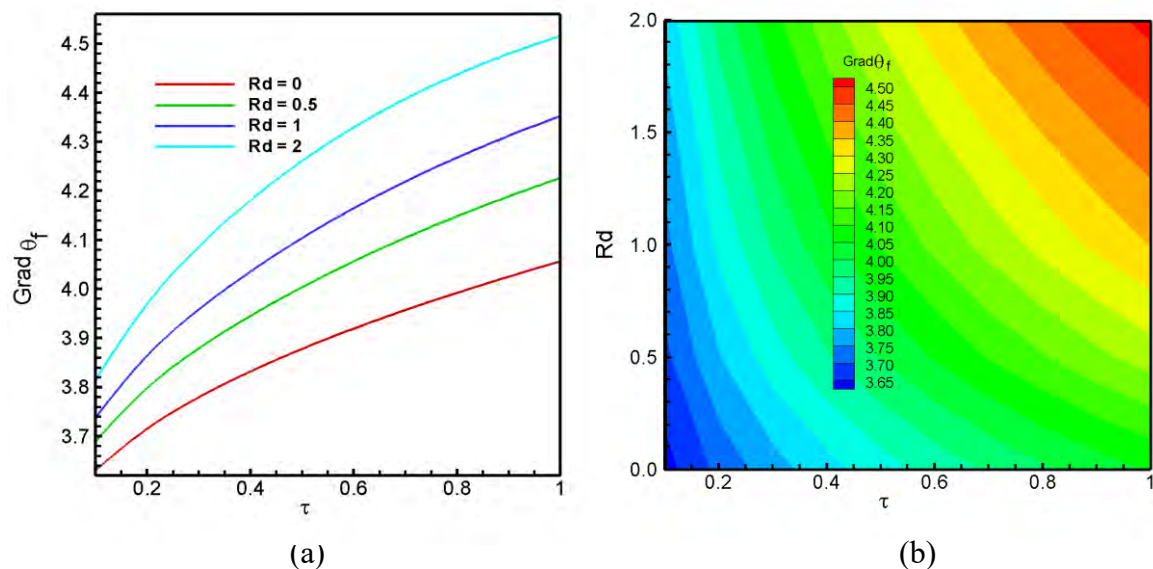


Figure 3.1.6: Effect of radiation parameter, Rd and dimensionless time τ on fluid temperature gradient at the fixed values of $Re = 100$, $Ri = 1$, $Ha = 10$, $\phi = 0.05$, $Pr = 23.004$.

Fluid temperature gradient magnitude (Grad θ_f) increases when there is an increase of heat transfer coefficient (h). Radiation causes the higher heat transfer coefficient

in the fluid, which causes a higher convective heat transfer rate. It is clear from figure 3.1.6 (a) that when there is an increase in radiation, there is a significant increase in convective heat transfer rate. The temperature gradient magnitude ($\text{Grad } \theta_f$) increases with the increase of radiation and dimensionless time. The same goes for figure 3.1.6 (b). In the surface plot, it is visible that the fluid temperature gradient magnitude ($\text{Grad } \theta_f$) increases with the increase of radiation parameter and dimensionless time at a fixed velocity, magnetohydrodynamics, and nanofluid concentration.

3.1.7 Effect on the Mean Heat Transfer Rate

Another observable property is the heated surface Nusselt number (Nu_h). This time while increasing the radiation value, the heat transfer near the heated wall decreases significantly. The reason behind it is the radiative heat transfer that took place along with the convective heat transfer. So that, the surface heat flux region has a significantly lesser heat transfer rate while increasing radiation. It is also noted that the surface Nusselt number decreases with time as the temperature difference between heated wall and fluid decreases with time. From figure 3.1.7 (a), it is also seen that the heated surface Nusselt number decreases with the increase of radiation and vice versa. From the transient point of view, the Nusselt number decreases with time as predicted. From the surface plot from figure 3.1.7 (b), the Nusselt number decreases with the increase of the radiation as well.

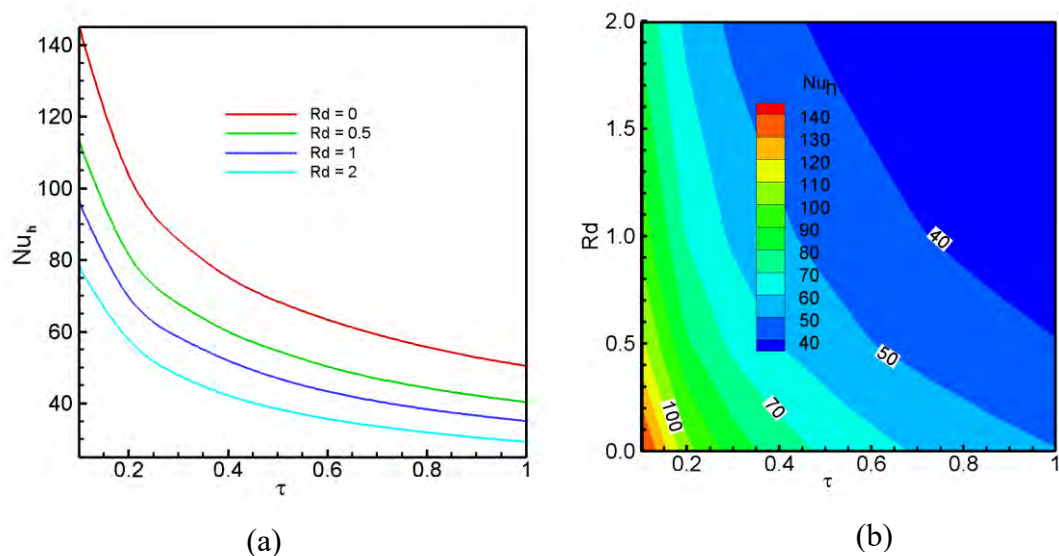


Figure 3.1.7: Effect of radiation parameter, Rd and dimensionless time τ on mean heat transfer rate from the heated surface at the fixed values of $Re = 100$, $Ri = 1$, $Ha = 10$, $\phi = 0.05$.

3.1.8 Effect on Average Fluid Temperature

As previously discussed, the heat transfer rate increases with the increase of radiation, there must be an increase in average temperature as well. From figure 3.1.8, it can be concluded that there is an impact of radiation on average fluid temperature. The average temperature of fluid increases with the increase of radiation, also with the dimensionless time.

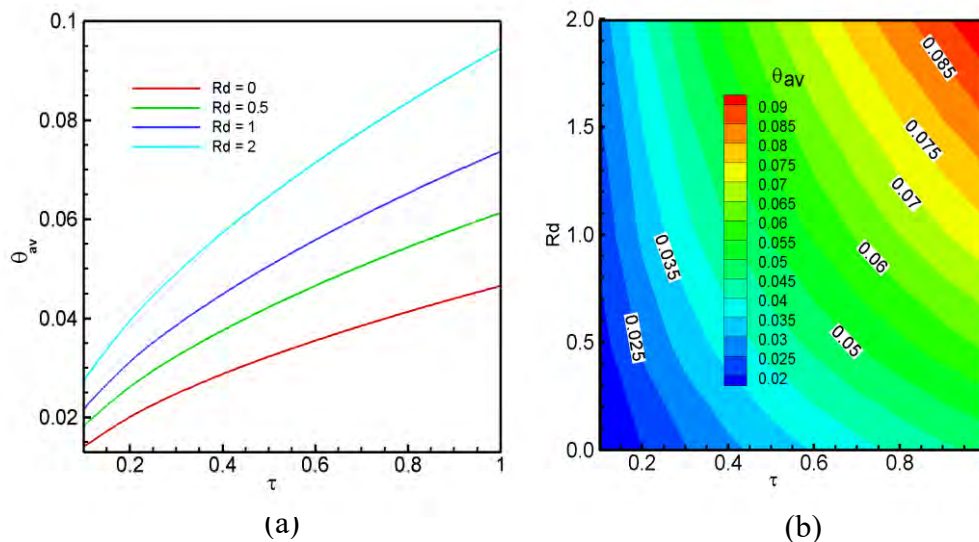


Figure: 3.1.8: Effect of radiation parameter, Rd and dimensionless time τ on the average temperature of the fluid at the fixed values of $Re = 100$, $Ri = 1$, $Ha = 10$, $\phi = 0.05$, $Pr = 23.004$.

3.1.9 Effect on the Bulk Temperature of the Fluid

For the bulk temperature of the fluid, it is clearly observed from figure: 3.1.9, that it increases with the increase of radiation. The line and surface plot show the change of bulk fluid temperature with changing the radiation and dimensionless time. As heat transfer increases with time the bulk fluid temperature also increases.

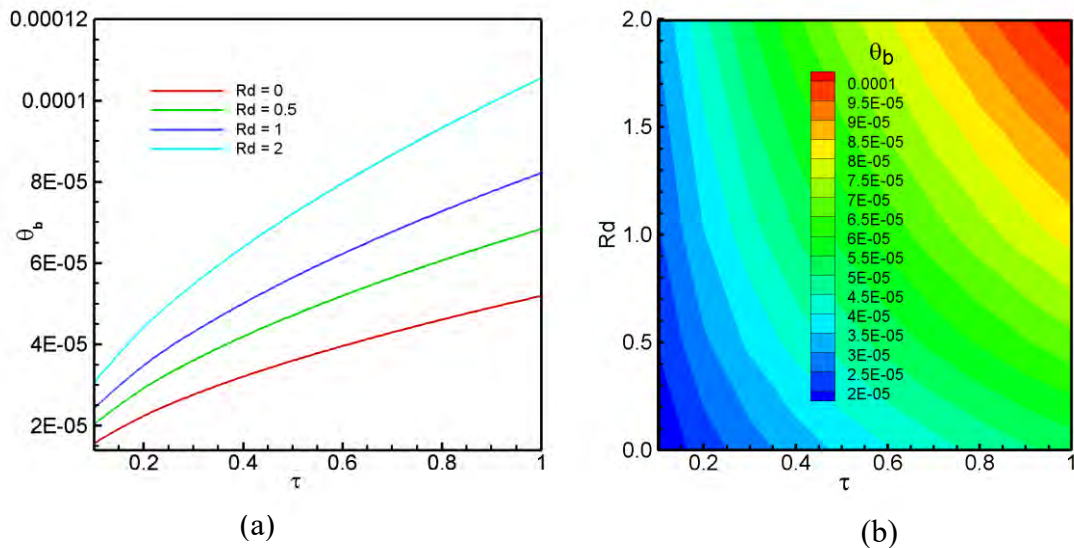


Figure 3.1.9: Effect of radiation parameter, Rd and dimensionless time τ on bulk temperature of the fluid at the fixed values of $Re = 100$, $Ri = 1$, $Ha = 10$, $\phi = 0.05$, $Pr = 23.004$.

3.2 EFFECT OF HARTMANN NUMBER

The magnetic field has an apparent effect on fluid flow and heat transfer. These results, including comparisons among magnetic field intensity by varying the Hartmann number (Ha) magnitude, are discussed in this section.

3.2.1 Effect on Flow Movement

Fluid flow movement can be observed from the streamline plot. Such plots with four different cases are placed in Figure 3.2.1 for the square cavity with a semicircular heater at the bottom. It shows the fluid flow streamlines through the fluid domain with various magnetic field conditions ($Ha = 0, 10, 20, 50$) considering constant Reynolds number ($Re = 100$), Radiation magnitude ($Rd = 1$), and Nanofluid concentration ($\phi = 0.05$), Richardson number ($Ri = 1$). The semicircular region deviates from the fluid flow pattern and generates vorticity near the area. Figure 3.2.1 depicts the velocity streamlines varying dimensionless time (0.1, 0.5, and 1). The vorticity magnitude increases with dimensionless time (τ). It increases by around

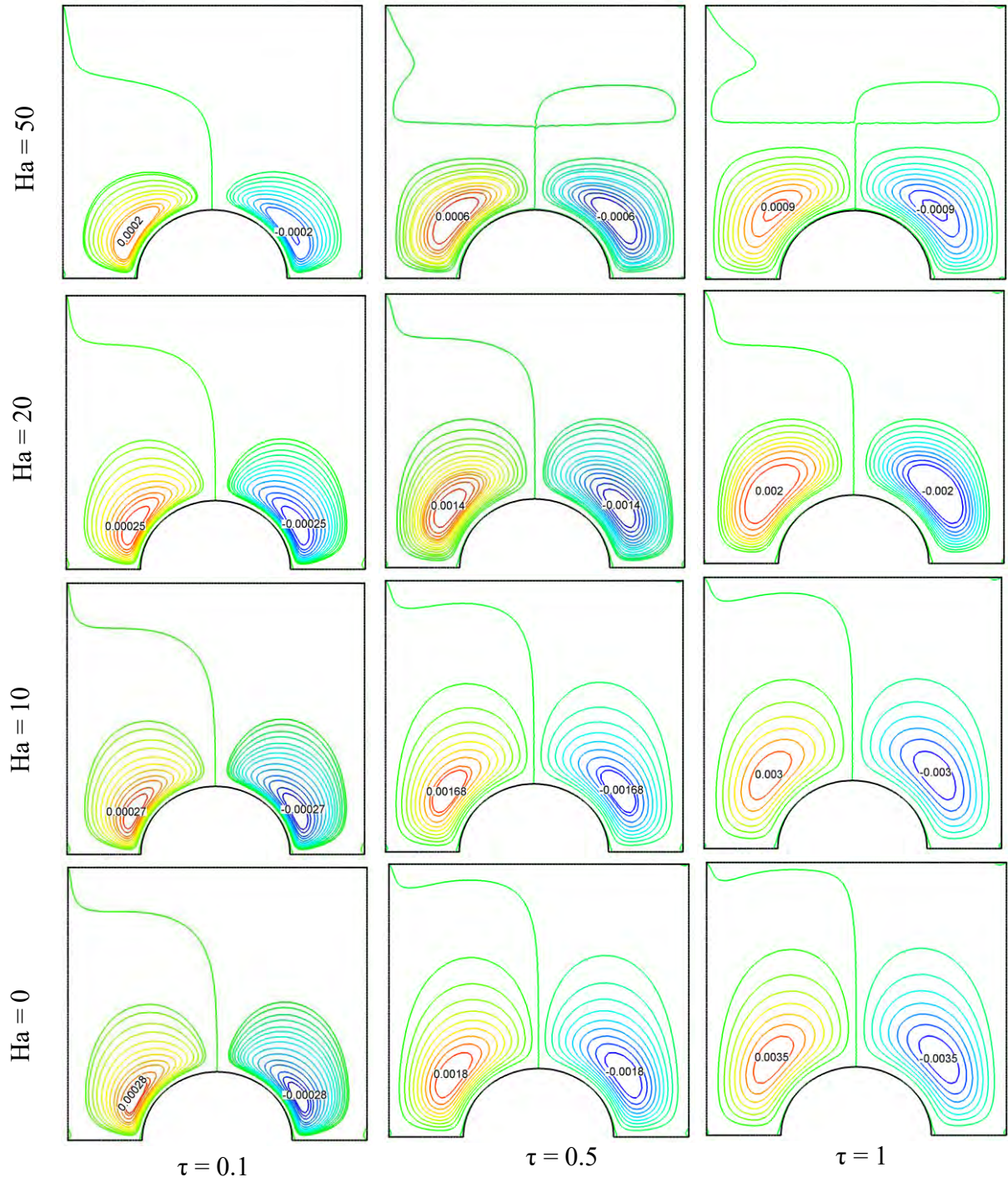


Figure 3.2.1: Effect of Hartmann number, Ha on streamlines for changed values of dimensionless time τ at $Re = 100$, $Ri = 1$, $Rd = 1$, $\phi = 0.05$, $Pr = 23.004$.

300% to 1500%, changing with the Hartmann number (Ha). Furthermore, the magnetohydrodynamics has an important impact on the fluid flow behavior. The magnetic field shows a negative impact on the velocity profile and vorticity. Vorticity reduces around three times after increasing the magnetic field magnitude from Hartmann number 0 to 50. When the highest magnetic field was placed in the cavity, the lowest vorticity was generated. So, it is concluded that the vorticity reduces for the rise of the magnetic field and vice versa.

3.2.2 Effect on the Temperature in the Flow Field

As the heat source took place at the semicircular area of the geometry, the temperature change near the wall can be found indeed. The temperature near the wall is also increased in the transient state with the increase of dimensionless time (τ). Additionally, the magnetic field effect on temperature is notable here. Isotherm plots are shown in Figure 3.2.2, where the temperature profile near the heated surfaces is placed. The temperature change with the change of Hartmann number is minimal, thus it is difficult to observe from the contour plot. However, later, it is discussed how much the temperature changes with detailed graph plot. For all the cases, the temperature increases with dimensionless time (τ) at the transient state, which is visible from the contour.

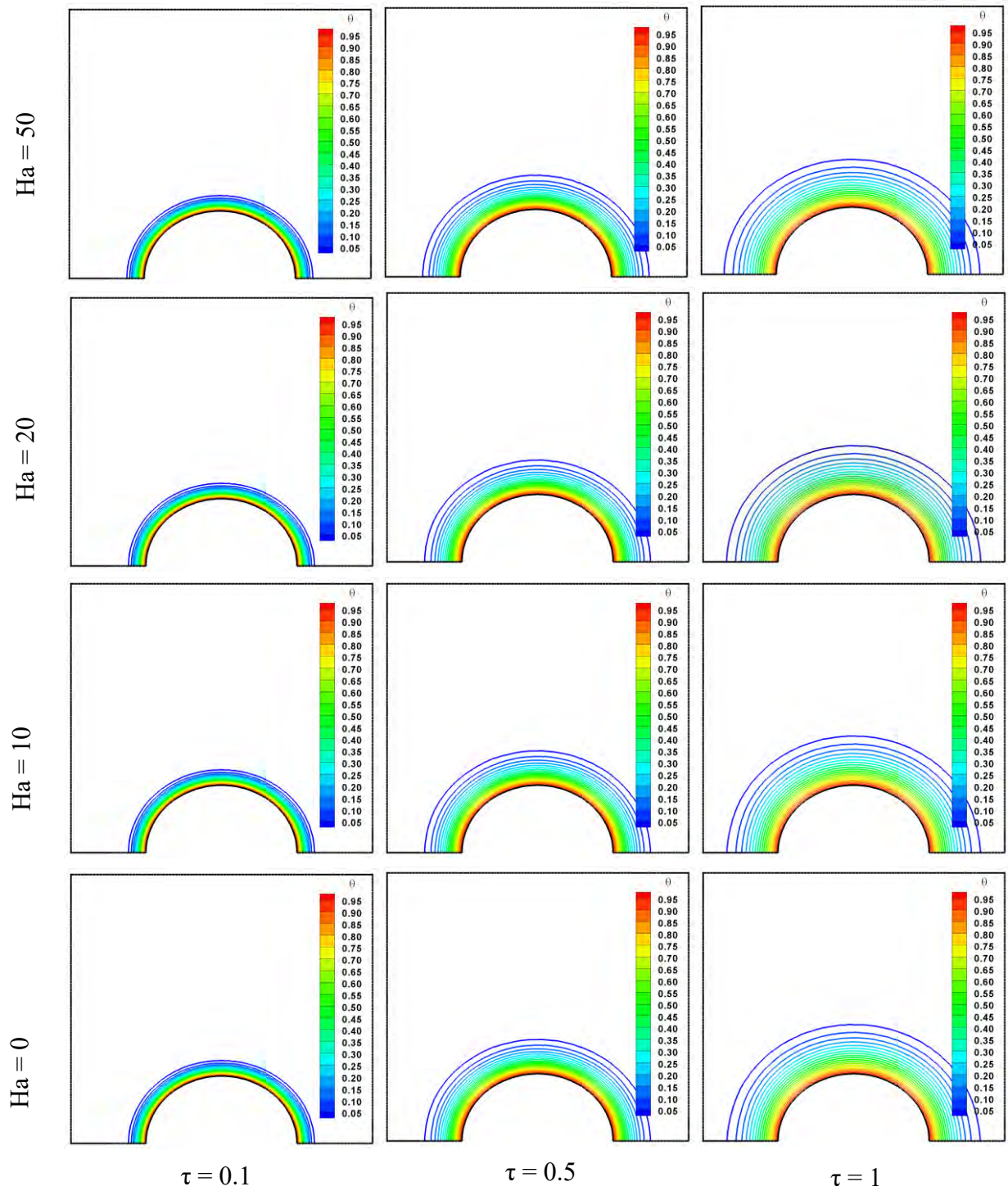


Figure 3.2.2: Effect of Hartmann number, Ha on isotherms for changed values of dimensionless time τ at $Re = 100$, $Ri = 1$, $Rd = 1$, $\phi = 0.05$, $Pr = 23.004$.

3.2.3 Effect on the Velocity Magnitude

Magnetic field hinders the fluid flow movement. Such phenomena can be noticed from the Figure 3.2.3. Figure 3.2.3 (a) depicts the velocity field plot vs dimensionless time (τ) considering magnetic field. The velocity field value decreases simultaneously with the increase of dimensionless time while the magnetic field increases. At the dimensionless time (τ) = 1, the velocity field is five times lesser with the Hartmann number 50, compared to no magnetic field condition. The velocity effect is lowest when Hartmann number is 50, and highest considering no magnetic field. There is increase of velocity gradient without considering magnetic field, and it increases commensurately with the dimensionless time (τ). However, when the magnetic field takes place, the velocity field deviates as it decreases with dimensionless time (τ). Moreover, when the magnetic field is higher, it deviates more and more from the commensurate state. So, with the rise of magnetic field, velocity field values become lesser with dimensionless time (τ).

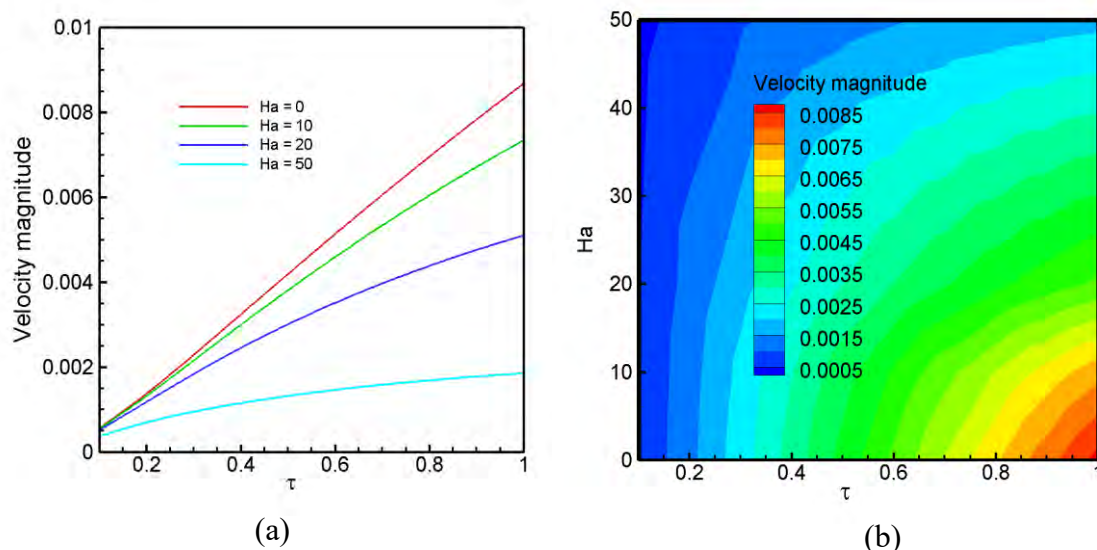


Figure. 3.2.3: Effect of Hartman number, Ha and dimensionless time τ on velocity magnitude at the fixed values of $Re = 100$, $Ri = 1$, $Rd = 1$, $\phi = 0.05$, $Pr = 23.004$.

Figure 3.2.3 (b) shows a surface plot where the velocity magnitude changes with the change of Hartmann number (Ha) and the dimensionless time (τ). From this plot, it can also be stated that the velocity magnitude becomes less when the Hartmann number (Ha) increases and becomes intense when the dimensionless time (τ) increases.

3.2.4 Effect on Drag Force

As there is a semi-circular curve surface on the fluid flow field, the drag force exists. And as there is a magnetic field condition throughout the flow field, drag force should be affected by magnetic force. Figure 3.2.4 visualizes the magnetic effect on the drag force in this study. At the transient state, drag force initially decreases with dimensionless time (τ), and after some time, it starts increasing for all the magnetic field conditions ($Ha = 0, 10, 20, 50$). It is clear from the Figure 3.2.4 (a) that without considering magnetic field, the drag force is lesser than the cases considering the magnetic field. When Hartmann number is 50, it has the highest drag force effect, and considering no magnetic field, it has the lowest impact on drag force. It is found from the graph that the drag force has increased 1.26 times with the magnetic field of Hartmann number 50 compared to no magnetic field. From these plots, it can be more confidently stated that the drag force magnitude is higher at the condition of the high magnetic field. Therefore, it is concluded that the drag force is increased with the increase of magnetic field intensity in the study.

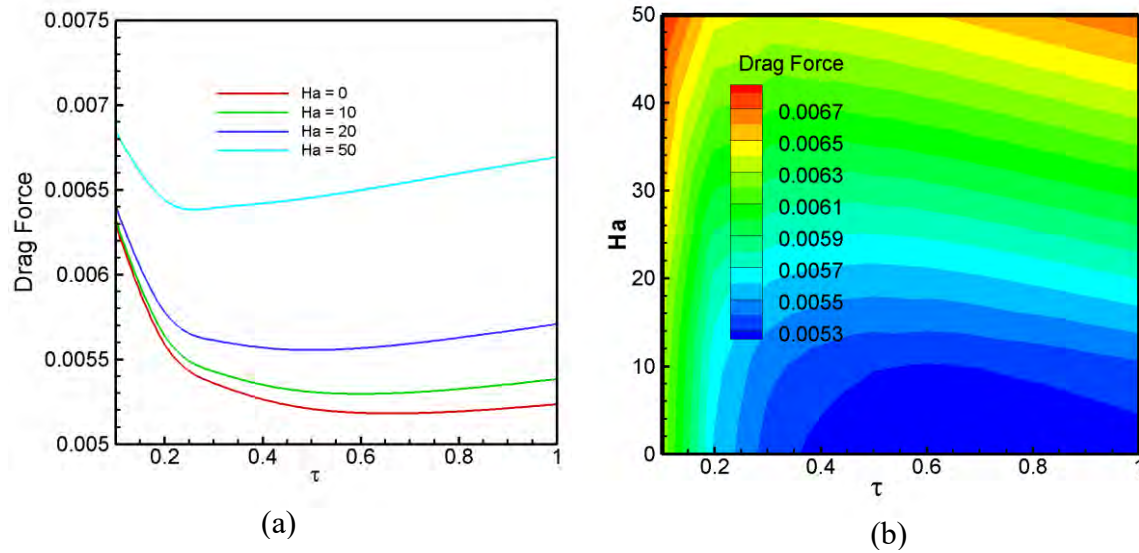


Figure 3.2.4: Effect of Hartmann number, Ha and dimensionless time τ on Drag force of the moving lid at the fixed values of $Re = 100$, $Ri = 1$, $Rd = 1$, $\phi = 0.05$, $Pr = 23.004$.

3.2.5 Effect on the Pressure Gradient

As the drag force increased significantly with dimensionless time (τ) and magnetic field magnitude, so pressure gradient ($Grad P$) must be affected. Figure 3.2.5 shows the comparison among the four different magnetic field magnitudes with pressure gradient ($Grad P$) values with respect to dimensionless time (τ). A clear distinction is observable where the pressure gradient ($Grad P$) increases with dimensionless time (τ) for all the cases in the Figure 3.2.5 (a) The case of no magnetic field has the highest pressure gradient ($Grad P$) magnitude, where the case of Hartmann number ($Ha = 50$) has the lowest impact compared to the other three cases. The pressure gradient ($Grad P$) decreases around 4%, 9%, 14% in the cases of Hartmann number ($Ha = 10, 20, 50$) respectively, compared to the case of Hartmann number ($Ha = 0$). A surface plot is shown in Figure 3.2.5 (b), where it is clear that the gradient pressure ($Grad P$) is increased with the dimensionless time (τ) and lessen with the intensity of the magnetic field.

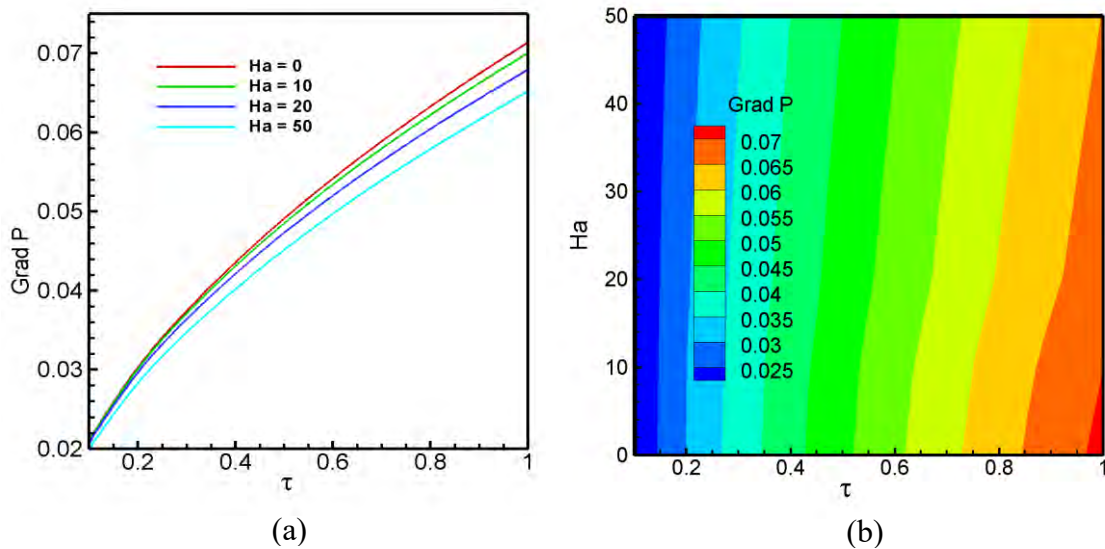


Figure 3.2.5: Effect of Hartman number, Ha and dimensionless time τ on pressure gradient of the fluid at the fixed values of $Re = 100$, $Ri = 1$, $Rd = 1$, $\phi = 0.05$, $Pr = 23.004$.

3.2.6 Effect on the Mean Heat Transfer Rate

As there is a heat source in the cavity region whose temperature is higher than the fluid temperature, the heat transfer must occur. Figure 3.2.6 represents the mean heat transfer rate varying with dimensionless time (τ) considering magnetohydrodynamics. The heat transfer rate reduces by the increase of the dimensionless time (τ) for all the cases considering the transient condition. From Figure 3.2.6 (a) it can be stated that higher Hartmann number (Ha) plays a negative role in heat transfer. It shows that the heat transfer rate lessens with the rise of Hartmann number (Ha) and vice versa. The highest Nusselt number (Nu_h) can be observed with no magnetic environment, and the lowest Nusselt number (Nu_h) is found with the case of Hartmann number ($Ha = 50$). From the 2D surface in Figure 3.2.6 (b), it can be said that the mean heat transfer is being high by lowering the magnetic field magnitude. Nusselt number (Nu_h) decreases with dimensionless time (τ) for all the cases.

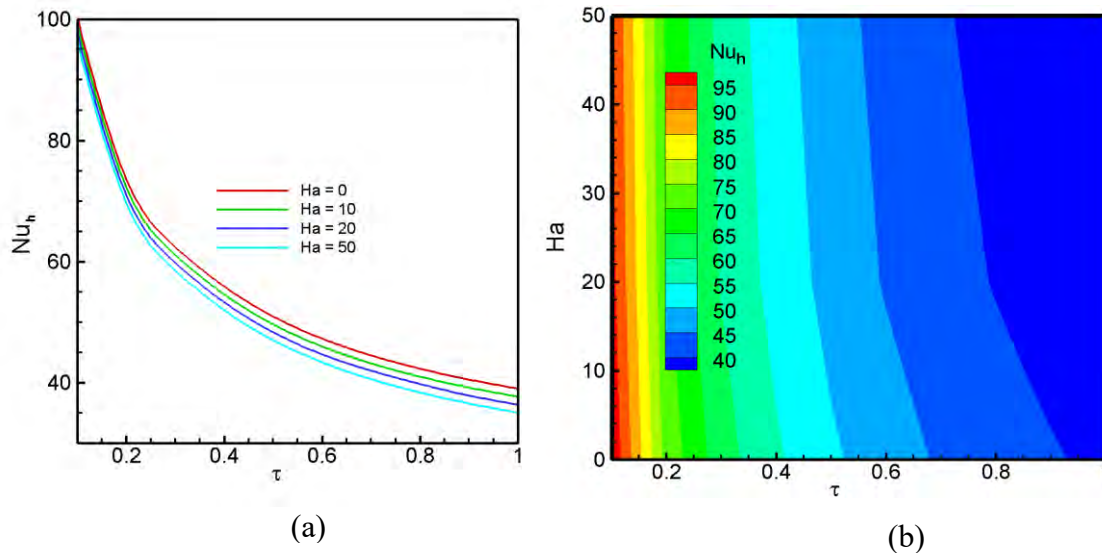


Fig. 3.2.6: Effect of Hartman number, Ha and dimensionless time τ on mean heat transfer rate from the heated surface at the fixed values of $Re = 100$, $Ri = 1$, $Rd = 1$, $\phi = 0.05$, $Pr = 23.004$.

3.2.7 Effect on the Fluid Temperature Gradient

To observe the magnetic field effect on the fluid temperature, three graphs are plotted in Figure 3.2.7. They show the fluid temperature gradient ($Grad \theta_f$) with respect to dimensionless time (τ) considering four different cases varying the magnetic field. For all the cases, it is found that the fluid temperature gradient ($Grad \theta_f$) rises with the rise of dimensionless time (τ), which is obvious. Like the heat transfer rate, fluid flow temperature has a negative effect on the magnetic field. From Figure 3.2.7 (a), it can be noticed that the fluid temperature gradient ($Grad \theta_f$) decreases as like the heat transfer rate with the rise of Hartmann number (Ha). As a result, the case of Hartmann number ($Ha = 0$) has the highest fluid temperature, where the case with the highest magnetic field has reported the lowest fluid temperature gradient ($Grad \theta_f$). Fluid temperature gradient ($Grad \theta_f$) in case of no magnetic field is 5%, 10%, and 16% higher than the cases of Hartmann number (Ha) 10, 20, and 50, respectively. A similar phenomenon can be observed from the 2D surface graph from Figure 3.2.7 (b). Here, it shows the variation of the fluid temperature gradient ($Grad \theta_f$) in a surface plot with the change of magnetic field and dimensionless time (τ).

From the graphical contour, it is clear that with the dimensionless time (τ), the fluid temperature gradient ($Grad \theta_f$) increases, and with the increase of magnetic field, the fluid temperature gradient ($Grad \theta_f$) decreases.

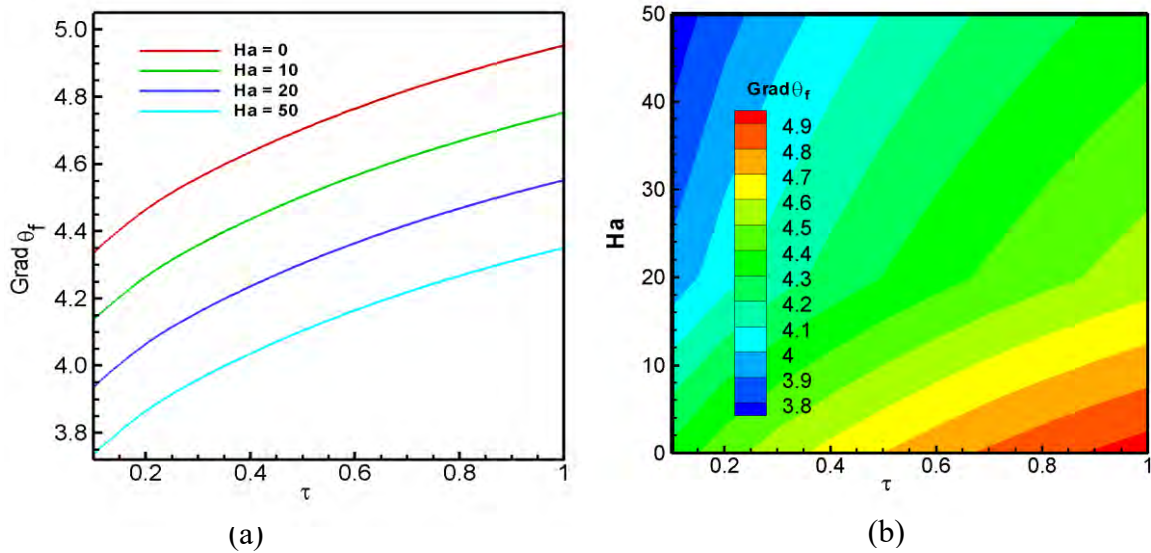


Figure 3.2.7: Effect of Hartman number, Ha and dimensionless time τ on fluid temperature gradient at the fixed values of $Re = 100$, $Ri = 1$, $Rd = 1$, $\phi = 0.05$, $Pr = 23.004$.

3.2.8 Effect on Average Fluid Temperature

Heat transfer occurs due to the difference between the heated region temperature and the fluid temperature, and heat is transferred to the fluid, which results in increasing the fluid temperature. When the transient condition is taken into consideration, the fluid temperature rises more and more with time. Figure 3.2.8 shows the average fluid temperature vs. dimensionless time (τ) graph where this phenomenon is clearly visible. The magnetic field affects the average fluid temperatures. The magnetic field increases the fluid temperature as the magnetic field intensity increases. Figure 3.2.8 (a) depicts that the Hartmann number (Ha) of 50 ensures the lowest fluid temperature value, and the Hartmann number (Ha) of 0 ensures the highest fluid temperature value in this study. From the surface plot in Figure 3.2.8 (b), it also can be concluded

that with the increase of dimensionless time (τ), the fluid temperature increases, but for the rise of Hartmann number (Ha), the fluid temperature value decreases.

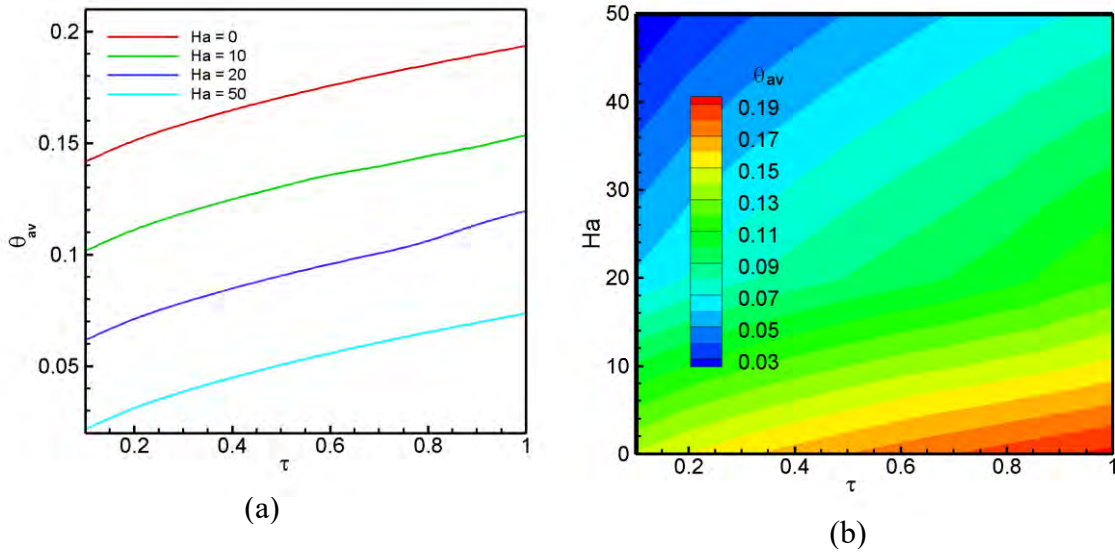


Fig. 3.2.8: Effect of Hartman number, Ha and dimensionless time τ on the average temperature of the fluid at the fixed values of $Re = 100$, $Ri = 1$, $Rd = 1$, $\phi = 0.05$, $Pr = 23.004$.

3.2.9 Effect on the Bulk Temperature of the Fluid

The average bulk fluid temperature vs. dimensionless time (τ) plot varying the magnetic field magnitude is represented in Figure 3.2.9. Like average fluid temperature, the bulk fluid temperature increases with the dimensionless time (τ). The bulk fluid temperature becomes low when there exists the magnetic field. It is clear from Figure 3.2.9 (a) that the higher temperature is found considering the case of $Ha = 10$ than the case of no magnetic field. The case of $Ha = 50$ ensures the lowest bulk fluid temperature value. Therefore, the magnetic field has a negative impact on the bulk fluid temperature. Figure 3.2.9 (b) represents a 2D surface plot, which shows the bulk fluid temperature change with the varying of magnetic field and dimensionless time (τ). It is observed that when magnetic field rises the bulk fluid temperature decreases.

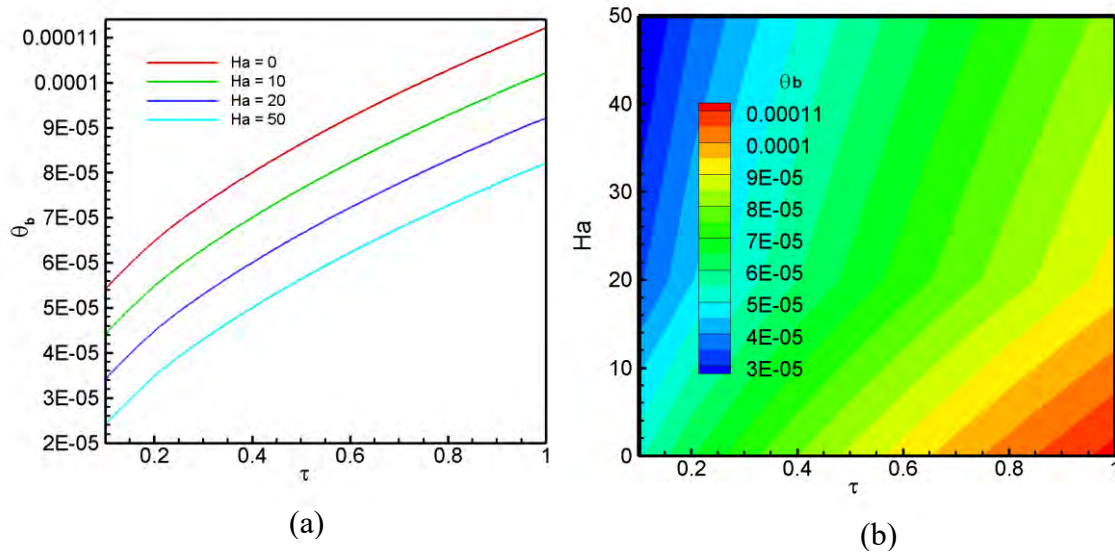


Figure 3.2.9: Effect of Hartman number, Ha and dimensionless time τ on bulk temperature of the fluid at the fixed values of $Re = 100, Ri = 1, Rd = 1, \phi = 0.05, Pr = 23.004$.

3.3 EFFECT OF SOLID VOLUME FRACTION

Kerosene oil-based CNT nanofluid with three different solid volume fractions is analyzed in a cavity with a semicircular heater. The magnetic field, radiation field, and mixed convection were considered. The effects of CNT volume fraction are discussed in this section.

3.3.1 Effect on Flow Movement

Figure 3.3.1 represents the fluid flow streamline plot of the fluid region. This study only focuses on the effect of the solid volume concentration of the nanoparticle. Only Kerosene with 0%, 1%, 4%, and 10% solid volume fractions of the nanofluid are chosen for the analysis. These four cases show four different velocity contours. It also varies with the dimensionless time (τ).

It is observed that during the fluid flow movement, the vorticity generates in the fluid domain where two vorticities have been created. One is before the semicircular region, and another is the flow pass region. The vorticities are similar in magnitude but opposite with the direction. It is noticed that when the *CNT* volume fraction increases, the vorticity also increases. There are significant differences between the case of 0% solid volume fraction and Kerosene with 1% or 4% or 10% solid volume

fractions for all the transient cases. The vorticities increase around 1.5, 2, 3.5 times higher than 0% solid volume concentration when the nanofluid concentrations are 1%,4%, and 10%, respectively.

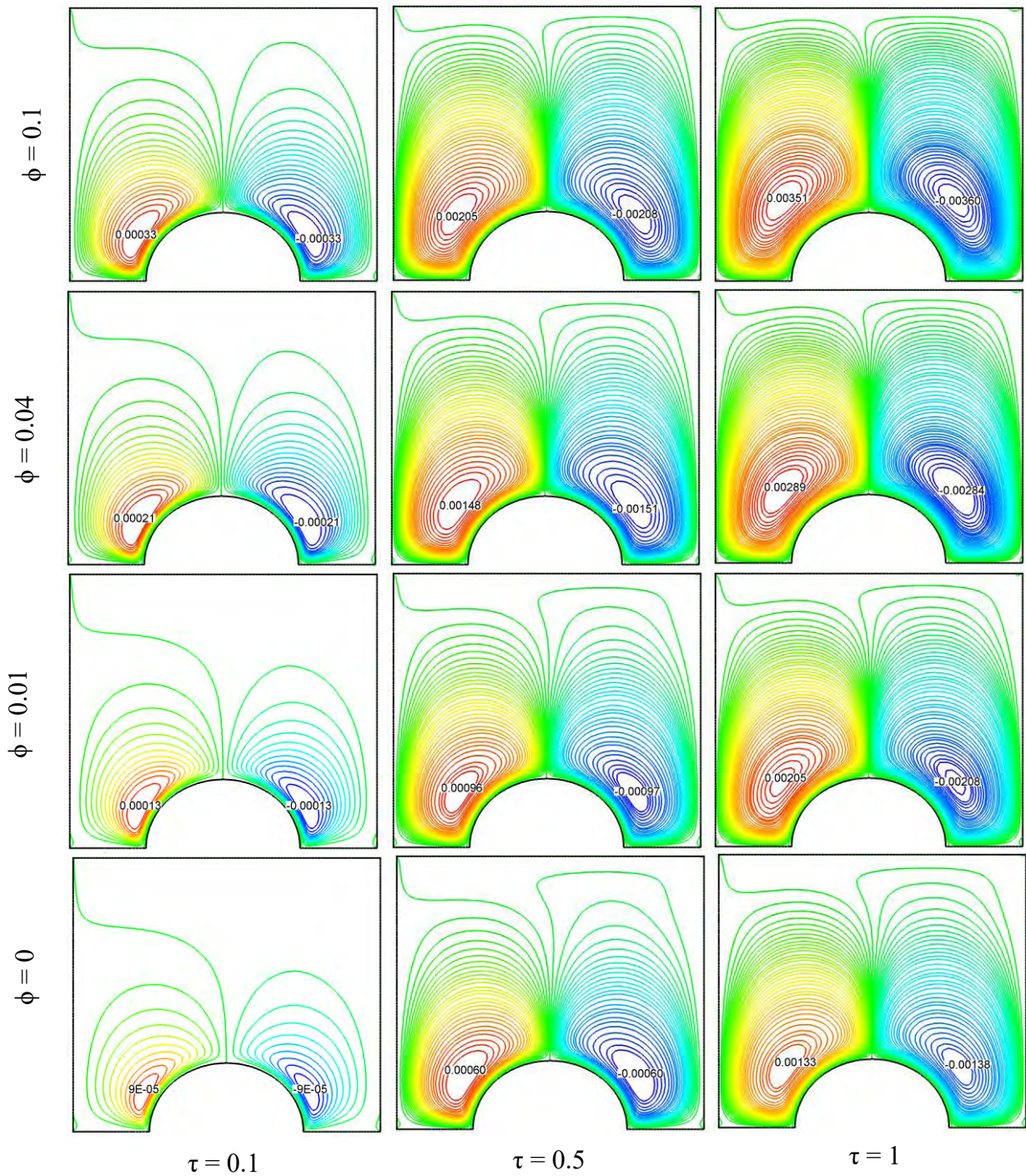


Figure 3.3.1: Effect of solid volume fraction, ϕ on streamlines for changed values of dimensionless time τ at $Re = 100$, $Ri = 1$, $Rd = 1$, $Ha = 10$, $Pr = 23.004$.

At transient conditions, the vorticity increases with time for all these cases. Vorticity rises about seven times when the dimensionless time (τ) moves to 0.1 to 0.5 and rises around double when the dimensionless time (τ) moves to 0.5 to 1. The highest vorticity is found around 0.00351 with the nanofluid concentration of 10% and at dimensionless time (τ) of 1. On the other hand, the lowest vorticity value is found around 0.00009, considering 0% concentration at dimensionless time (τ) of 0.1. From the discussion, it can be stated that the concentration of the nanofluid has an impact in the fluid flow movement where higher volume concentration ensures a higher amount of vorticity.

3.3.2 Effect on the Temperature in the Flow Field

Nanoparticles are very high thermally conductive materials. As the thermal conductivity is high, they show tremendous heat transfer performance rather than normal fluids. The suspension of *CNT* nanoparticles on the Kerosene enhances the heat transfer rate. Figure 3.2 depicts the isotherm plot of the fluid domain where the heated surface is placed at the semicircular region. The heat is transferred to the fluid, and it solely depends on the fluid properties how much heat should be transferred to the fluid. Four cases of concentrations 0%, 1%, 4%, and 10% are chosen for the analysis. Isotherm plots describe that the fluid temperature is higher at the heated surface for all the cases. When the nanofluid concentration gets higher, the fluid near the heated region becomes more heated. It is clear from the plot that the fluid temperature is greater when the solid volume fraction is 1%, 4%, and 10%, rather than 0% nanofluid concentration. Furthermore, it is observed that the temperature is increased for four different nanofluid concentration cases with the increase of dimensionless time (τ). Thus, it can be concluded that the nanofluid concentration tends to augment the heat transfer in such flow in a cavity.

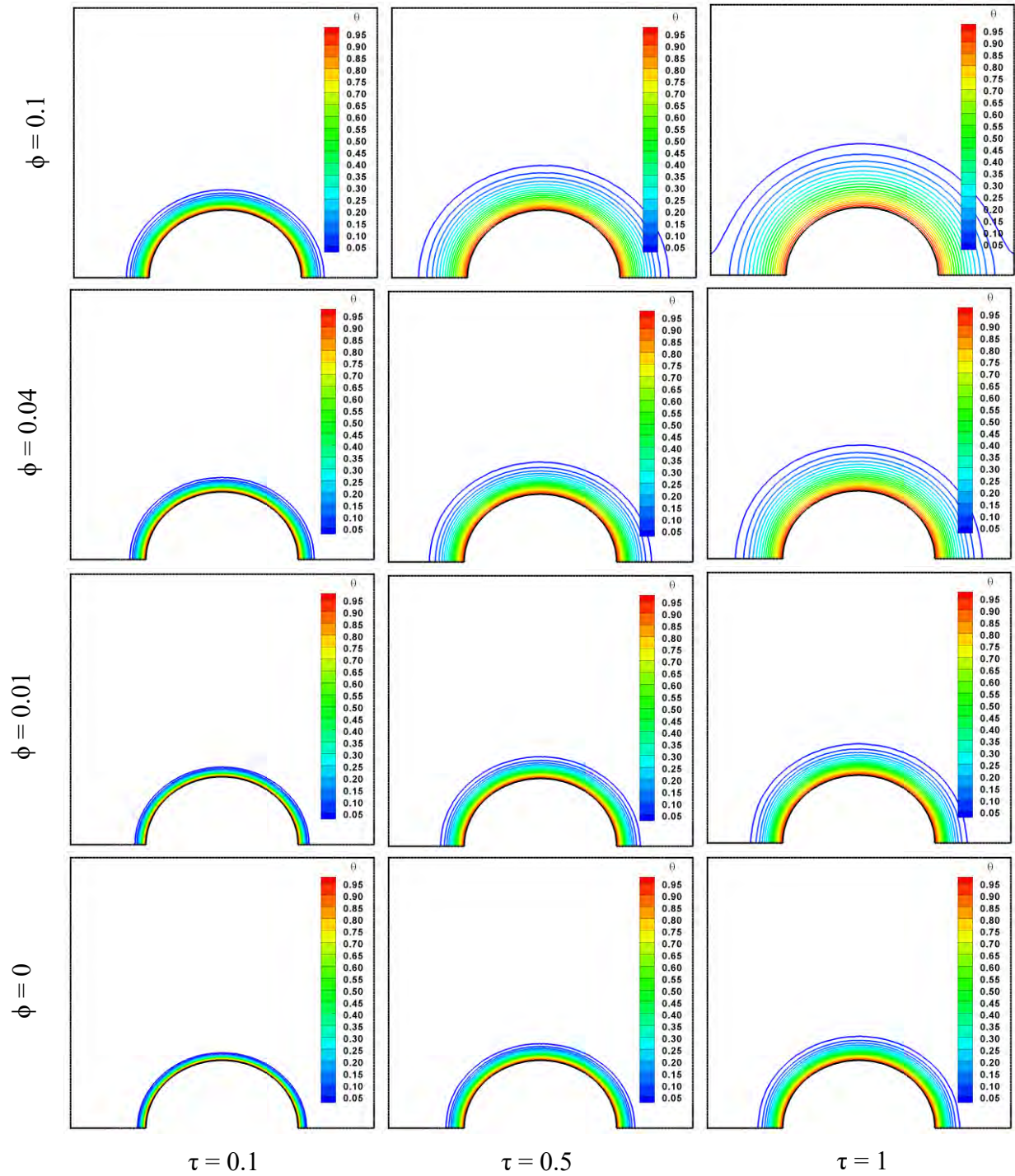


Figure 3.3.2: Effect of solid volume fraction, ϕ on isotherms for changed values of dimensionless time τ at $Re = 100$, $Ri = 1$, $Rd = 1$, $Ha = 10$, $Pr = 23.004$.

3.3.3 Effect on the Velocity Magnitude

Velocity field vs. dimensionless time plot (τ) is presented in Figure 3.3.3, varying the percentage of nanofluid concentration. It is notable from the plot in Figure 3.3.3 (a) that the velocity field is found higher when the nanoparticle volume fraction is higher. Velocity field magnitude increases about 2, 3, and 4 times using nanofluid of 1%, 4%, and 10% respectively than the case of 0% volume concentration. Therefore, the 10% nanofluid concentration case ensures the highest velocity field, and Kerosene with no nanoparticles reports the lowest value in this study. More precise observation can be seen from a surface plot shown in Figure 3.3.3 (b). Here, the contour denotes that the velocity field is higher at the location where solid volume fraction and dimensionless time (τ) are high.

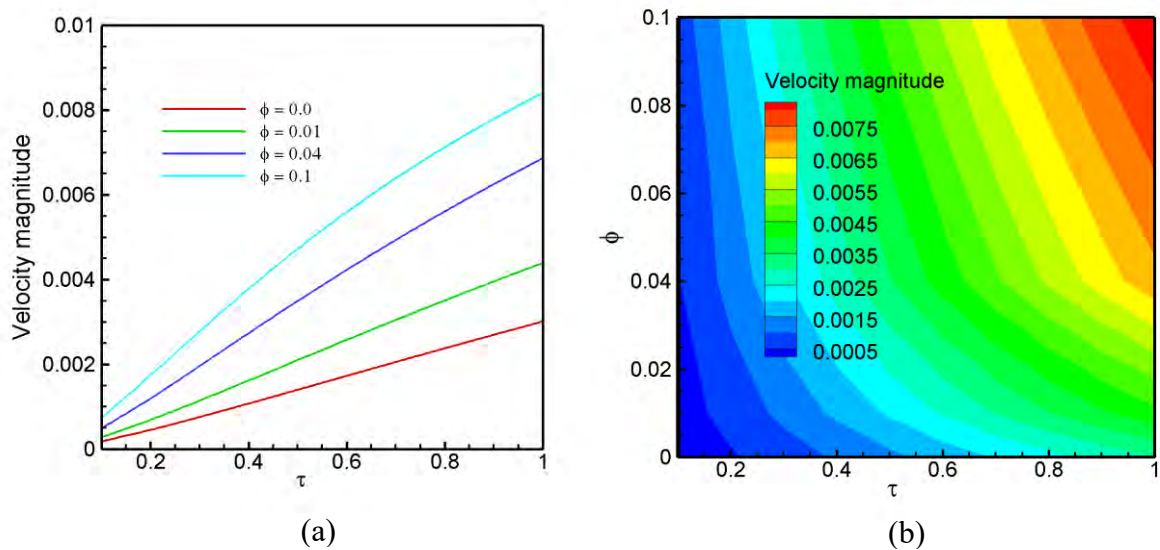


Figure 3.3.3: Effect of solid volume fraction, ϕ and dimensionless time τ on velocity fields at the fixed values of $Re = 100$, $Ri = 1$, $Ha = 10$, $Rd = 1$, $Pr = 23.004$.

3.3.4 Effect on Drag Force

The fluid flows through the square cavity on the semicircular region, creating drag force in the opposite direction of the flow. Nanofluid solid volume fraction has a significant impact on this drag force. This impact is shown in Figure 3.3.4, considering four cases of different concentrations of the nanoparticle.

In the case of pure Kerosene with no nanoparticles, the drag force reduces with dimensionless time (τ), and at 0.7, it becomes constant. The 1% nanoparticle concentration case shows a similar attitude; however, the cases of 4% and 10% nanoparticle concentration are slightly different. In these cases, the drag force reduces, and at specific dimensionless time (τ), it shoots up with dimensionless time (0.6 for $\phi = 4\%$ and 0.3 for $\phi = 10\%$) illustrated in Figure 3.3.4(a). From 2D surface plot in Figure 3.3.4 (b), it is clear that solid volume fraction increases the drag force. So, the highest drag force produces in the case of 10% solid volume fraction of nanofluid and the lowest in the case of 0% solid volume fraction. At dimensionless time =1, the drag force is 1.1 times higher than the case of pure Kerosene with no nanoparticle. Due to the high amount of drag force, the pressure will be increased, which is discussed next.

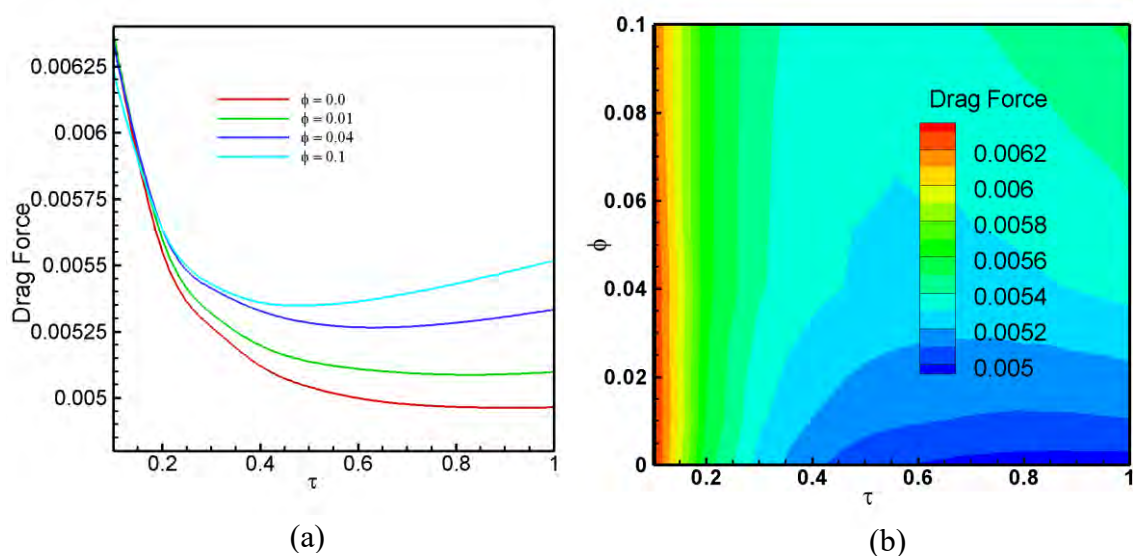


Figure 3.3.4: Effect of solid volume fraction, ϕ and dimensionless time τ on Drag force of the moving lid at the fixed values of $Re = 100$, $Ri = 1$, $Ha = 10$, $Rd = 1$, $Pr = 23.004$.

3.3.5 Effect on the Pressure Gradient

As discussed earlier, the drag force rises with the rise of nanofluid concentration, and there should be an effect on the pressure gradient ($Grad P$). Usually, the pressure gradient ($Grad P$) increases if the drag force increases. Such phenomenon is conspicuous in Figure 3.3.5. The first plot shows the pressure gradient ($Grad P$) vs. dimensionless time (τ) graph with different nanoparticle concentrations considering the same magnetic and radiative fields. Reynolds number and Richardson number are also constant, the only parameter that affects the pressure gradient ($Grad P$) is the solid volume fraction. It is observed that the pressure gradient ($Grad P$) increases almost commensurately for all the cases through dimensionless time (τ) explained in Figure 3.3.5(a). However, the higher the volume concentration, the higher the rate of the pressure gradient ($Grad P$) is observed from the surface plot in Figure 3.3.5 (b). The case of 10% solid volume fraction results the highest rate of pressure gradient ($Grad P$), whereas Kerosene with no nanoparticle shows the lowest. The pressure gradient ($Grad P$) is around 1.3, 2, 3 times higher in the cases of 1%,4%,10% solid volume concentration than the case with no nanoparticles at the dimensionless time (τ) at 1.

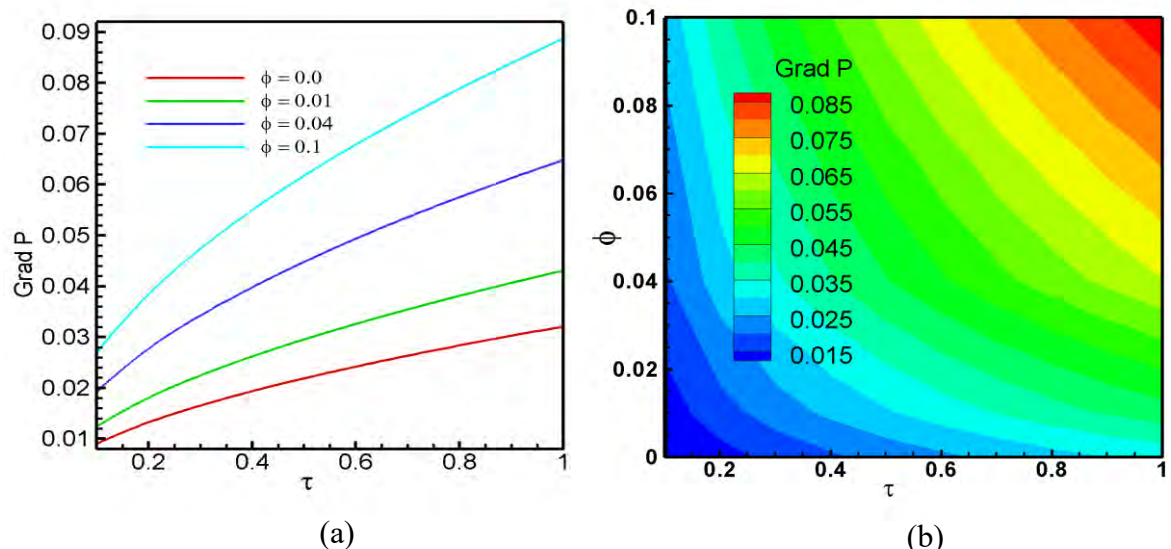


Figure 3.3.5: Effect of solid volume fraction, ϕ and dimensionless time τ on pressure gradient of the fluid at the fixed values of $Re = 100$, $Ri = 1$, $Ha = 10$, $Rd = 1$, $Pr = 23.004$.

3.3.6 Effect on Mean Heat Transfer Rate

Figure 3.3.6(a) depicts the nanoparticle concentration effect on the heat transfer rate with respect to dimensionless time (τ). For a constant concentration case, the heat transfer rate falls down with dimensionless time (τ) and suddenly gets a constant rate at the transient condition. For thermophysical characteristics, the heat transfer rate is higher when the nanoparticle concentration is higher. Here, 10% solid volume fraction ensures the highest amount of heat transfer rate among the cases. As no nanoparticle exists in the case of 0% nanoparticle volume concentration, the Nusselt number (Nu_h) is found the lowest. A surface plot is shown in Figure 3.3.6(b). The heat transfer rate of the cases 1%, 4%, and 10% solid volume fractions is 1.25, 2, and 3 times higher, respectively, than the case of 0% nanofluid concentration.

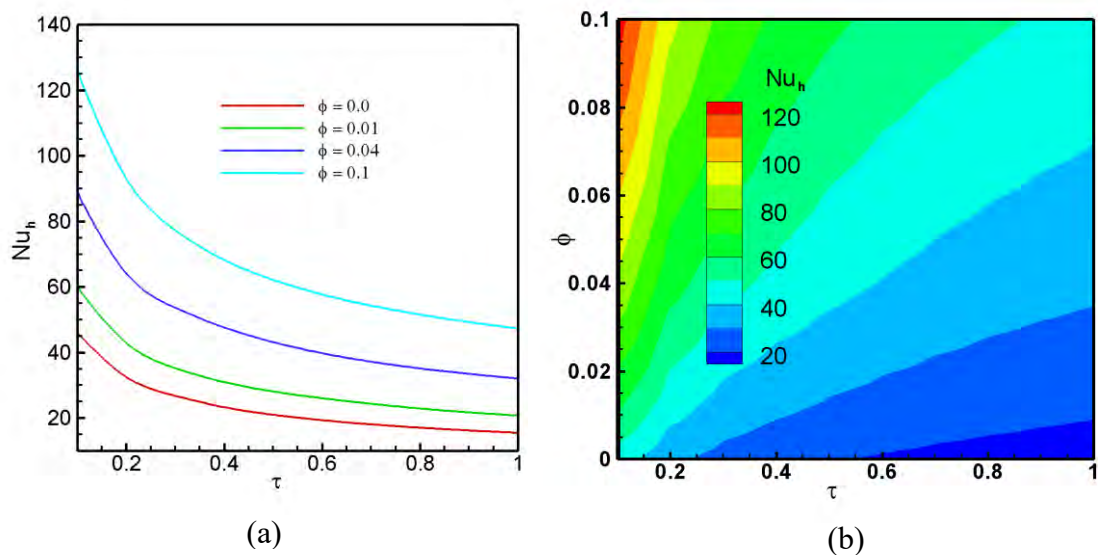


Figure 3.3.6: Effect of solid volume fraction, ϕ and dimensionless time τ on mean heat transfer rate from the heated surface at the fixed values of $Re = 100$, $Ri = 1$, $Ha = 10$, $Rd = 1$, $Pr = 23.004$.

3.3.7 Effect on Fluid Temperature Gradient

As the heater temperature is higher than the fluid temperature, the heat transfer occurs, and there will be change of fluid temperature. Three plots are shown in Figure 3.3.7 where the fluid temperature gradient variation is placed with the change of dimensionless time (τ) and the solid volume fraction to observe such phenomenon. The graphs describe that the fluid temperature gradient increases when the solid volume fraction is greater. Concentration with 10% nanoparticle ensures the highest fluid temperature gradients, and the case with no concentration is the lowest. The fluid temperature gradient in the case of 10% solid volume fraction is almost 2.5, 5, and 9 times higher than the case of 4%, 1%, and 0% concentrations respectively.

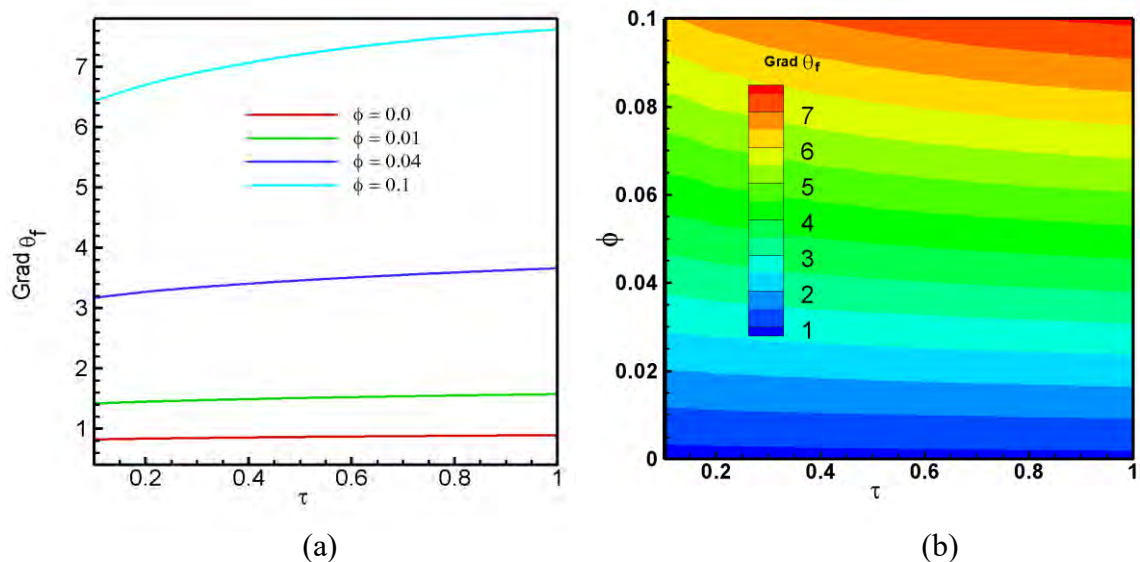


Figure 3.3.7: Effect of solid volume fraction, ϕ and dimensionless time τ on fluid temperature gradient at the fixed values of $Re = 100$, $Ri = 1$, $Ha = 10$, $Rd = 1$, $Pr = 23.004$.

3.3.8 Effect on the Average Fluid Temperature

At the transient state, the average fluid temperature will increase with dimensionless time (τ). From Figure 3.3.8(a), this thing can be observed for the four cases. The average fluid temperature has the effect of nanoparticle volume fraction. The graph describes that for higher solid volume concentration, the average fluid temperature is found higher too. As a result, the highest average fluid temperature value is obtained by using the nanofluid with 10% concentration. Then the cases of 4% and 1% concentration. Kerosene with 0% nanoparticles ensures the lowest average fluid temperature among the four cases. The average fluid temperature is 3.3 times higher when 10% concentration is used than the case of $\phi = 0\%$. A 2D surface plot is placed in Figure 3.3.8(b), which describes that the average fluid temperature increases when solid volume fraction increases.

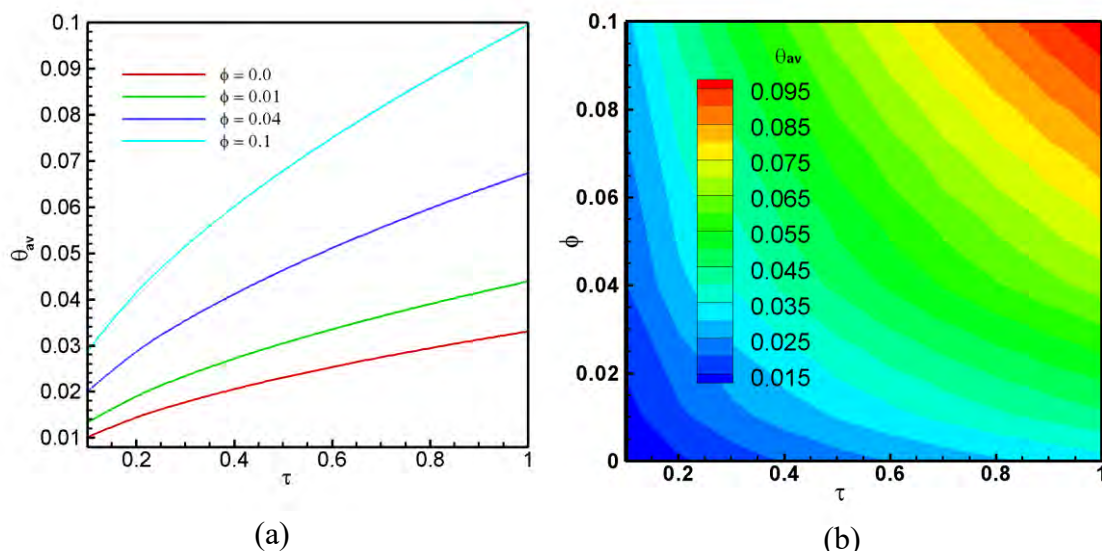


Figure 3.3.8: Effect of solid volume fraction, ϕ and dimensionless time τ on the average temperature of the fluid at the fixed values of $Re = 100$, $Ri = 1$, $Ha = 10$, $Rd = 1$, $Pr = 23.004$.

3.3.9 Effect on Bulk Temperature of the Fluid

Similar to average temperature, the bulk fluid temperature also varies with the concentration of solid volume fraction. Figure 3.3.9 (a) represents a graph of bulk fluid temperature vs. dimensionless time (τ) considering four different cases of nanofluid volume concentration. The highest temperature is reported in the case of 10% nanofluid concentration, and the lowest is found in the case of 0% nanofluid concentration. Using a 10% solid volume fraction, the bulk fluid temperature is 3.6 times higher than using Kerosene without *CNT* nanoparticles. From the surface plot in Figure 3.3.9 (b), bulk fluid temperature is higher when the solid volume fraction is higher. At transient conditions, the bulk fluid temperature increases with dimensionless time (τ).

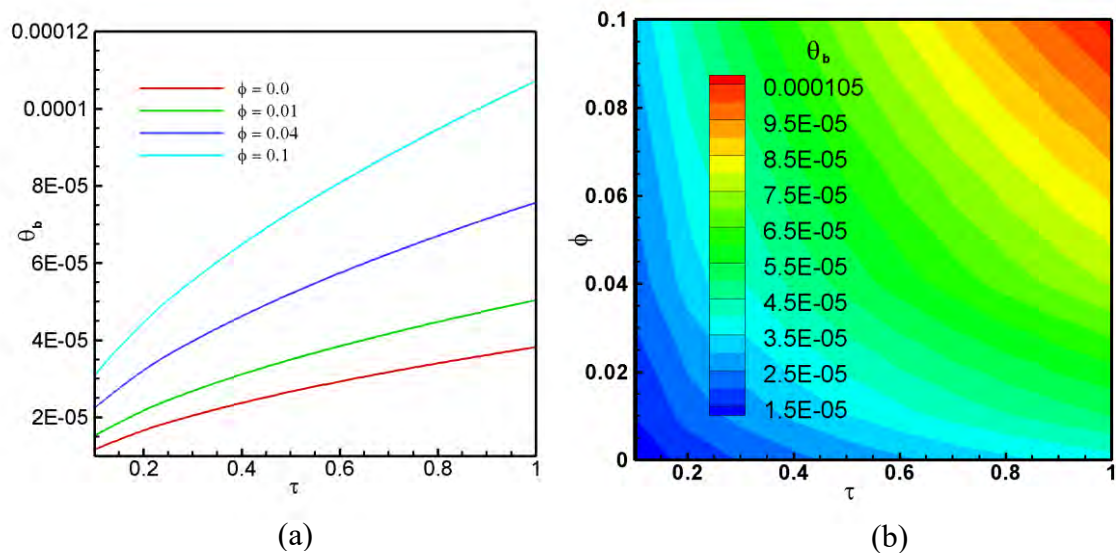


Figure 3.3.9: Effect of solid volume fraction, ϕ and dimensionless time τ on bulk temperature of the fluid at the fixed values of $Re = 100$, $Ri = 1$, $Ha = 10$, $Rd = 1$, $Pr = 23.004$.

3.4 EFFECTS OF REYNOLDS NUMBER

This section discusses the effect of different velocity magnitude in the form of Reynolds number (Re) on several fluid and heat transfer properties considering mixed convection MHD radiative flow in a semicircular cavity using CNT-Kerosene nanofluid.

3.4.1 Effect on Flow Movement

Constant value of nanoparticle concentration ($\phi = 0.05$), constant magnetic field magnitude Hartmann number ($Ha = 10$), constant radiation parameter (Rd) value 1, and mixed convection parameter Richardson number (Ri) value 1, are chosen to analyze the study. The only changeable parameter here is the velocity magnitude. Figure 3.4.1 represents the fluid flow streamlines for all twelve cases considering four different Reynolds number value ($Re = 50, 100, 150, 200$) and three different dimensionless time ($\tau = 0.1, 0.5, 1$). Due to the presence of the semicircular cavity, vorticity creates around the region. By observing the streamlines and the vorticity value, it can be said that changing the Reynolds number (Re) has an apparent effect on the fluid flow movement. Vorticity value depends upon the value of the angular velocity of the flow. As Reynolds number (Re) is proportional to the fluid velocity, the vorticity changes with Reynolds number (Re). The lowest vorticity value is found 0.00024 in the case of $Re = 50$ at the dimensionless time (τ) 0.1. In the case of $Re = 100$ and at the 0.1 dimensionless time (τ) value, vorticity increases by 12%. After increasing the value to $Re = 200$, the vorticity value increases around 54%.

Furthermore, vorticity rises with the dimensionless time (τ). The vorticity increases 6.75 times when the dimensionless time (τ) increases 0.1 to 0.5. Similarly, vorticity increases around 10 times when the dimensionless time (τ) becomes 0.1 to 1. The highest vorticity value 0.00461 has found in the case of $Re = 200$ at the dimensionless time (τ) 1. Therefore, it is concluded that, increasing the Reynolds number (Re) the vorticity of the flow increases.

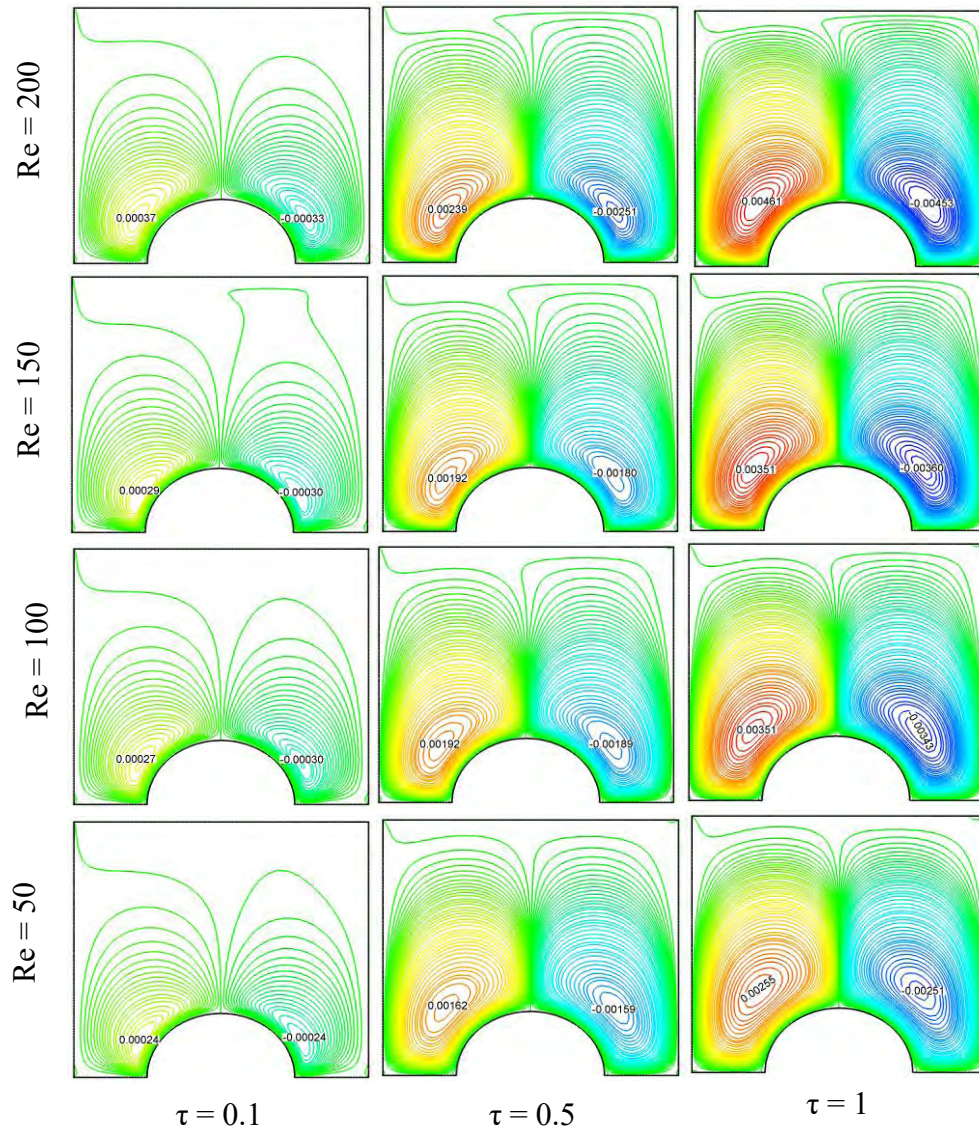


Figure 3.4.1: Effect of Reynolds number, Re on streamlines for changed values of dimensionless time τ at $\phi = 0.05$, $Ri = 1$, $Rd = 1$, $Ha = 10$ $Pr = 23.004$.

3.4.2 Effect on the Temperature in the Flow Field

For observing the temperature variation through the fluid domain, isotherm plots are placed in Figure 3.4.2. It is observed that the temperature collapse with the increase of fluid velocity. Therefore, the highest temperature variation is got in the case of ($Re = 50$) and the lowest temperature variation is found in the case of ($Re = 200$) compared to the other three cases. This phenomenon is also true for all the dimensionless time (τ) conditions. Additionally, the temperature variation increases when the dimensionless time (τ) increases considering a constant fluid flow velocity.

As a result, it is found that the case of $Re = 50$ and dimensionless time ($\tau = 1$) has shown the highest temperature variation among the cases. The case of ($Re = 200$) and dimensionless time ($\tau = 0.1$) has shown the lowest temperature variation.

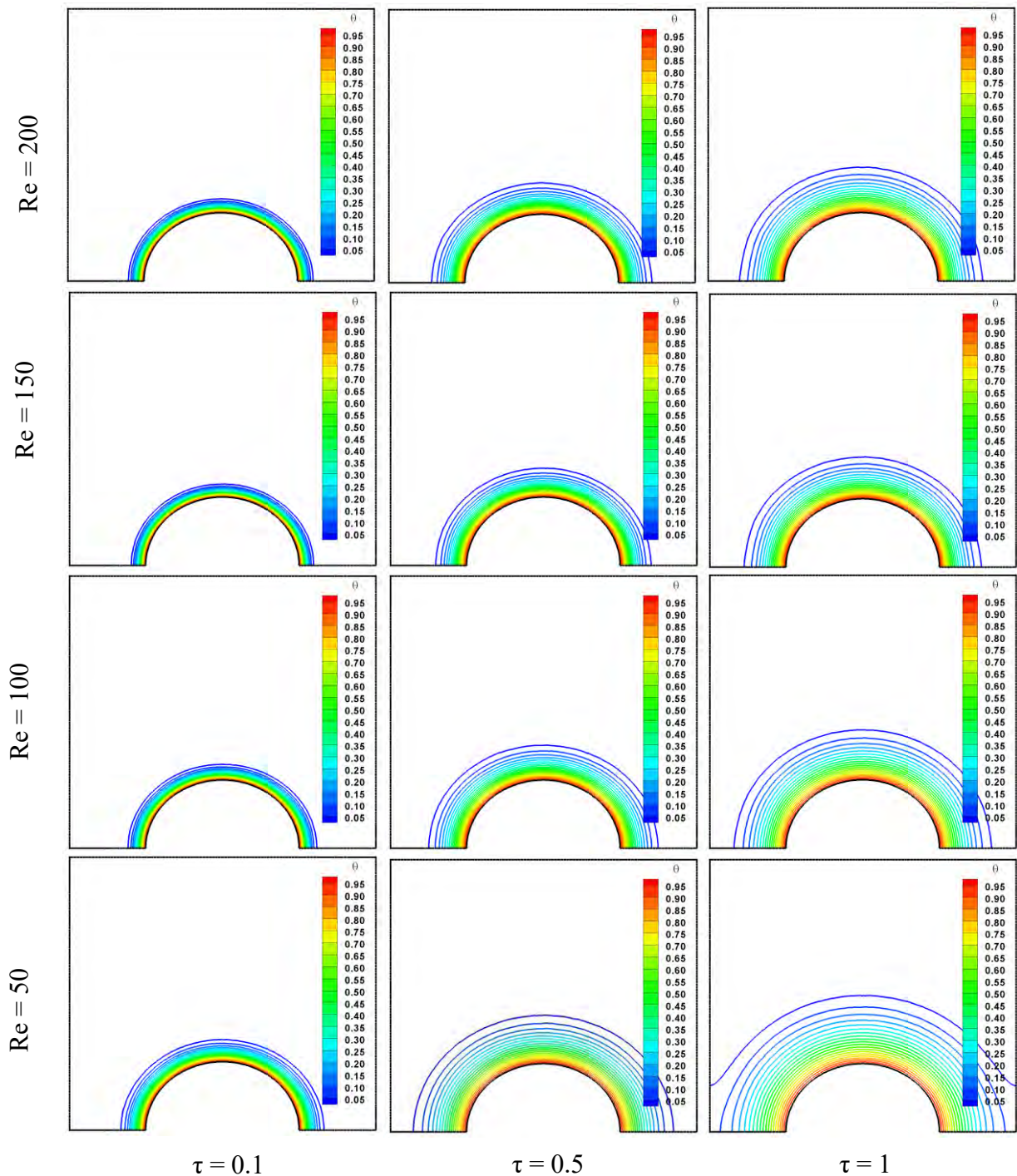


Figure 3.4.2 Effect of Reynolds number, Re on isotherms for changed values of dimensionless time τ at $\phi = 0.05$, $Ri = 1$, $Rd = 1$, $Ha = 10$, $Pr = 23.004$.

3.4.3 Effect on the Velocity Magnitude

As this study is only focused on the Reynolds number (Re), the same velocity profile will not be through the fluid domain for all the cases. Figure 3.4.3 (a) shows a velocity field vs. dimensionless time (τ) plot varying the four different Reynolds number (Re) cases. There are some overlapped lines in this graph, and it is difficult to understand how the velocity profile changes. A surface plot is placed in Figure 3.4.3(b), which represents a perfect visualization of the effect of fluid velocity. It says that the high value of Reynolds number (Re) increases the velocity field. So, the case of $Re = 200$ has the highest value of the velocity field, and $Re = 50$ reports the lowest. Furthermore, the velocity field increases with dimensionless time (τ) for all the cases. However, for the case of $Re = 50$, it falls after increasing the dimensionless time (τ) compared to the other three cases, despite at $\tau = 0$ the velocity field value being the highest.

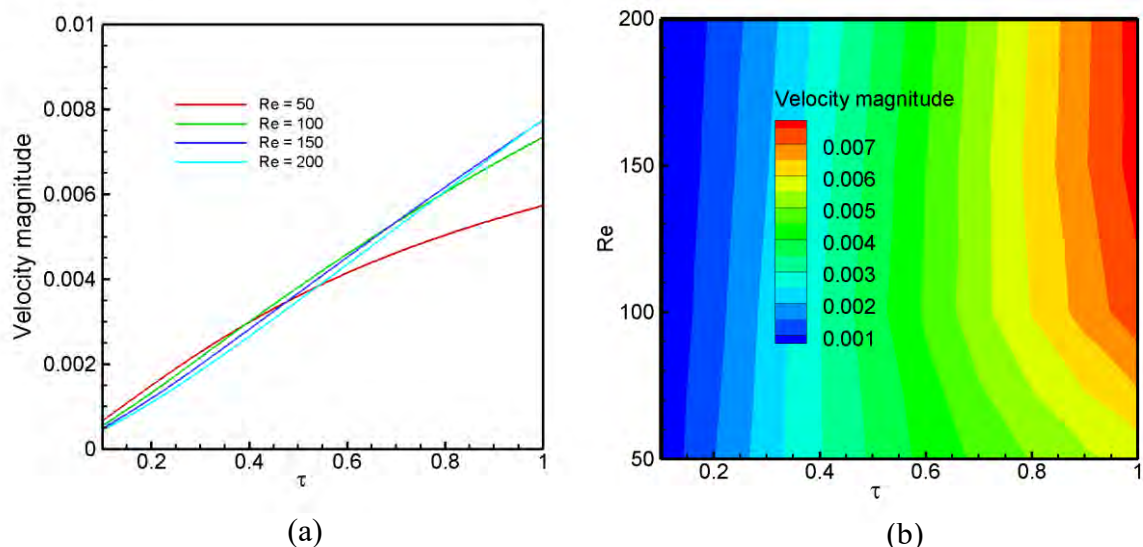


Figure 3.4.3: Effect of Reynolds number, Re and dimensionless time τ on velocity field at the fixed values of $Rd = 1$, $Ri = 1$, $Ha = 10$, $\phi = 0.05$, $Pr = 23.004$.

3.4.4 Effect on Drag Force

The drag force is a resistive force exerted by the obstacle in the fluid flow. As the semicircular heater is acted as the obstacle in the flow path, the drag force is created. For changing the Reynolds number (Re), the drag force magnitude also changes. This variation of the drag force is shown in Figure 3.4.4 with three different graph plots. Figure 3.4.4 (a) is a graph of drag force vs. dimensionless time (τ) considering the four cases of Reynolds number (Re). It is clear from the graph that there is an effect of changing the velocity on Drag force. The drag force is initially high, and with the rise of dimensionless time (τ), it reduces and becomes constant. From Figure 3.4.4 (b) surface plot, it is observed that by the increase of Reynolds number (Re), the drag force also increases because the drag force is proportional to the square of fluid velocity. The highest drag force is found in the case of $Re = 200$, and the lowest drag force is got from the case of $Re = 50$. It is also observed that the case of $Re = 100$ has the 2 times drag force than the drag force exerted in the case of $Re = 50$. Following that, the case of $Re = 150$ and $Re = 200$ has the 2.6 and 3.6 times drag force, respectively, compared to the case of $Re = 50$. So, it is concluded that the drag force increases with the rise of the fluid velocity and vice versa.

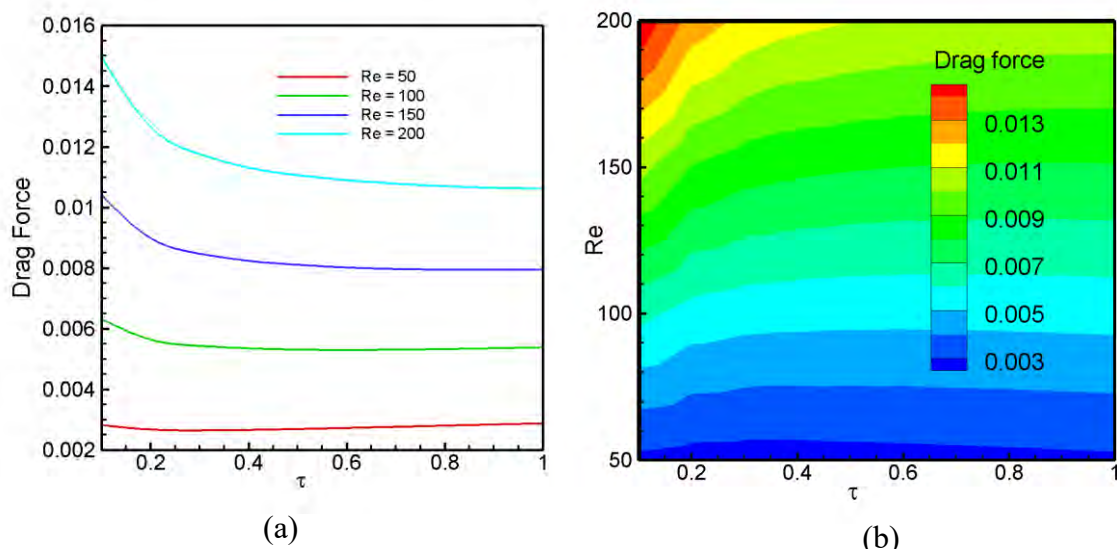


Figure 3.4.4: Effect of Reynolds number, Re and dimensionless time τ on Drag force of the moving lid at the fixed values of $Rd = 1$, $Ri = 1$, $Ha = 10$, $\phi = 0.05$, $Pr = 23.004$.

3.4.5 Effect on the Pressure Gradient

As Reynolds number (Re) varies in this study, there should be a change of pressure gradient through the fluid domain. Figure 3.4.5 (a) depicts a graph of the pressure gradient ($Grad P$) vs. dimensionless time (τ) varying Reynolds number (Re). Higher Reynolds number (Re) results in a lower pressure gradient ($Grad P$). As a result, $Re = 200$ case shows the lowest pressure gradient ($Grad P$) value, and $Re = 50$ case reports the highest pressure gradient ($Grad P$) among the four cases. The pressure gradient ($Grad P$) value is 22% higher in the case of $Re = 150$ than in the case of $Re = 200$. The case of $Re = 50$ and $Re = 100$ gives 122% and 55% more pressure gradient ($Grad P$) value than the case of $Re = 200$. A surface plot of the change of pressure gradient ($Grad P$) is shown in Figure 3.4.5 (b) with the variation of Reynolds number (Re) and dimensionless time (τ). It is observed that with the increase of dimensionless time (τ), the pressure gradient ($Grad P$) also increases. The rate of pressure gradient change is higher when the fluid velocity is low.

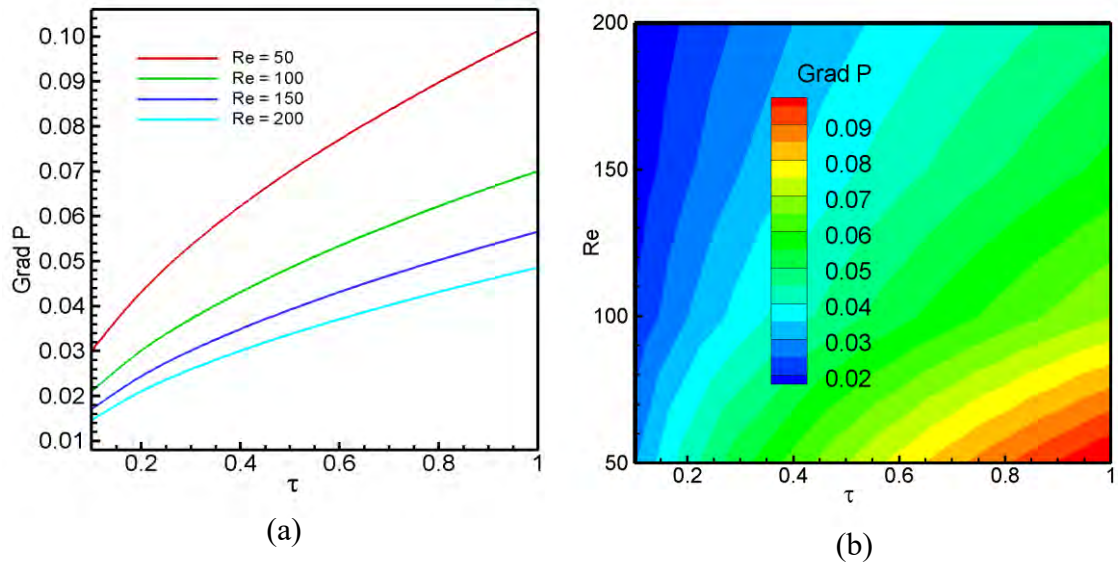


Figure 3.4.5: Effect of Reynolds number, Re and dimensionless time τ on pressure gradient at the fixed values of $Rd = 1$, $Ri = 1$, $Ha = 10$, $\phi = 0.05$, $Pr = 23.004$.

3.4.6 Effect on the Mean Heat Transfer Rate

Heat flux is situated in the semicircular heated region and heat is transferred to the fluid. The mean heat transfer rate is not the same throughout the dimensionless time (τ) at the transient condition. A graph is plotted in Figure 3.4.6 (a), which shows the Nusselt number (Nu_h) change with the rise of dimensionless time (τ), varying the Reynolds number (Re) value. The graph shows that the mean heat transfer rate stays initially high and with the dimensionless time (τ) it decreases for all the cases. It is also observed that with the increase of velocity, the Nusselt number (Nu_h) also increases. Figure 3.4.6 (b) denotes a surface plot showing the Nusselt number (Nu_h) variation by changing the value of Reynolds number (Re) and dimensionless time (τ). The case of $Re=200$ reports the highest Nusselt number (Nu_h) value and the case of $Re=50$ shows the lowest Nusselt number (Nu_h) value.

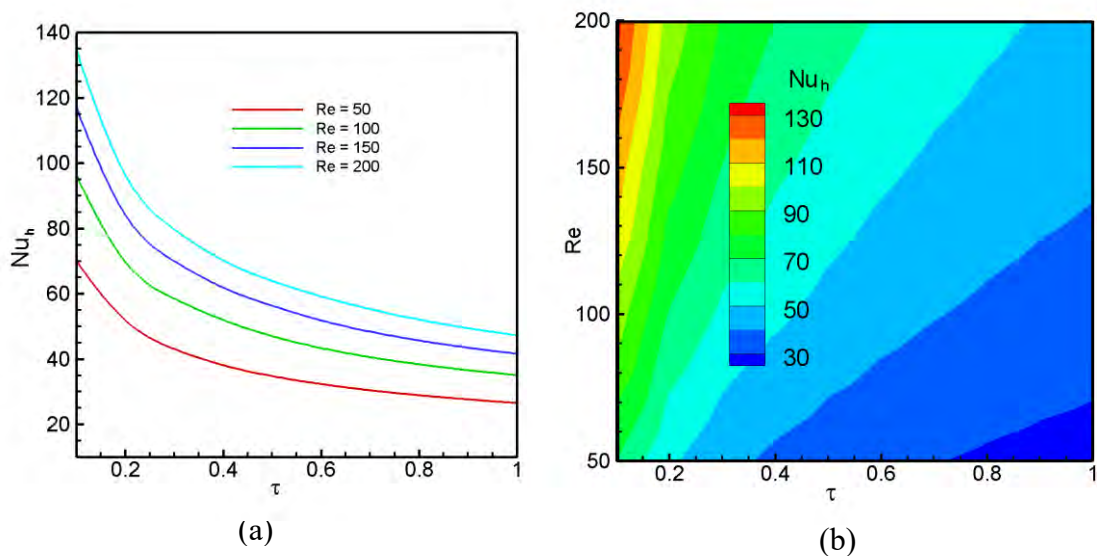


Figure 3.4.6: Effect of Reynolds number, Re and dimensionless time τ on mean heat transfer rate from the heated surface at the fixed values of $Rd = 1$, $Ri = 1$, $Ha = 10$, $\phi = 0.05$, $Pr = 23.004$.

3.4.7 Effect on the Fluid Temperature Gradient

Reynolds number (Re) has a significant impact on the fluid temperature gradient. Figure 3.4.7 (a) represents the fluid temperature gradient vs dimensionless time (τ) plot where it is observed that with the increase of dimensionless time (τ) the fluid temperature gradient rises. However, observing the four different Reynolds number (Re) cases, the fluid gradient temperature decreases when the Reynolds number (Re) increases. As a result, the highest fluid gradient temperature is found in the case of $Re = 50$. Moreover, the fluid gradient temperature is got lowest in the case of $Re = 200$. Fluid gradient temperature in the case of $Re = 150$ is 2.5% greater than the case of $Re = 200$. Moreover, the cases of $Re = 100$ and $Re = 50$ report around 7% and 12% higher fluid temperature gradient, respectively, than the case of $Re = 200$. So, it is concluded that fluid gradient temperature falls when the nanofluid velocity increases and vice versa.

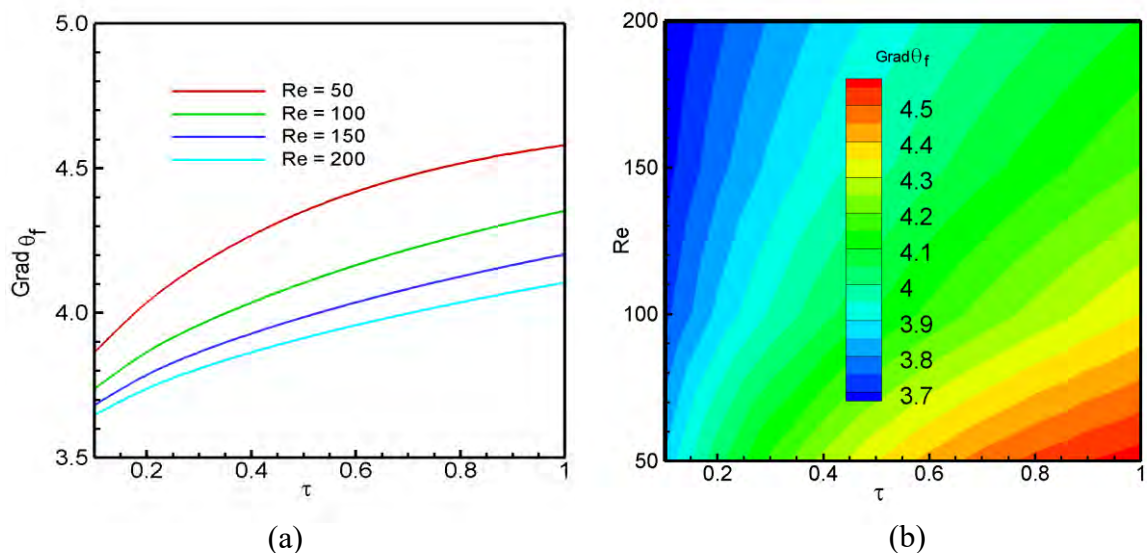


Figure 3.4.7: Effect of Reynolds number, Re and dimensionless time τ on fluid temperature gradient at the fixed values of $Rd = 1$, $Ri = 1$, $Ha = 10$, $\phi = 0.05$, $Pr = 23.004$.

3.4.8 Effect on Average Fluid Temperature

Likewise, fluid gradient temperature, the average fluid temperature changes with fluid velocity magnitude. When the Reynolds number (Re) rises, the average fluid temperature falls accordingly. Such a thing is noticed in Figure 3.4.8 (a), which is average fluid temperature vs. dimensionless time (τ) plot varying four Reynolds numbers (Re). At the transient conditions, it shows that the average fluid temperature increases with dimensionless time (τ) and vice versa. The surface plot in Figure 3.4.8 (b) gives a better visualization. The highest average fluid temperature value is found in the case of $Re = 50$ and the lowest is found in the case of $Re = 200$. At the dimensionless time (τ) 1, the average fluid temperature is 2.2 times higher in the case of $Re = 50$ than in the case of $Re = 200$. So, it is concluded that the higher the fluid velocity, the lower the fluid temperature is found.

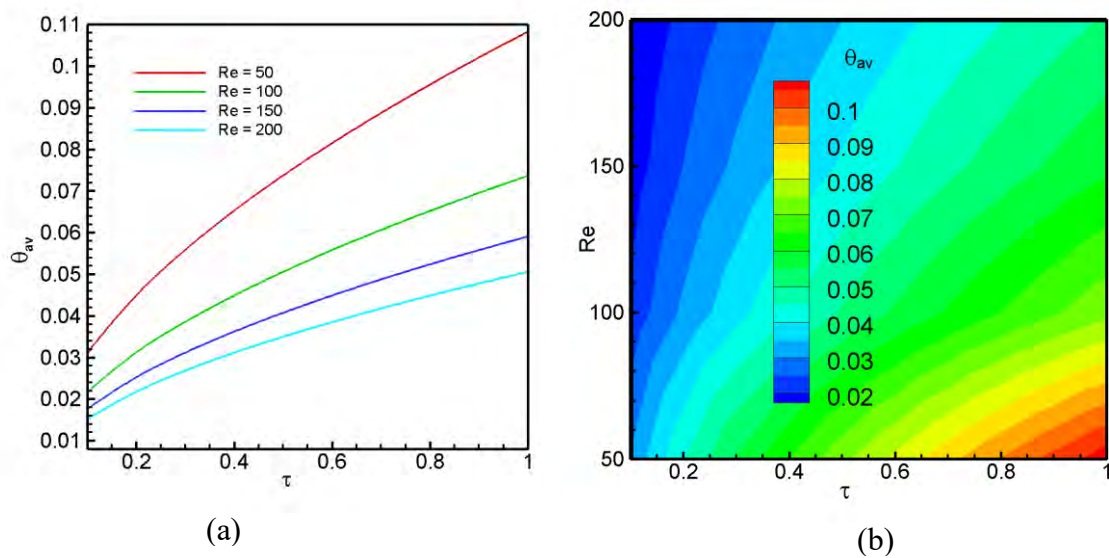


Figure 3.4.8: Effect of Reynolds number, Re and dimensionless time τ on average temperature of the fluid at the fixed values of $Rd = 1$, $Ri = 1$, $Ha = 10$, $\phi = 0.05$, $Pr = 23.004$.

3.4.9 Effect on the Bulk Temperature of the Fluid

The bulk fluid temperature affects Reynolds number (Re) considering the constant MHD radiative mixed convection with the fixed value of nanofluid concentration. Like average fluid temperature, bulk fluid temperature also decreases with the rise of fluid velocity. Figure 3.4.9 (a) shows a plot of the effect of Reynolds number (Re) on bulk fluid temperature. In the case of $Re = 50$ the highest bulk temperature of fluid is found, and in the case of $Re = 200$ it is found the lowest. Figure 3.4.9 (b) shows a surface plot, which states that the bulk fluid temperature increases with dimensionless time (τ) for all the cases. The contour on the top resembles the highest value of the bulk fluid temperature in the case of the lowest possible Reynolds number (Re). So, it is concluded that when the fluid flow is minimal, the bulk fluid temperature is the maximum.

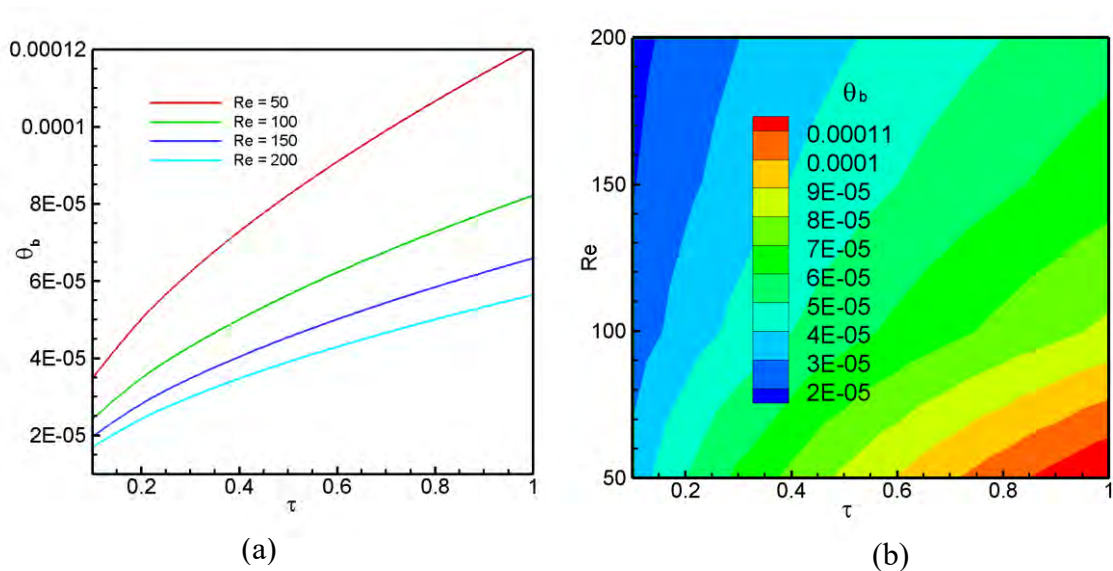


Figure 3.4.9: Effect of Reynolds number, Re and dimensionless time τ on bulk temperature of the fluid at the fixed values of $Rd = 1$, $Ri = 1$, $Ha = 10$, $\phi = 0.05$, $Pr = 23.004$.

3.5 EFFECT OF RICHARDSON NUMBER

This study analyzes the Richardson number (Ri) effect in a cavity flow using CNT Kerosene-based nanofluid. Richardson number (Ri) is a parameter that defines the heat transfer condition as natural or forced convection. Four Richardson numbers ($Ri = 0.1, 1, 5, 10$) are considered for this study using the constant value of the magnetic field, radiation parameter, nanofluid concentration, and fluid flow velocity. The case of $Ri = 1$ indicates the convection is neither natural nor forced dominant. Both the conditions are taken place in this case. The case of $Ri = 0.1$ indicates the forced convection. And finally, the natural convection dominant cases are the cases of $Ri = 5$ and $Ri = 10$.

3.5.1 Effect on Flow Movement

Figure 3.5.1 represents the velocity streamline plot varying Richardson number (Ri) and dimensionless time (τ) to observe the fluid flow pattern in the fluid domain. Three different dimensionless times ($\tau = 0.1, 0.5, 1$) are considered to observe how the streamline changes with time. As the fluid passes over the semicircular region, the vorticity creates in two sides of the cavity. It is observed that by the rise of dimensionless time (τ), the vorticity increases for all the cases. So, at dimensionless time $\tau = 1$, the highest vorticity value is found considering a constant Richardson number (Ri).

The vorticity is found lowest in the $Ri = 0.1$ case, which means the forced convection lessens the vorticity effect on the flow. In the case of $Re = 1$, the vorticity increases around 10 times than the case of $Ri = 0.1$. The highest vorticity is reported in the case of $Ri = 10$, where there is less significance of forced convection. The $Ri = 0.1$ case reports the lowest vorticity among the cases. Therefore, it is concluded that high value of Richardson number (Ri) ensures the higher vorticity near the semicircular region. The higher the dominance of natural convection, the higher the vorticity value in this study is noticed. Among all the cases and states, the highest vorticity value is found 0.03825 in $Ri = 10$ and the dimensionless time $\tau = 1$ case. The lowest value is got is 0.00003 in case of $Ri = 0.1$ and dimensionless time $\tau = 0.1$ case.

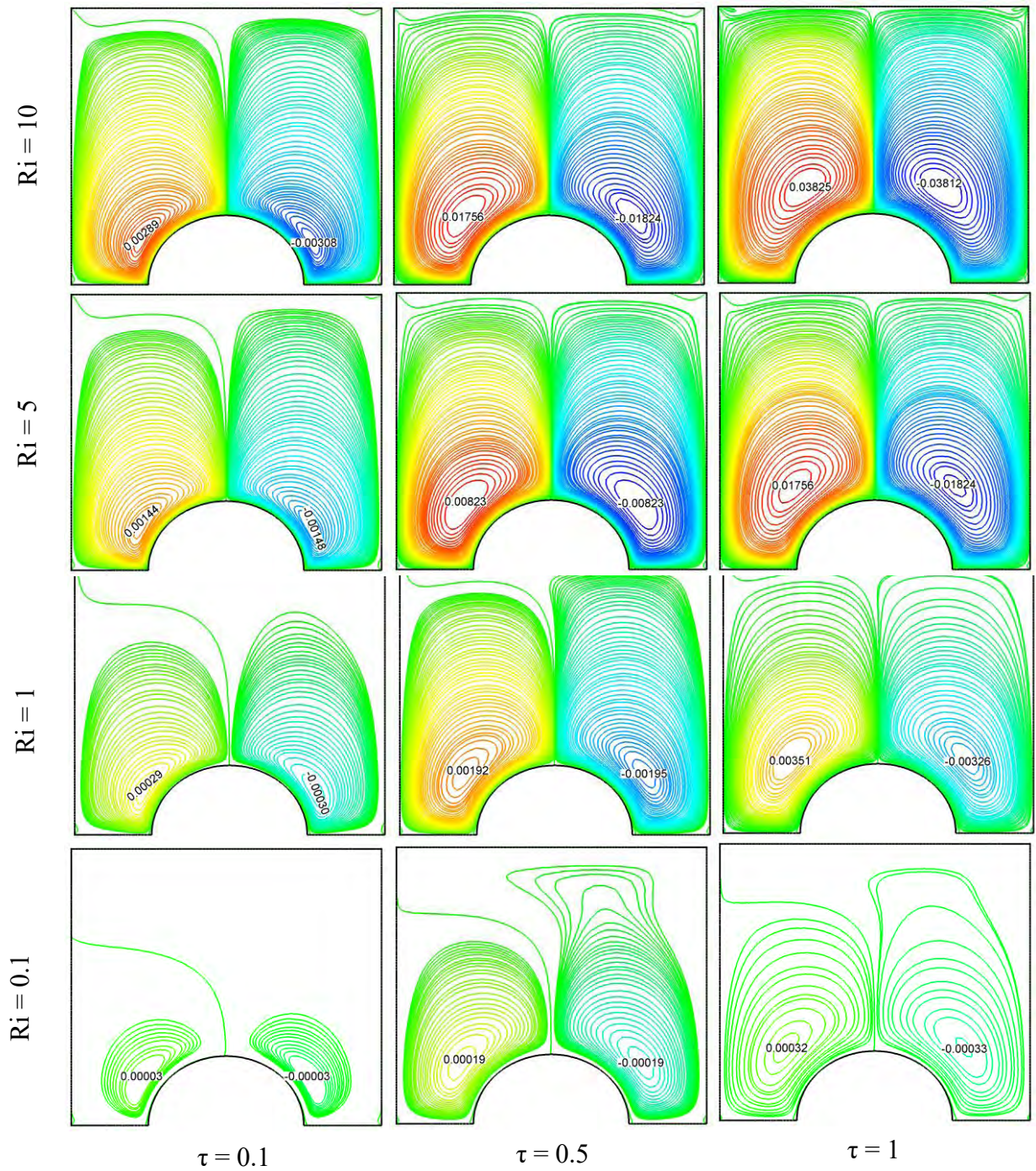


Figure 3.5.1: Effect of Richardson number, Ri on streamlines for changed values of dimensionless time τ at $\phi = 0.05$, $Re = 100$, $Rd = 1$, $Ha = 10$, $Pr = 23.004$.

3.5.2 Effect on the Temperature in the Flow Field

Isotherm plots for four different cases of Richardson number (Ri) varying the dimensionless time (τ) are placed in Figure 3.5.2. From these plots, the temperature distribution in the fluid domain can be observed. The heater is placed at the semicircular region, and it transfers heat to the nanofluid. The temperature variation is evident, and it is clear from the figure that the temperature variation becomes intense with the rise of the Richardson number (Ri). With the increase of dimensionless time (τ), the temperature variation also increases for all the cases of the Richardson number (Ri). The highest temperature variation is found in the $Ri = 10$ case, and the lowest is found in the $Ri = 0.1$ case. In other words, when the natural convection took place in the study, the temperature variation became the highest, and when the forced convection took place, the temperature variation became the lowest.

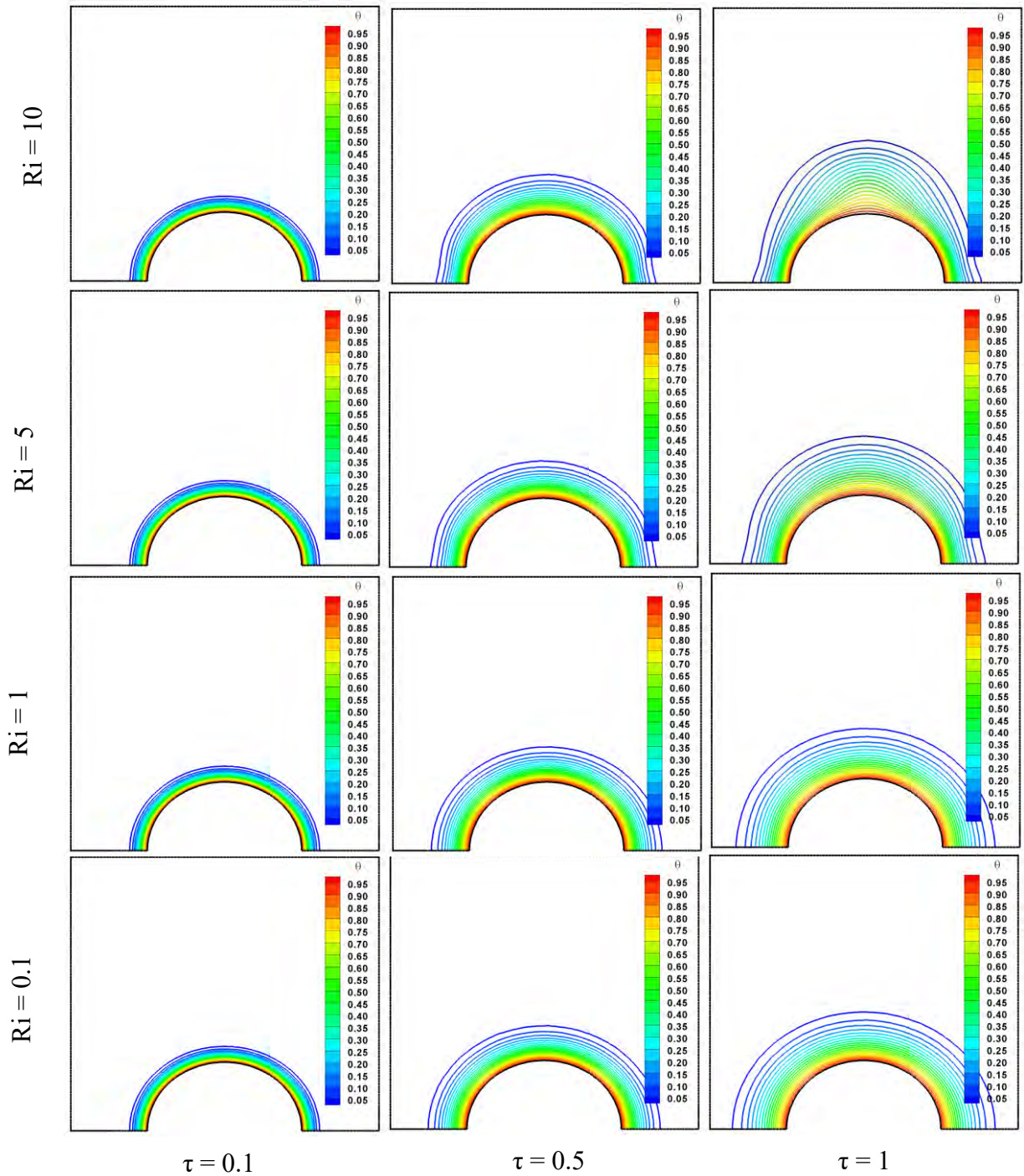


Figure 3.5.2. Effect of Richardson number, Ri on isotherms for changed values of dimensionless time τ at $\phi = 0.05$, $Re = 100$, $Rd = 1$, $Ha = 10$, $Pr = 23.004$.

3.5.3 Effect on the Velocity Magnitude

The velocity field is not the same through the fluid domain. Figure 3.5.3 (a) represents a velocity field magnitude plot varying the dimensionless time (τ) and the Richardson number (Ri). The velocity magnitude is high at the natural convection state and low at the forced convection condition. It is observed from the plot that the higher the Richardson number (Ri), the higher the velocity magnitude is reported. Therefore, the highest velocity magnitude is found in the $Ri = 10$ case, and the lowest is found in the $Ri = 0.1$ case. Figure 3.5.3 (b) shows a surface plot of velocity magnitude varying the Richardson number (Ri) and dimensionless time (τ). At the dimensionless time ($\tau = 1$), the velocity magnitude is 18 times higher in the $Ri = 10$ case than in the $Ri = 1$ case. Similarly, the velocity magnitude is 2.3 times higher in the $Ri = 10$ case than in the $Ri = 5$ case. The velocity magnitude increases for the case of $Ri = 1, 5, \text{ and } 10$ with the rise of dimensionless time (τ). In the $Ri = 0.1$ case, the velocity magnitude does not increase with dimensionless time (τ).

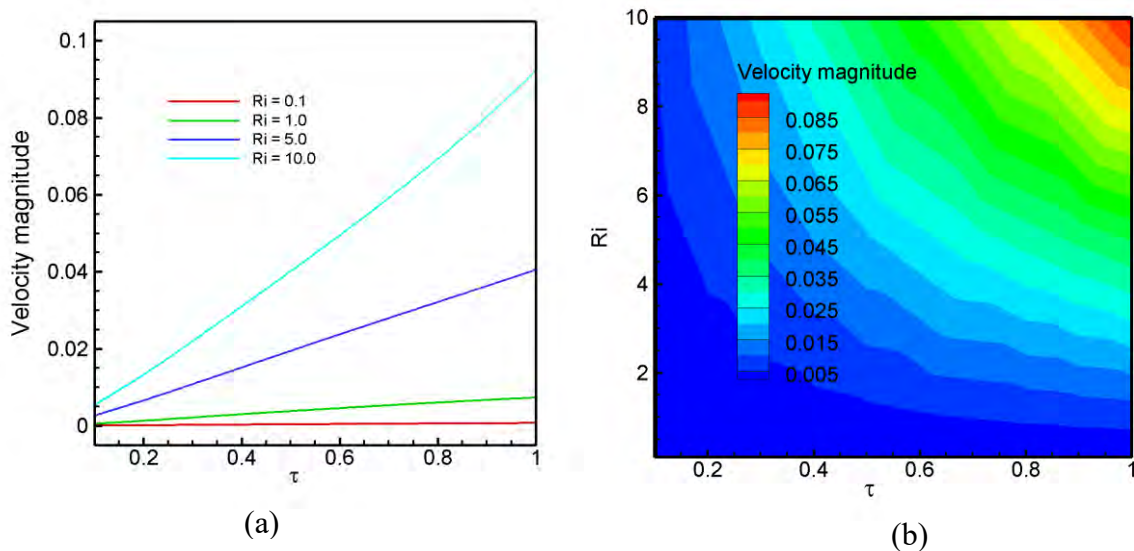


Figure 3.5.3: Effect of Richardson number, Ri and dimensionless time τ on velocity field at the fixed values of $Re = 100$, $Rd = 1$, $Ha = 10$, $\phi = 0.05$, $Pr = 23.004$.

3.5.4 Effect on Drag Force

The nanofluid passes over a semicircular cavity which causes the drag force in the fluid domain. The natural or forced convection condition significantly affects the drag force, which can be observed in Figure 3.5.4 (a). It is a drag force vs. dimensionless time (τ) graph considering the four cases of Richardson number (Ri). It is observed that in the $Ri = 0.1$ and the $Ri = 1$ cases, the drag force decreases with dimensionless time (τ), and at a specific dimensionless time (τ) it becomes constant. In natural convection cases ($Ri = 5$ and 10), the drag force becomes high with dimensionless time (τ). From the surface plot in Figure 3.5.4 (b), it is observed that when the Richardson number (Ri) rises, the drag force is also increased and vice versa. As a result, the highest drag force is observed in the $Ri = 10$ case, which is natural convection dominant. The case of $Ri = 0.1$, reports the lowest drag force in this study. At the dimensionless time ($\tau = 1$), the case of $Ri = 10$ produces 2.8 times higher drag force than the case of $Ri = 0.1$.

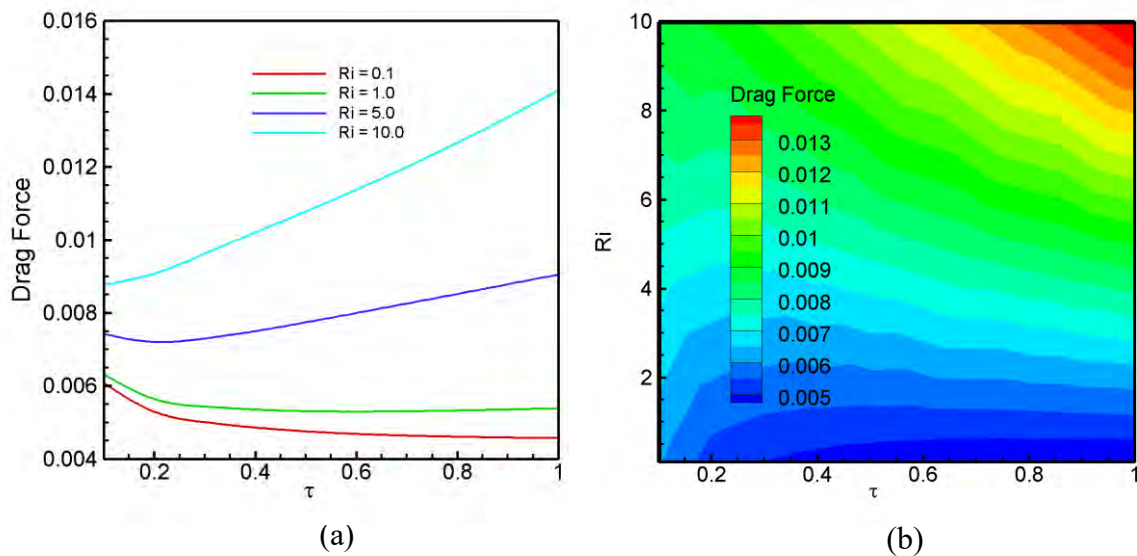


Figure 3.5.4: Effect of Richardson number, Ri and dimensionless time τ on Drag force of the moving lid at the fixed values of $Re = 100$, $Rd = 1$, $Ha = 10$, $\phi = 0.05$.

3.5.5 Effect on the Pressure Gradient

Richardson number (Ri) affects the pressure in the fluid domain. Figure 3.5.5 (a) represents a graph of the pressure gradient ($Grad P$) varying the Richardson number (Ri) and dimensionless time (τ). It is observed that the pressure gradient ($Grad P$) rises when the Richardson number (Ri) increases. So, the highest value of pressure gradient ($Grad P$) is reported in the $Ri = 10$ case, and the lowest value is got from the $Ri = 0.1$ case. At the transient condition, the pressure gradient ($Grad P$) increases with dimensionless time (τ) except for the condition of $Ri = 0.1$, which is forced convection dominant. Similar phenomena can be observed from a surface plot placed in Figures 4.5 (b). It is observed that at the dimensionless time (τ) = 1, the pressure gradient ($Grad P$) at the case of $Ri = 10$ is 15 times higher than at the case of $Ri = 1$. So, it is concluded that natural convection causes greater pressure gradient ($Grad P$) than forced convection considering other parameters as constant.

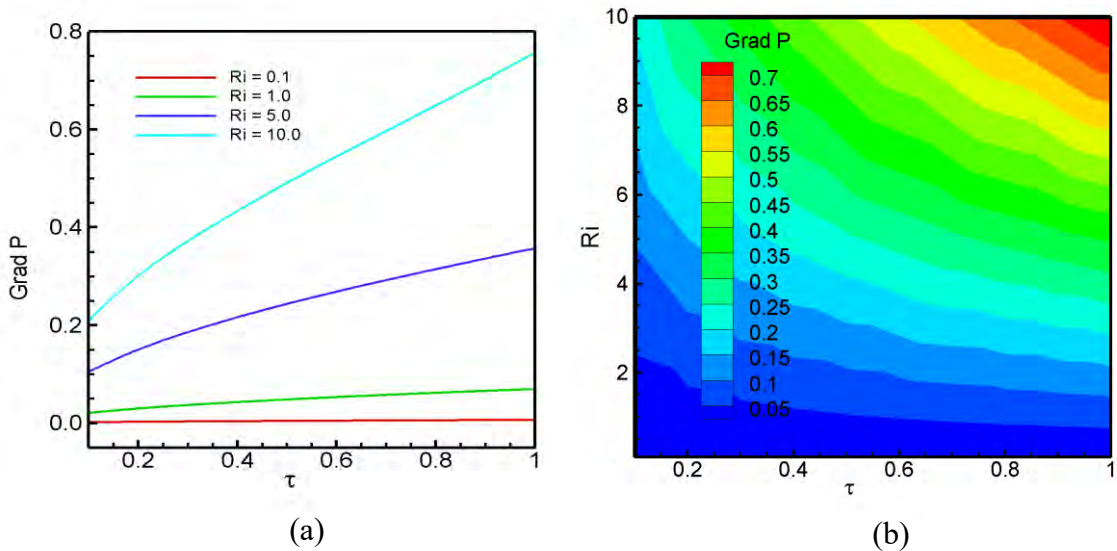


Figure 3.5.5: Effect of Richardson number, Ri and dimensionless time τ on pressure gradient of the fluid at the fixed values of $Re = 100$, $Rd = 1$, $Ha = 10$, $\phi = 0.05$, $Pr = 23.004$.

3.5.6 Effect on the Mean Heat Transfer Rate

Heat transfer took place due to the temperature difference between the heated surface and the nanofluid. Figure 3.5.6 (a) shows the mean heat transfer rate varying the dimensionless time (τ) and Richardson number (Ri). The case of $Ri = 10$, which is natural convection dominant case, shows the highest heat transfer rate. The $Ri = 1$ case, considered a forced convection case, reports the lowest heat transfer rate. A similar result can be seen from the surface plot placed in Figure 3.5.6 (b). It is clear from the plot that the Richardson number (Ri) increases the Nusselt number (Nu_h). Furthermore, the heat transfer rate becomes low with dimensionless time (τ) for all the cases.

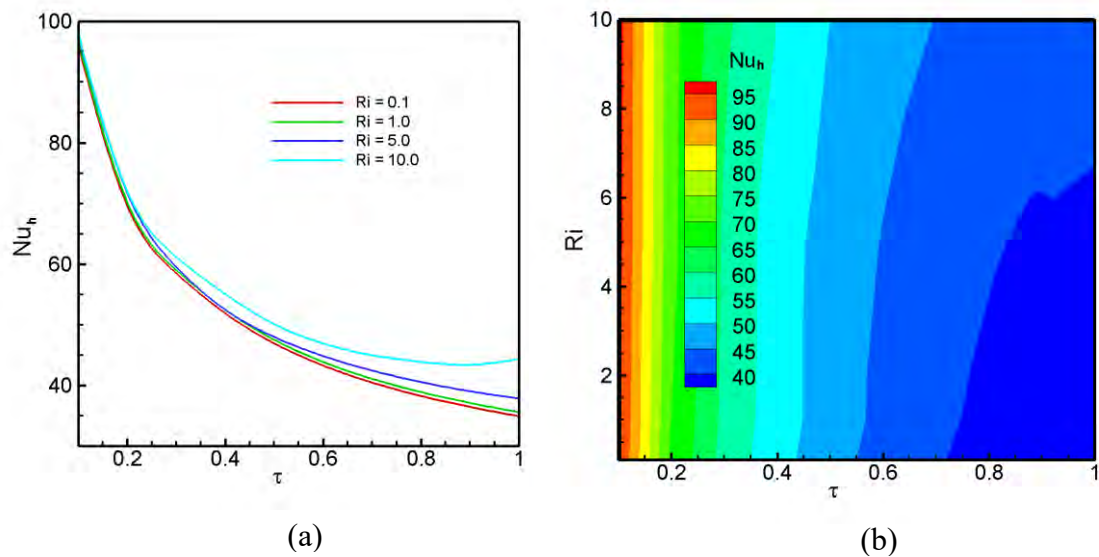


Figure 3.5.6: Effect of Richardson number, Ri and dimensionless time τ on mean heat transfer rate from the heated surface at the fixed values of $Re = 100$, $Rd = 1$, $Ha = 10$, $\phi = 0.05$, $Pr = 23.004$.

3.5.7 Effect on the Fluid Temperature Gradient

Figure 3.5.7 (a) represents a graph of fluid temperature gradient vs. dimensionless time (τ) varying the heat transfer conditions. The higher the Richardson number (Ri), the higher the fluid temperature gradient is observed from the figure. As a result, the highest fluid temperature gradient is got when the condition is natural convection dominant. The lowest fluid temperature gradient is found in the $Ri = 0.1$ case, which is a forced convection dominant case. Figure 3.5.7 (b) shows a surface plot describing the fluid temperature gradient variation. It is clear from the plot that the fluid temperature gradient increases with dimensionless time (τ). The fluid temperature gradient in the $Ri = 10$ case increases approximately 18% than in the $Ri = 0.1$ case. So, it is concluded that natural convection condition helps to increase the fluid temperature gradient.

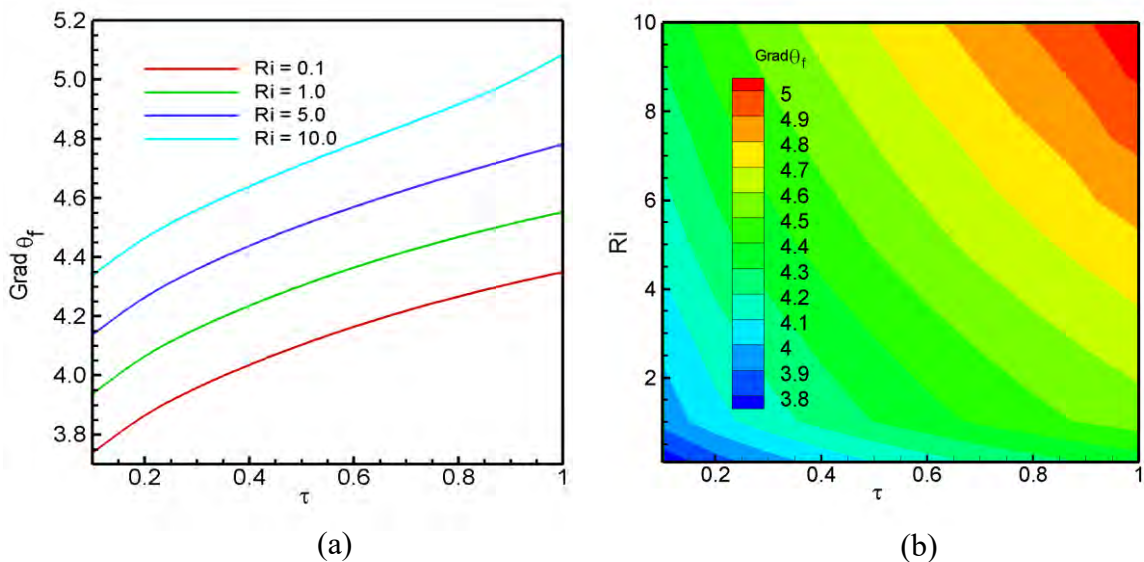


Figure 3.5.7 Effect of Richardson number, Ri and dimensionless time τ on fluid temperature gradient at the fixed values of $Re = 100$, $Rd = 1$, $Ha = 10$, $\phi = 0.05$, $Pr = 23.004$.

3.5.8 Effect on Average Fluid Temperature

Similar to the fluid temperature gradient, the average fluid temperature changes with the change of Richardson number (Ri). Figure 3.5.8 (a) shows a graph representing average fluid temperature varying the dimensionless time (τ) and Richardson number (Ri). The average fluid temperature becomes high with the rise of dimensionless time (τ) and vice versa. Moreover, a surface plot is placed in Figure 3.5.8 (b). The higher the value of Richardson number (Ri), the higher the average fluid temperature is found. Natural convection-dominated $Ri = 10$ case reports the highest value of average fluid temperature, whereas forced convection-dominated $Ri = 0.1$ case shows the lowest. The average fluid temperature in the case of $Ri = 10$ is 1.85 times higher than the $Ri = 0.1$ case. Therefore, it is concluded that natural convection affects the average fluid temperature the most.

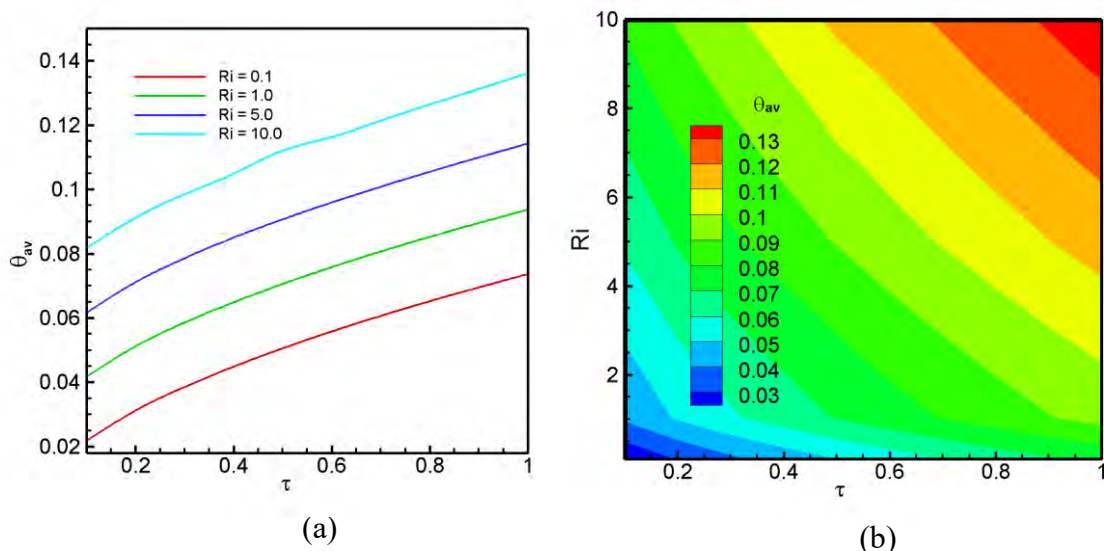


Figure 3.5.8: Effect of Richardson number, Ri and dimensionless time τ on average temperature of the fluid at the fixed values of $Re = 100$, $Rd = 1$, $Ha = 10$, $\phi = 0.05$, $Pr = 23.004$.

3.5.9 Effect on the Bulk Temperature of the Fluid

The bulk fluid temperature depends on the condition of heat transfer. When the natural convection dominates, the bulk fluid temperature becomes high. Also, when the forced convection exists, the bulk fluid temperature becomes low. Such thing is observed from Figure 3.4.9 (a). It is a bulk fluid temperature vs. dimensionless time (τ) graph considering four Richardson number (Ri) cases. A surface plot is also shown in Figure 3.4.9 (b). It is observed that the highest bulk fluid temperature reports in the case of $Ri = 10$, and the lowest bulk fluid temperature is found in the $Ri = 0.1$ case. When the dimensionless time (τ) increases at transient conditions, the bulk fluid temperature also increases. The highest bulk fluid temperature is found at dimensionless time (τ) = 1 considering a constant heat transfer condition. So, it is concluded that the higher the dimensionless number (τ) and the Richardson number (Ri), the higher the bulk fluid temperature will be.

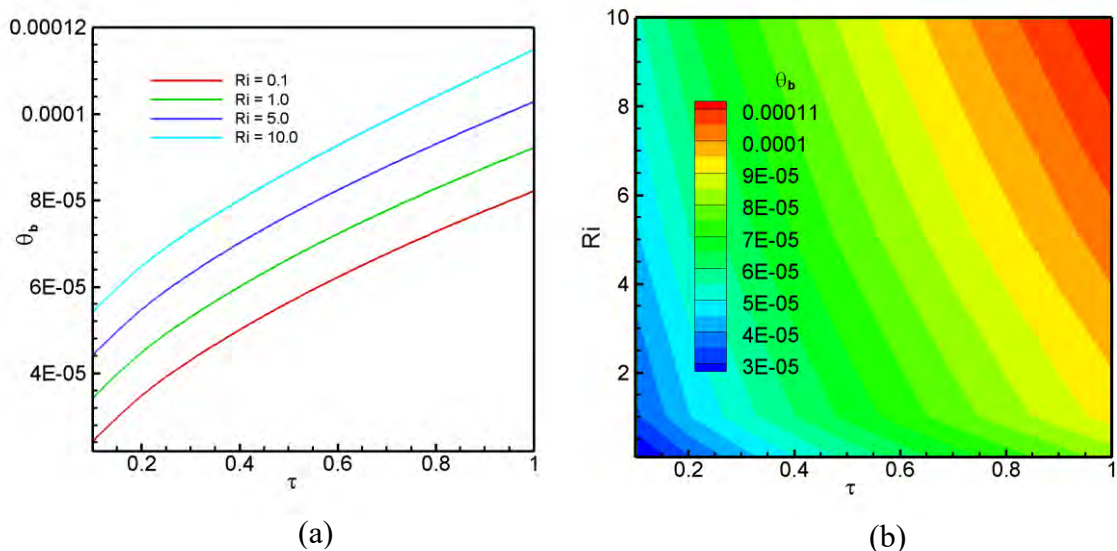


Figure 3.5.9: Effect of Richardson number, Ri and dimensionless time τ on bulk temperature of the fluid at the fixed values of $Re = 100$, $Rd = 1$, $Ha = 10$, $\phi = 0.05$. $Pr = 23.004$

CHAPTER 4

CONCLUSIONS

The MHD mixed convection of a kerosene oil-based carbon nanotube nanofluid in a square lid driven cavity is analyzed using finite element analysis, considering the unsteady radiative heat flow. Authors demonstrated the application of a semicircular heater with constant temperature in the bottom wall and including a radiative source term in the energy equation. In addition, for Brownian motion of the nanoparticle, it takes the effective thermal conductivity and dynamic viscosity into account. The effects of radiation parameter on drag force, streamlines, isotherm, Nusselt number, fluid temperature gradient magnitude, velocity magnitude, average temperature of the domain, bulk temperature and pressure gradient are explored. Additionally, a section on the scope of future study in related topics of inquiry is offered.

4.1 SUMMARY OF THE MAJOR OUTCOMES

Five different parameters are used: the Radiation parameter ($Rd = 0 - 2$), the Hartmann number ($Ha = 0 - 50$), the solid volume fraction ($\phi = 0 - 10\%$), the Reynolds number ($Re = 50 - 200$), and the Richardson number ($Ri = 0.1 - 10$). The Prandtl number is set to 23.004 and Kerosene oil-based nanofluids are used. The following main conclusions are drawn from the present study:

- Radiation Parameter: Radiation strengthens the fluid flow that travels through the greater vorticity. After increasing the radiation from 0 to 2, the fluid temperature increases nearly thrice at the near-wall. With increasing radiation intensity, the magnitude of velocity, drag force, pressure gradient magnitude, fluid temperature gradient magnitude, average fluid temperature, and fluid bulk temperature all increase. The heat transfer rate of the semicircular heater reduces as the radiation parameter increases. In the fluid domain, the magnitudes of velocity, pressure gradient, temperature gradient, average temperature, and bulk temperature all grow as dimensionless time increases. However, after a period, it begins to behave stable. The drag force of the moving lid and the heat transfer rate of the semicircular heater diminish as the

dimensionless time value increases and, after a time, consistent behavior begins.

- Hartmann number: The magnetic field hinders the fluid flow, resulting in reduced vorticity and velocity field value. The heat transfer rate also reduced with the increase of Hartmann number (Ha) and the case of $Ha = 50$ has the highest Nusselt number (Nu) value. The average temperature, mean temperature, bulk temperature, and pressure gradient of the fluid decreases when the magnetic field becomes intense. With the increase of dimensionless time (τ), the velocity, vorticity, drag force, pressure gradient, and fluid temperature increase.
- Solid Volume fraction: Particle concentration raises the fluid's thermophysical characteristics as well as the heater's heat transfer rate. The magnitude of the fluid temperature gradient is at pic, and it is approximately 9 times more than the 0% particle concentration. The velocity magnitudes, pressure gradient, temperature gradient, average temperature, and bulk temperature all increase with increasing dimensionless time in the fluid domain. However, after a period of time, it begins to exhibit stable behavior. As the dimensionless time value increases, the drag force of the sliding lid and the heat transfer rate of the semicircular heater decrease, and after a period, consistent behavior occurs.
- Reynolds number: the velocity streamlines showed the vorticity increases by 54% in the $Re=200$ case than the $Re=50$ case. The mean heat transfer rate and drag force increase with the increase of velocity magnitude. The case of Reynolds number (Re) = 200 reported the highest Nusselt number (Nu_h) in the study. When the Reynolds number (Re) rises, the pressure gradient, average temperature, mean temperature, and bulk temperature of the fluid decreases. At transient conditions, the fluid's velocity, vorticity, temperature, and pressure gradient increase with dimensionless time (τ), whereas the mean heat transfer rate and drag force decrease (τ).
- Mixed convection parameter (Ri): the fluid velocity is lower at the natural convection case than the forced convection. When the heat transfer condition becomes natural convection dominant, the fluid temperature becomes intense.

Drag force is 2.8 times higher in the $Ri=10$ case than in the $Ri=0.1$ case. At the natural convection state, the pressure gradient was also reported higher. Higher Nusselt number (Nuh) is also found in natural convection conditions. Velocity, average temperature, bulk temperature, the temperature gradient of the fluid, drag force, and pressure increase with dimensionless time (τ) at unsteady conditions. But mean heat transfer decreases for all the cases of natural and forced convection.

4.2 FURTHER WORKS

The following may be proposed for further investigation as follow-ups to the current study:

- ❖ The governing equations of concentration conservation may be used to study double diffusive mixed convection.
- ❖ Magnetic fluid may be used in place of electrically conducting fluid inside the porous medium, and the boundary conditions of the cavity's walls can be changed.
- ❖ The analysis may be expanded to include turbulent flow with various fluids and thermal boundary conditions such as constant heat flux.
- ❖ This thesis analyzes just two-dimensional fluid flow and heat transmission. As a result, this discussion may be expanded to three-dimensional studies in order to study the impact of factors on flow fields and heat transfer in cavities.

REFERENCES

- [1] Azad, A., "MHD combined convection in a channel with cavity using nanofluids," 2016, Accessed: Aug. 06, 2021. [Online]. Available: <http://lib.buet.ac.bd:8080/xmlui/handle/123456789/4539>.
- [2] Powell, K. G., Roe, P. L., Linde, T. J., Gombosi, T. I., and De Zeeuw, D. L., "A Solution-Adaptive Upwind Scheme for Ideal Magnetohydrodynamics," *J. Comput. Phys.*, vol. 154, no. 2, pp. 284–309, Sep. 1999, doi: 10.1006/JCPH.1999.6299.
- [3] Shercliff, J. A., "Textbook of magnetohydrodynamics.," 1965.
- [4] Roberts, P. H., "*An introduction to magnetohydrodynamics.*" UMI, 1967.
- [5] Howell J. R., Menguc M. P., and Siegel R., "Thermal Radiation Heat Transfer," *Therm. Radiat. Heat Transf.*, Sep. 2010, doi: 10.1201/9781439894552.
- [6] Khanafer K. and Vafai K., "A critical synthesis of thermophysical characteristics of nanofluids," *Int. J. Heat Mass Transf.*, vol. 54, no. 19–20, pp. 4410–4428, Sep. 2011, doi: 10.1016/J.IJHEATMASSTRANSFER.2011.04.048.
- [7] Yu W. and Choi S. U. S., "The Role of Interfacial Layers in the Enhanced Thermal Conductivity of Nanofluids: A Renovated Maxwell Model," *J. Nanoparticle Res. 2003 51*, vol. 5, no. 1, pp. 167–171, Apr. 2003, doi: 10.1023/A:1024438603801.
- [8] Yu W. and Choi S. U. S., "The role of interfacial layers in the enhanced thermal conductivity of nanofluids: A renovated Hamilton-Crosser model," *J. Nanoparticle Res.*, vol. 6, no. 4, pp. 355–361, Aug. 2004, doi: 10.1007/s11051-004-2601-7.
- [9] Jang S. P. and Choi S. U. S., "Role of Brownian motion in the enhanced thermal conductivity of nanofluids," *Appl. Phys. Lett.*, vol. 84, no. 21, pp. 4316–4318, May 2004, doi: 10.1063/1.1756684.
- [10] Prasher R., Bhattacharya P., and Phelan P. E., "Brownian-motion-based convective-conductive model for the effective thermal conductivity of nanofluids," *J. Heat Transfer*, vol. 128, no. 6, pp. 588–595, Jun. 2006, doi: 10.1115/1.2188509.
- [11] Corcione M., "Empirical correlating equations for predicting the effective thermal conductivity and dynamic viscosity of nanofluids," *Energy Convers. Manag.*, vol. 52, no. 1, pp. 789–793, Jan. 2011, doi: 10.1016/J.ENCONMAN.2010.06.072.
- [12] Brinkman H. C., "The viscosity of concentrated suspensions and solutions," *J.*

- Chem. Phys.*, vol. 20, no. 4, p. 571, 1952, doi: 10.1063/1.1700493.
- [13] Batchelor G. K., “The effect of Brownian motion on the bulk stress in a suspension of spherical particles,” *J. Fluid Mech.*, vol. 83, no. 1, pp. 97–117, 1977, doi: 10.1017/S0022112077001062.
- [14] Lundgren T. S., “Slow flow through stationary random beds and suspensions of spheres,” *J. Fluid Mech.*, vol. 51, no. 2, pp. 273–299, Jan. 1972, doi: 10.1017/S002211207200120X.
- [15] Nguyen C. T., Desgranges F., Roy G., Galanis N., Maré T., Boucher S., Angue Mintsu H., “Temperature and particle-size dependent viscosity data for water-based nanofluids - Hysteresis phenomenon,” *Int. J. Heat Fluid Flow*, vol. 28, no. 6, pp. 1492–1506, Dec. 2007, doi: 10.1016/j.ijheatfluidflow.2007.02.004.
- [16] Namburu P. K., Kulkarni D. P., Misra D., and Das D. K., “Viscosity of copper oxide nanoparticles dispersed in ethylene glycol and water mixture,” *Exp. Therm. Fluid Sci.*, vol. 32, no. 2, pp. 397–402, Nov. 2007, doi: 10.1016/j.expthermflusci.2007.05.001.
- [17] Kulkarni D. P., Das D. K., and Vajjha R. S., “Application of nanofluids in heating buildings and reducing pollution,” *Appl. Energy*, vol. 86, no. 12, pp. 2566–2573, Dec. 2009, doi: 10.1016/j.apenergy.2009.03.021.
- [18] Fan S. and Li W., “Nanophotonic control of thermal radiation for energy applications [Invited],” *Opt. Express*, vol. 26, no. 12, pp. 15995–16021, Jun. 2018, doi: 10.1364/OE.26.015995.
- [19] Hunt J. C. R., “Lewis fry richardson and his contributions to mathematics, meteorology, and models of conflict,” *Annu. Rev. Fluid Mech.*, vol. 30, no. 1, pp. xiii–xxxvi, 1998, doi: 10.1146/annurev.fluid.30.1.0.
- [20] Rahman M. M., Parvin S., Saidur R., and Rahim N. A., “Magnetohydrodynamic mixed convection in a horizontal channel with an open cavity,” *Int. Commun. Heat Mass Transf.*, vol. 38, no. 2, pp. 184–193, 2011, doi: 10.1016/j.icheatmasstransfer.2010.12.005.
- [21] Manca O., Nardini S., Khanafer K., and Vafai K., “Effect of heated wall position on mixed convection in a channel with an open cavity,” *Numer. Heat Transf. Part A Appl.*, vol. 43, no. 3, pp. 259–282, Feb. 2003, doi: 10.1080/10407780307310.
- [22] Moallemi M. K. and Jang K. S., “Prandtl number effects on laminar mixed convection heat transfer in a lid-driven cavity,” *Int. J. Heat Mass Transf.*, vol. 35, no. 8, pp. 1881–1892, 1992, doi: 10.1016/0017-9310(92)90191-T.
- [23] Oztop H. F., Al-Salem K., and Pop I., “MHD mixed convection in a lid-driven cavity with corner heater,” *Int. J. Heat Mass Transf.*, vol. 54, no. 15–16, pp. 3494–3504, Jul. 2011, doi:

- 10.1016/J.IJHEATMASSTRANSFER.2011.03.036.
- [24] Ghorbani N., Taherian H., Gorji M., and Mirgolbabaei H., “Experimental study of mixed convection heat transfer in vertical helically coiled tube heat exchangers,” *Exp. Therm. Fluid Sci.*, vol. 34, no. 7, pp. 900–905, Oct. 2010, doi: 10.1016/J.EXPTHERMFLUSCI.2010.02.004.
- [25] Geridonmez B. P. and Oztop H. F., “Mixed Convection Heat Transfer in a Lid-Driven Cavity under the Effect of a Partial Magnetic Field,” *Heat Transf. Eng.*, pp. 1–13, 2020, doi: 10.1080/01457632.2020.1792622.
- [26] Chen X., Wu Y. T., Wang C., Wang X., and Ma C. F., “Flow and mixed convection heat transfer of Hitec salt in multi-sided heating pipes,” *Sustain. Energy Technol. Assessments*, vol. 47, p. 101375, Oct. 2021, doi: 10.1016/j.seta.2021.101375.
- [27] Rahman M. M., Öztop H. F., Saidur R., Mekhilef S., and Al-Salem K., “Finite element solution of MHD mixed convection in a channel with a fully or partially heated cavity,” *Comput. Fluids*, vol. 79, pp. 53–64, Jun. 2013, doi: 10.1016/J.COMPFLUID.2013.03.003.
- [28] Sheremet M. A., Oztop H. F., and Pop I., “MHD natural convection in an inclined wavy cavity with corner heater filled with a nanofluid,” *J. Magn. Magn. Mater.*, vol. 416, pp. 37–47, Oct. 2016, doi: 10.1016/j.jmmm.2016.04.061.
- [29] Mansour M. A., Rashad A. M., Mallikarjuna B., Hussein A. K., Aichouni M., and Kolsi L., “MHD mixed bioconvection in a square porous cavity filled by gyrotactic microorganisms,” *Int. J. Heat Technol.*, vol. 37, no. 2, pp. 433–445, 2019, doi: 10.18280/ijht.370209.
- [30] Rabbi K. M., Saha S., Mojumder S., Rahman M. M., Saidur R., and Ibrahim T. A., “Numerical investigation of pure mixed convection in a ferrofluid-filled lid-driven cavity for different heater configurations,” *Alexandria Eng. J.*, vol. 55, no. 1, pp. 127–139, Mar. 2016, doi: 10.1016/j.aej.2015.12.021.
- [31] Öztop H.F., RahmanM.M., Ahsan A., Hasanuzzaman M., Saidur R., KhaledAl-Salem, Rahimc N.A., “MHD natural convection in an enclosure from two semi-circular heaters on the bottom wall,” *Int. J. Heat Mass Transf.*, vol. 55, no. 7–8, pp. 1844–1854, Mar. 2012, doi: 10.1016/J.IJHEATMASSTRANSFER.2011.11.037.
- [32] Hasanuzzaman M., Öztop H. F., Rahman M. M., Rahim N. A., Saidur R., and Varol Y., “Magnetohydrodynamic natural convection in trapezoidal cavities,” *Int. Commun. Heat Mass Transf.*, vol. 39, no. 9, pp. 1384–1394, Nov. 2012, doi: 10.1016/J.ICHEATMASSTRANSFER.2012.08.009.
- [33] Selimefendigil F. and Öztop H. F., “Analysis of MHD mixed convection in a flexible walled and nanofluids filled lid-driven cavity with volumetric heat

- generation,” *Int. J. Mech. Sci.*, vol. 118, pp. 113–124, Nov. 2016, doi: 10.1016/j.ijmecsci.2016.09.011.
- [34] Barnoon P., Toghraie D., Dehkordi R. B., and Abed H., “MHD mixed convection and entropy generation in a lid-driven cavity with rotating cylinders filled by a nanofluid using two phase mixture model,” *J. Magn. Magn. Mater.*, vol. 483, pp. 224–248, Aug. 2019, doi: 10.1016/J.JMMM.2019.03.108.
- [35] Rashad A. M., Ismael M. A., Chamkha A. J., and Mansour M. A., “MHD mixed convection of localized heat source/sink in a nanofluid-filled lid-driven square cavity with partial slip,” *J. Taiwan Inst. Chem. Eng.*, vol. 68, pp. 173–186, Nov. 2016, doi: 10.1016/j.jtice.2016.08.033.
- [36] Hayat T., Khan M. I., Waqas M., Alsaedi A., and Farooq M., “Numerical simulation for melting heat transfer and radiation effects in stagnation point flow of carbon–water nanofluid,” *Comput. Methods Appl. Mech. Eng.*, vol. 315, pp. 1011–1024, Mar. 2017, doi: 10.1016/J.CMA.2016.11.033.
- [37] Bhuiyan A. A., Banna M. H., Barna S. F., Amin M. R., and Sadrul Islam A. K. M., “Numerical modelling of thermal characteristics in a microstructure filled porous cavity with mixed convection,” *Int. J. Heat Mass Transf.*, vol. 93, pp. 464–476, Feb. 2016, doi: 10.1016/J.IJHEATMASSTRANSFER.2015.10.004.
- [38] Çolak E., Ekici Ö., and Öztop H. F., “Mixed convection in a lid-driven cavity with partially heated porous block,” *Int. Commun. Heat Mass Transf.*, vol. 126, p. 105450, Jul. 2021, doi: 10.1016/J.ICHEATMASSTRANSFER.2021.105450.
- [39] Sheikholeslami M., “Magnetic field influence on nanofluid thermal radiation in a cavity with tilted elliptic inner cylinder,” *J. Mol. Liq.*, vol. 229, pp. 137–147, Mar. 2017, doi: 10.1016/J.MOLLIQ.2016.12.024.
- [40] Kalteh M., Javaherdeh K., and Azarbarzin T., “Numerical solution of nanofluid mixed convection heat transfer in a lid-driven square cavity with a triangular heat source,” *Powder Technol.*, vol. 253, pp. 780–788, Feb. 2014, doi: 10.1016/J.POWTEC.2013.12.039.
- [41] Shekaramiz M., Fathi S., Ataabadi H. A., Kazemi-Varnamkhasti H., and Toghraie D., “MHD nanofluid free convection inside the wavy triangular cavity considering periodic temperature boundary condition and velocity slip mechanisms,” *Int. J. Therm. Sci.*, vol. 170, p. 107179, Dec. 2021, doi: 10.1016/J.IJTHERMALSCI.2021.107179.
- [42] Toghraie D., “Numerical simulation on MHD mixed convection of Cu-water nanofluid in a trapezoidal lid-driven cavity,” *Int. J. Appl. Electromagn. Mech.*, vol. 62, no. 4, pp. 683–710, Jan. 2020, doi: 10.3233/JAE-190123.
- [43] Azad A. K., Parvin S., and Chowdhury M. M. K., “Effects of Hartmann

- number on combined convection in a channel with cavity using Cu-water nanofluid,” *AIP Conf. Proc.*, vol. 1851, no. 1, p. 020081, Jun. 2017, doi: 10.1063/1.4984710.
- [44] Hussain S. and Öztop H. F., “Impact of inclined magnetic field and power law fluid on double diffusive mixed convection in lid-driven curvilinear cavity,” *Int. Commun. Heat Mass Transf.*, vol. 127, p. 105549, Oct. 2021, doi: 10.1016/J.ICHEATMASSTRANSFER.2021.105549.
- [45] Veera Krishna M., Ahamad N. A., and Chamkha A. J., “Numerical investigation on unsteady MHD convective rotating flow past an infinite vertical moving porous surface,” *Ain Shams Eng. J.*, vol. 12, no. 2, pp. 2099–2109, Jun. 2021, doi: 10.1016/J.ASEJ.2020.10.013.
- [46] Sheikholeslami M., Hayat T., and Alsaedi A., “On simulation of nanofluid radiation and natural convection in an enclosure with elliptical cylinders,” *Int. J. Heat Mass Transf.*, vol. 115, pp. 981–991, Dec. 2017, doi: 10.1016/j.ijheatmasstransfer.2017.07.119.
- [47] Kumar V., Pare A., Tiwari A. K., and Ghosh S. K., “Efficacy evaluation of oxide-MWCNT water hybrid nanofluids: An experimental and artificial neural network approach,” *Colloids Surfaces A Physicochem. Eng. Asp.*, vol. 620, p. 126562, Jul. 2021, doi: 10.1016/J.COLSURFA.2021.126562.
- [48] Krishna M. V., Ahammad N. A., and Chamkha A. J., “Radiative MHD flow of Casson hybrid nanofluid over an infinite exponentially accelerated vertical porous surface,” *Case Stud. Therm. Eng.*, vol. 27, p. 101229, Oct. 2021, doi: 10.1016/J.CSITE.2021.101229.
- [49] Rafiq M., Shafique M., Azam A., and Ateeq M., “Transformer oil-based nanofluid: The application of nanomaterials on thermal, electrical and physicochemical properties of liquid insulation-A review,” *Ain Shams Eng. J.*, vol. 12, no. 1, pp. 555–576, Mar. 2021, doi: 10.1016/J.ASEJ.2020.08.010.
- [50] Jain D. S., Srinivas Rao S., and Srivastava A., “Rainbow schlieren deflectometry technique for nanofluid-based heat transfer measurements under natural convection regime,” *Int. J. Heat Mass Transf.*, vol. 98, pp. 697–711, Jul. 2016, doi: 10.1016/J.IJHEATMASSTRANSFER.2016.03.062.
- [51] Mei S., Qi C., Luo T., Zhai X., and Yan Y., “Effects of magnetic field on thermo-hydraulic performance of Fe_3O_4 -water nanofluids in a corrugated tube,” *Int. J. Heat Mass Transf.*, vol. 128, pp. 24–45, Jan. 2019, doi: 10.1016/J.IJHEATMASSTRANSFER.2018.08.071.
- [52] Siddiqui F. R., Tso C. Y., Fu S. C., Qiu H. H., and Chao C. Y. H., “Droplet evaporation and boiling for different mixing ratios of the silver-graphene hybrid nanofluid over heated surfaces,” *Int. J. Heat Mass Transf.*, vol. 180, p. 121786, Dec. 2021, doi: 10.1016/J.IJHEATMASSTRANSFER.2021.121786.

- [53] Modi M., Kangude P., and Srivastava A., “Performance evaluation of alumina nanofluids and nanoparticles-deposited surface on nucleate pool boiling phenomena,” *Int. J. Heat Mass Transf.*, vol. 146, p. 118833, Jan. 2020, doi: 10.1016/J.IJHEATMASSTRANSFER.2019.118833.
- [54] Gholinia M., Armin M., Ranjbar A. A., and Ganji D. D., “Numerical thermal study on CNTs/ C₂H₆O₂– H₂O hybrid base nanofluid upon a porous stretching cylinder under impact of magnetic source,” *Case Stud. Therm. Eng.*, vol. 14, p. 100490, Sep. 2019, doi: 10.1016/J.CSITE.2019.100490.
- [55] Hosseinzadeh K., Asadi A., Mogharrebi A. R., Khalesi J., Mousavisani S., and Ganji D. D., “Entropy generation analysis of (CH₂OH)₂ containing CNTs nanofluid flow under effect of MHD and thermal radiation,” *Case Stud. Therm. Eng.*, vol. 14, p. 100482, Sep. 2019, doi: 10.1016/J.CSITE.2019.100482.
- [56] Srinivasulu T. and Goud B. S., “Effect of inclined magnetic field on flow, heat and mass transfer of Williamson nanofluid over a stretching sheet,” *Case Stud. Therm. Eng.*, vol. 23, p. 100819, Feb. 2021, doi: 10.1016/J.CSITE.2020.100819.
- [57] Dehghani M. S., Toghraie D., and Mehmandoust B., “Effect of MHD on the flow and heat transfer characteristics of nanofluid in a grooved channel with internal heat generation,” *Int. J. Numer. Methods Heat Fluid Flow*, vol. 29, no. 4, pp. 1403–1431, Jun. 2019, doi: 10.1108/HFF-05-2018-0235/FULL/PDF.
- [58] Selimefendigil F. and Öztop H. F., “Mixed convection of nanofluid filled cavity with oscillating lid under the influence of an inclined magnetic field,” *J. Taiwan Inst. Chem. Eng.*, vol. 63, pp. 202–215, Jun. 2016, doi: 10.1016/J.JTICE.2016.03.003.
- [59] Selimefendigil F., Öztop H. F., and Chamkha A. J., “Analysis of mixed convection of nanofluid in a 3D lid-driven trapezoidal cavity with flexible side surfaces and inner cylinder,” *Int. Commun. Heat Mass Transf.*, vol. 87, pp. 40–51, Oct. 2017, doi: 10.1016/J.ICHEATMASSTRANSFER.2017.06.015.
- [60] Ismael M. A., Mansour M. A., Chamkha A. J., and Rashad A. M., “Mixed convection in a nanofluid filled-cavity with partial slip subjected to constant heat flux and inclined magnetic field,” *J. Magn. Magn. Mater.*, vol. 416, pp. 25–36, Oct. 2016, doi: 10.1016/J.JMMM.2016.05.006.
- [61] Rehman W. U., Zulkifli Merican Aljunid Merican, Aamir HussianBhat, Beh GuanHoe, Aliyu AdebayoSulaimon, Omid Akbarzadeh, Muhammad Saad Khan, Ahmad Mukhtar, Sidra Saqib, Ayesha Hameed, Nurhayati Mellon, Hafeez Ullah, Sami Ullahh, Mohammed Ali Assiri, “Synthesis, characterization, stability and thermal conductivity of multi-walled carbon nanotubes (MWCNTs) and eco-friendly jatropa seed oil based nanofluid: An experimental investigation and modeling approach,” *J. Mol. Liq.*, vol. 293, p. 111534, Nov. 2019, doi: 10.1016/J.MOLLIQ.2019.111534.

- [62] Kavitha M., Rajesh V., Mallesh M. P., and Chamka A. J., “Unsteady CNTs kerosene nanofluid flow past a vertical plate with heat transfer under the influence of thermal radiation,” *AIP Conf. Proc.*, vol. 2246, no. 1, p. 020045, Jul. 2020, doi: 10.1063/5.0014577.
- [63] Awais M., Saad M., Ayaz H., Ehsan M. M., and Bhuiyan A. A., “Computational assessment of Nano-particulate ($\text{Al}_2\text{O}_3/\text{Water}$) utilization for enhancement of heat transfer with varying straight section lengths in a serpentine tube heat exchanger,” *Therm. Sci. Eng. Prog.*, vol. 20, p. 100521, Dec. 2020, doi: 10.1016/J.TSEP.2020.100521.
- [64] Al Kalbani K. S., Alam M. S., and Rahman M. M., “Finite element analysis of unsteady natural convective heat transfer and fluid flow of nanofluids inside a tilted square enclosure in the presence of oriented magnetic field,” *Am. J. Heat Mass Transf.*, vol. 3, no. 3, pp. 186–224, 2016, doi: 10.7726/ajhmt.2016.1012.
- [65] Sheikholeslami M., Ganji D. D., Gorji-Bandpy M., and Soleimani S., “Magnetic field effect on nanofluid flow and heat transfer using KKL model,” *J. Taiwan Inst. Chem. Eng.*, vol. 45, no. 3, pp. 795–807, May 2014, doi: 10.1016/J.JTICE.2013.09.018.
- [66] Mahmud S. and Fraser R. A., “Analysis of mixed convection—Radiation interaction in a vertical channel: Entropy generation,” *Exergy, An Int. J.*, vol. 2, no. 4, pp. 330–339, 2002, doi: 10.1016/s1164-0235(02)00075-4.
- [67] Zienkiewicz O. C., Taylor R. L., and Zhu J. Z., “Finite Element Method - Its Basis and Fundamentals (6th Edition),” *Elsevier*, p. 749, Dec. 2005.
- [68] Malleswaran A., Sivasankaran S., and Bhuvaneshwari M., “Effect of heating location and size on MHD mixed convection in a lid-driven cavity,” *Int. J. Numer. Methods Heat Fluid Flow*, vol. 23, no. 5, pp. 867–884, 2013, doi: 10.1108/HFF-04-2011-0082.
- [69] Sheikholeslami M., Hayat T., and Alsaedi A., “MHD free convection of Al_2O_3 –water nanofluid considering thermal radiation: A numerical study,” *Int. J. Heat Mass Transf.*, vol. 96, pp. 513–524, May 2016, doi: 10.1016/J.IJHEATMASSTRANSFER.2016.01.059.